

**Genetic Analysis of Insulin and
Insulin-like Growth Factor-1 Signaling
in the Central Nervous System**

Inaugural-Dissertation

zur

Erlangung des Doktorgrades

der Mathematisch-Naturwissenschaftlichen Fakultät

der Universität zu Köln

vorgelegt von

Linda Koch

aus Köln

Köln 2007

Berichterstatter: Prof. Dr. Jens Brüning
Prof. Dr. Thomas Langer

Tag der mündlichen Prüfung: 06.02.2008

Figure Index	VI
Table Index	IX
Abbreviations	X
1 Introduction	1
1.1 Diabetes mellitus	1
1.2 Insulin	2
1.2.1 Structure and Biosynthesis	2
1.2.2 Metabolic Effects	2
1.3 The Insulin Receptor	3
1.3.1 Molecular Mechanisms of Insulin Signaling	4
1.4 Conditional Gene Targeting	6
1.4.1 Generation of loxP-flanked Alleles	6
1.4.2 Cre-transgenic Mice	7
1.5 RNA interference	9
1.5.1 Small hairpin RNAs	10
1.6 Mouse Mutants of Insulin and IGF-1 Receptor Signaling	11
1.7 Insulin and IGF-1 Receptor Signaling Redundancy	12
1.7.1 Insulin and IGF-1 Signaling in the CNS	14
1.7.2 IGF-1 Signaling in Learning and Memory Formation	15
1.8 Objectives	16
2 Material and Methods	17
2.1 Chemicals	17
2.2 Molecular Biology	19
2.2.1 Isolation of Genomic DNA	19
2.2.2 Quantification of Nucleic Acids	19
2.2.3 Polymerase Chain Reaction (PCR)	20
2.2.4 Southern Blot Analysis	20
2.2.5 RNA Extraction, RT PCR and Quantitative Realtime PCR	21
2.2.6 ELISA	22
2.3 Cell Biology	23
2.3.1 Gene Targeting and Generation of IGF-1R ^{ASyn} Mice	23
2.3.2 Histological Analysis and Immunohistochemistry	24
2.4 Biochemistry	25
2.4.1 Protein Extraction	25
2.4.2 Western Blot Analysis	25
2.5 Mouse Experiments	26
2.5.1 Animals	26
2.5.2 Experimental Setup	27
2.5.3 Body Weight and Blood Glucose Levels	28
2.5.4 Food Intake	28
2.5.5 Glucose and Insulin Tolerance Test	28
2.5.6 Glucose-stimulated Insulin Secretion	28
2.5.7 Insulin Signaling	28
2.5.8 Intracerebroventricular Insulin Infusion	29
2.5.9 Leptin Restoration	29
2.5.10 Kainic Acid-induced Seizures	29
2.5.11 Analysis of Body Composition	30
2.5.12 Behavioral Analysis	30
2.6 Computer Analysis	32

Table of contents

2.6.1	Densitometrical Analysis	32
2.6.2	Statistical Methods	32
3	Results	33
3.1	Inducible inactivation of the insulin receptor gene in peripheral tissues of adult mice	33
3.2	Inducible inactivation of the insulin receptor in peripheral tissues and the central nervous system of adult mice	39
3.3	Combined central and peripheral insulin resistance leads to a more severe lipodystrophy than peripheral insulin resistance	41
3.4	Intracerebroventricular infusion of insulin leads to increased lipogenesis	43
3.5	Insulin inhibits adipocyte-autonomous leptin secretion	46
3.6	Peripheral and central insulin action regulate hepatic ObRb expression	48
3.7	Central insulin action regulates hepatic IL-6 mRNA levels	51
3.8	IR^{Awb} mice display a higher degree of impaired peripheral glucose metabolism	52
3.9	Leptin administration improves glucose metabolism in IR^{Awb} mice	54
3.10	Peripheral insulin resistance results in β cell hyperplasia but unaltered insulin secretion	56
3.11	Targeted disruption of the IGF-1 receptor allele	59
3.12	Conditional inactivation of the IGF-1 receptor gene in the central nervous system	62
3.13	Physiological characterization of IGF-1R^{ASyn} mice	66
3.13.1	Energy homeostasis	66
3.13.2	Glucose homeostasis	68
3.14	Brain weight is unaffected by central IGF-1R deficiency	70
3.15	Unaltered susceptibility to kainic acid of IGF-1R^{ASyn} mice	71
3.16	Central IGF-1 receptor deficiency results in loss of spatial memory formation and anxiety-like behavior	73
4	Discussion	77
4.1	Inducible mouse models of insulin resistance	77
4.2	Peripheral versus central insulin signaling	78
4.2.1	The role of central insulin action in lipogenesis	78
4.2.2	Insulin-mediated inhibition of adipocyte-autonomous leptin secretion	80
4.2.3	Hepatic Stat-3 activation and its role in peripheral glucose homeostasis	82
4.2.4	Effects of peripheral and central insulin deficiency on insulin concentrations and its secretion from the pancreatic β cell	83
4.3	IGF-1 receptor signaling in the central nervous system	84
4.3.1	Contribution of central IGF-1 receptor signaling to insulin-mediated effects in the periphery	84
4.3.2	Neuroprotective effects of IGF-1 receptor signaling	85
4.3.3	IGF-1 receptor signaling in learning and memory formation	86
4.4	Perspectives and experimental approaches	86
5	Summary	88
6	Zusammenfassung	89
7	References	91
8	Acknowledgements	113

9	<i>Erklärung</i>	114
10	<i>Curriculum Vitae</i>	115

Figure Index

Fig. 1: Metabolic effects of insulin signaling.....	3
Fig. 2: Insulin signal transduction pathway.....	5
Fig. 3: General scheme of the ligand-activated CreLBD fusion protein.....	8
Fig. 4: RNA interference.....	10
Fig. 5: General scheme of the inducible peripheral insulin receptor knockout mouse (IR ^{Δper})... 33	33
Fig. 6: Genomic map of the mouse insulin receptor locus surrounding exon 4.....	34
Fig. 7: Southern blot analysis of insulin receptor recombination.....	34
Fig. 8: Western blot analysis of insulin receptor expression.....	36
Fig. 9: Insulin receptor deficiency in peripheral organs of IR ^{Δper} mice.....	37
Fig. 10: Abrogated insulin signaling in peripheral organs of IR ^{Δper} mice.....	38
Fig. 11: General scheme of the inducible whole body insulin receptor knockout mouse (IR ^{Δwb}).	39
Fig. 12: Insulin receptor deficiency in central and peripheral organs of IR ^{Δwb} mice.....	40
Fig. 13 Changes in body weight in insulin receptor deficient mice.....	41
Fig. 14: Reduction of white adipose tissue mass in insulin receptor deficient mice.....	42
Fig. 15: Body composition in insulin receptor deficient mice.....	42
Fig. 16: Adipose tissue-specific hypoplasia in IR ^{Δwb} mice.....	43
Fig. 17: Chronic icv infusion of insulin has no effect on peripheral insulin concentrations in C57BL/6 mice.....	44
Fig. 18: Chronic icv infusion of insulin increases adipose tissue mass without changes in body weight or food intake in C57BL/6 mice.....	45
Fig. 19: Chronic icv infusion of insulin increases lipogenesis in C57BL/6 mice.....	46
Fig. 20: Peripheral insulin resistance results in an increase in total serum leptin concentrations.	46
Fig. 21: Whole body insulin resistance results in a decrease in total serum leptin concentrations.	47
Fig. 22: Serum adipokine levels correlated with white adipose tissue mass in insulin receptor deficient mice.....	47
Fig. 23: Peripheral and central insulin receptor deficiency increases hepatic ObRb mRNA expression.....	48
Fig. 24: Peripheral and central insulin receptor deficiency increases hepatic ObRb protein expression.....	49
Fig. 25: Peripheral but not central insulin receptor deficiency results in an increase in hepatic Stat-3 phosphorylation.....	50

Fig. 26: Peripheral insulin receptor deficiency results in an increase in hepatic IL-6 mRNA expression.....	51
Fig. 27: Unaltered IL-6 mRNA expression in the liver of IR ^{Δwb} mice.....	52
Fig. 28: Loss of central insulin receptor signaling results in more pronounced hyperglycemia.	53
Fig. 29: Impaired glucose tolerance in IR ^{Δper} mice.....	53
Fig. 30: Impaired glucose tolerance in IR ^{Δwb} mice.....	54
Fig. 31: Restoration of serum leptin concentrations of IR ^{Δwb} mice.....	55
Fig. 32: Chronic infusion of leptin increases hepatic Stat-3 phosphorylation in IR ^{Δwb} mice.....	55
Fig. 33: Restoration of hepatic Stat-3 phosphorylation ameliorates blood glucose concentrations.	56
Fig. 34: Peripheral and whole body insulin receptor deficiency results in hyperinsulinemia.....	57
Fig. 35: Glucose-stimulated insulin secretion in IR ^{Δper} and IR ^{Δwb} mice.....	57
Fig. 36: Peripheral and central insulin resistance results in β cell hyperplasia.....	58
Fig. 37: Increased β cell mass in IR ^{Δper} and IR ^{Δwb} mice.....	59
Fig. 38: Conditional gene targeting strategy.....	60
Fig. 39: Correct construct integration into the endogenous IGF-1 receptor locus.....	60
Fig. 40: Chimeras heterozygous for the mutated IGF-1 receptor allele.....	61
Fig. 41: Germline transmission of the mutated IGF-1 receptor allele.....	61
Fig. 42: Central IGF-1 receptor protein expression.....	63
Fig. 43: Peripheral IGF-1 receptor protein expression.....	64
Fig. 44: Synapsin Cre expression in brain regions of SynCre-LacZ mice.....	65
Fig. 45: Reduced IGF-1 receptor expression in the dentate gyrus of IGF1R ^{ΔSyn} mice.....	66
Fig. 46: Body weight of IGF-1R ^{ΔSyn} mice.....	67
Fig. 47: Unaltered body composition of IGF-1R ^{ΔSyn} mice.....	67
Fig. 48: Central IGF-1 receptor deficiency has no impact on adipose tissue mass or serum leptin and insulin concentrations.....	68
Fig. 49: Loss of central IGF-1 receptor signaling has no impact on blood glucose concentrations.....	69
Fig. 50: Unaltered glucose tolerance in IGF-1R ^{ΔSyn} mice.....	69
Fig. 51: Unaltered insulin sensitivity in IGF-1R ^{ΔSyn} mice.....	70
Fig. 52: Unaltered brain weight of IGF-1R ^{ΔSyn} mice.....	71
Fig. 53: Central IGF-1 receptor deficiency has no impact on kainic acid-induced seizures.....	72
Fig. 54: Kainic acid-induced neuronal damage occurs to similar extent in IGF-1R ^{ΔSyn} and control mice.....	73
Fig. 55: Spatial navigation working memory is impaired in IGF-1R ^{ΔSyn} mice.....	74
Fig. 56: IGF-1R ^{ΔSyn} mice do not display signs of anxiety.....	74

Figure Index

Fig. 57: Unaltered motor coordination in IGF-1R ^{ΔSyn} mice.	75
Fig. 58: Unaltered spontaneous novelty preference and exploratory activity in IGF-1R ^{ΔSyn} mice.	76
Fig. 59: Proposed model for insulin action in the CNS and in the periphery in the regulation of glucose and adipose tissue metabolism.	80
Fig. 60: Proposed model for the effects of insulin resistance on circulating leptin levels.	81

Table Index

Table 1: Excerpt of transgenic and knockout mouse models involving genes of the insulin or IGF-1 receptor signaling pathway.....	12
Table 2: Chemicals.....	19
Table 3: Oligonucleotides used for genotyping.	20
Table 4: Oligonucleotides used to amplify the Southern blot probes.	21
Table 5: Probes used for Realtime PCR.....	22
Table 6: Primary antibodies used for Western blot analysis.....	26

Abbreviations

aa	amino acid
Akt	proteinkinase B
Avertin	tribromoethyl alcohol and <i>tert</i> -amyl alcohol
β-me	β-mercaptoethanol
bp	base pair
c	DNA concentration
C	cytosine
°C	degrees Celsius
cDNA	complementary DNA
cpm	counts per minute
Cre	site-specific recombinase (<u>causes</u> <u>recombination</u>)
CreER ^{T2}	Cre recombinase and mutated ER-LBD fusion protein
Ctrl	Control
ddH ₂ O	double distilled water
DEPC	diethylpyrocarbonate
dNTP	desoxynucleotide-triphosphate
DMSO	dimethylsulfoxide
DNA	desoxyribonucleic acid
ds	doublestranded
DTT	1,4-Dithio-DL-threitol
E ₂	17-β-estradiol
ECL	enhanced chemiluminescence
EDTA	ethylene-diaminetetraacetic acid
EF	embryonic fibroblasts
ER	estrogen receptor
ER ^{T2}	mutated ligand binding domain of the human ER
ES	embryonic stem
EtBr	ethidium bromide
G	guanine
G418	geneticin

GTT	glucose tolerance test
h	hour
HEPES	N-2-hydroxyethylpiperazine-N'-2-ethansulfonic acid
HR	homologous recombinant
HRE	hormone response element
HSV-tk	thymidine kinase of the <i>Herpes simplex</i> virus
icv	intracerebroventricular
IGF-1R	insulin-like growth factor-1 receptor
i.p.	intraperitoneal
IR	insulin receptor
IRS	insulin receptor substrate
ITT	insulin tolerance test
KA	kainic acid
kbp	kilobase pairs
kDa	kilodalton
loxP	locus of x (crossing) over of P1
min	minute
NaCl	sodium chloride
NaOH	sodium hydroxide
neo ^r	neomycine resistance gene
LBD	ligand binding domain
NLS	nuclear localization sequence
OD	optical density
PBS	phosphate buffered saline
PCR	polymerase chain reaction
per	peripheral
PH	pleckstrin homology
PI3K	phosphatidylinositol-3 kinase
PIP ₂	phosphatidylinositol-4,5-biphosphate
PIP ₃	phosphatidylinositol-3,4,5-triphosphate
p.o.	per os
PTB	phosphotyrosine binding
RNA	ribonucleic acid
RNAi	RNA interference

Abbreviations

rpm	rounds per minute
RT	room temperature
sec	second
s.c.	subcutaneous
SDS	sodium dodecyl sulfate
SH	src homology
shRNA	small/short hairpin RNA
siRNA	small interfering RNA
ss	singlestranded
SSC	sodium chloride/ sodium citrate buffer
TAE	Tris-acetic acid-EDTA buffer
Taq Pol	polymerase from <i>Thermus aquaticus</i>
TE	Tris-EDTA buffer
Tris	2-amino-2-(hydroxymethyl)-1,3-propanediol
TWEEN	polyoxethylene-sorbitan-monolaureate
U	units
v/v	volume per volume
WAT	white adipose tissue
wb	whole body
w/v	weight per volume
wt	wildtype
5'	five prime end of DNA sequences
3'	three prime end of DNA sequences

1 Introduction

1.1 Diabetes mellitus

Diabetes mellitus is a chronic disease, accounting for an estimated 224,000 deaths every year in the United States (US) alone, establishing itself as the 6th leading cause of death. As of 2005, an estimate of 7% of the US population, approximately 20.8 million people, suffers from diabetes. Diabetes and complications arising from it cost an estimated \$132 billion each year in terms of healthcare and lost productivity in the US (1).

The first reference to diabetes is attributed to an Egyptian papyrus, written as early as 1550 BC, which describes remedies for the treatment of excessive urination. Around 100 AD, Aretaeus, a disciple of Hippocrates, provided the first accurate description of the disease and termed it “diabetes”, based on the Greek word *diabainein*, “to pass through”, a reference to the polyuria, one of its major symptoms (for review see (2, 3)). Not until the late 18th century, the physicians Johann Peter Frank and John Rollo appended the Latin term “mellitus”, for honey, to distinguish diabetes from other diseases causing polyuria (for review see (4)).

In the early modern period, one of the first publicized works relating to diabetes originates from 1675, when the British physician Thomas Willis found the urine of diabetic patients to be abnormally sweet (5), an observation which was confirmed a century later, in 1776, by his compatriot and colleague Matthew Dobson. Dobson also found that sugar was not only present in the urine but in the blood of patients, thereby establishing the systemic nature of the disorder (6). Twelve years later, the physician Thomas Cawley first noted a correlation between diabetes and damaged pancreas while performing an autopsy on a diabetic patient, yet his observation would not be acknowledged for another hundred years (7). In 1889, the Polish-German physician Oscar Minkowski and his German colleague Joseph von Mering discovered that after surgical removal of the pancreas, dogs displayed all symptoms associated with diabetes and died shortly afterwards, providing the first link between the pancreas and diabetes ((8), (for review see (9))). However, although it had been deduced by several scientists that a substance must be secreted from the pancreas to regulate carbohydrate metabolism and that loss of this substance causes diabetes (10), it was not until 1921 that physician Frederick Banting and medical student Charles Best in the lab of J.J.R.

MacLeod at the University of Toronto finally made the discovery which would revolutionize the treatment of diabetes mellitus (11). In 1923, Banting and MacLeod were awarded the Nobel Prize in Medicine for their discovery of insulin.

1.2 Insulin

1.2.1 Structure and Biosynthesis

Insulin is synthesized in the β cells of the pancreatic islets of Langerhans, endocrine cells within the predominantly exocrine pancreatic tissue. It is cleaved from an inactive precursor, proinsulin, consisting of two peptide chains linked by a third, the so-called C-peptide (12). Proinsulin is synthesized in the endoplasmatic reticulum, then transported to the Golgi apparatus where it is packed into secretory granules (13). Within these vesicles, it is processed to insulin through site-specific proteolytic cleavage by two endopeptidases and one carboxypeptidase (14-16). The C-peptide is removed from proinsulin, leading to a conformational change of the protein which enables the interaction of the mature molecule with its receptor, the insulin receptor (17). After binding to and activating its receptor, insulin is either returned into the circulation intact or internalized and degraded by the Insulin-degrading enzyme (for review see (18)).

1.2.2 Metabolic Effects

Elevated plasma glucose concentration (hyperglycemia) is the predominant stimulus causing insulin secretion from the pancreatic β cells into the bloodstream, although insulin is also secreted in response to glucagon, adrenalin or increased amino acid concentrations. Activation of insulin signaling results in the translocation of the glucose transporter GLUT-4 into the cell membrane of skeletal muscle cells and adipocytes, thereby increasing glucose uptake into these tissues (19-21). In addition to glucose clearance from the blood, insulin increases glycolysis and inhibits its reverse process, gluconeogenesis (for review see (22)). Concomitantly, insulin promotes the storage of substrates by stimulating amino acid uptake and protein synthesis in muscle, glycogen synthesis in liver and lipogenesis in adipose tissue. Catabolic processes, on the

other hand, such as glycogenolysis, lipolysis and proteolysis are inhibited by insulin (Fig. 1).

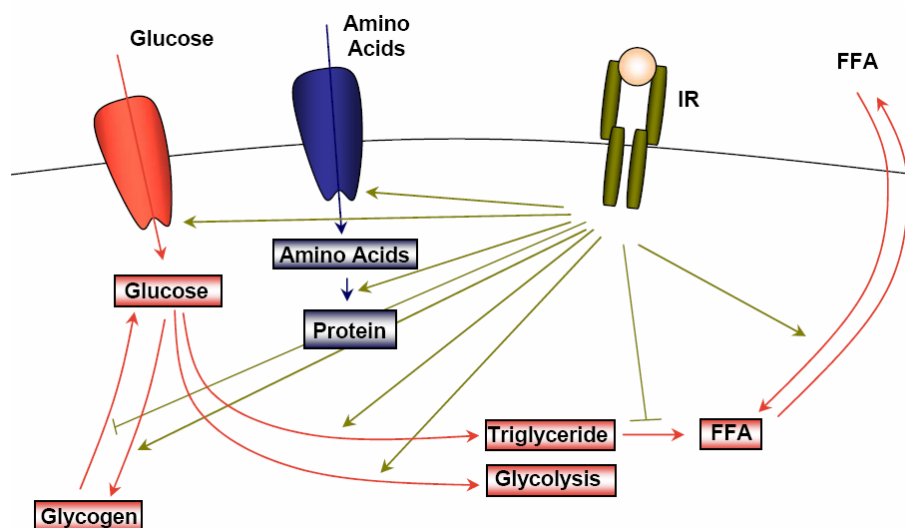


Fig. 1: Metabolic effects of insulin signaling.

Overview of insulin's effects on the cellular level. Insulin signaling results in the increase of glucose and amino acid uptake, glycogen and protein synthesis, lipogenesis and glycolysis, while it inhibits gluconeogenesis, lipolysis and proteolysis (adapted from (23)).

1.3 The Insulin Receptor

The family of ligand-activated receptor tyrosine kinases represents the connecting link between extra- and intracellular signal transduction of insulin and insulin-like peptides. This subfamily of receptor kinases comprises the insulin receptor, the insulin-like growth factor (IGF)-1 receptor and an orphan receptor, known as the insulin receptor-related receptor (24-26). These receptors are heterotetrameric proteins, consisting of two $\alpha\beta$ -dimers connected by disulfide bridges (27, 28). The α -subunits form an extracellular ligand binding domain, while the transmembrane region and the intracellular C-terminal part encompassing the intrinsic receptor tyrosine kinase activity are formed by the β -subunit (29-32). Each receptor is the product of a separate gene, whose transcript is translated into a precursor or proreceptor that, after removal of the precursor signaling peptide, is post-translationally processed by a furin-like enzyme to yield a single $\alpha\beta$ -dimer (33).

In humans, the gene encoding the insulin receptor is located on the short arm of chromosome 19, spanning a region of more than 120 kilobase pairs (kbp) which

comprise a total of 22 exons (34, 35). In mammals, insulin receptors are expressed in all tissues, including classic insulin responsive tissues such as skeletal muscle, liver and adipose tissue, as well as tissues previously thought to be unresponsive to insulin like the central nervous system, the pancreas or lymphatic cells (36-38).

1.3.1 Molecular Mechanisms of Insulin Signaling

Insulin and the related insulin-like growth factor (IGF)-1 exert their pleiotropic functions by binding to and activating their membrane-bound tyrosine kinase receptors (25, 39, 40) (Fig. 2). Functionally, the insulin receptor acts as a classical allosteric enzyme. Ligand binding results in receptor autophosphorylation on three intracellular tyrosine residues of the β -subunits, thereby activating the intrinsic tyrosine kinase activity in the C-terminal region of the receptor (41). Upon autophosphorylation, intracellular signaling proteins are recruited to the receptor through their phosphotyrosine binding (PTB) domain and there become tyrosine phosphorylated (42-44). In addition to the PTB domain, intracellular substrates contain an N-terminal Pleckstrin homology (PH) domain which, through interaction with inositol phosphates in the cell membrane, allows for the localization of the substrate to the membrane (45-47). Intracellular signaling molecules of the insulin receptor are the insulin receptor substrates (IRS)-1-4 and the Grb2-associated binder (Gab)-1-4 proteins (48-54). These substrates, when tyrosine phosphorylated, serve as docking platforms for Src-homology (SH)-2 domain containing proteins such as the regulatory subunit of the phosphatidylinositol 3 kinase (PI3K), the growth factor receptor binding protein (Grb)-2 and the SH-2 domain containing phosphatase (Shp)-2, among others, resulting in the activation of the PI3K and the Ras/Raf Mitogen-activated protein (MAP)-kinase pathway (55-59). The PI3K is a heterodimer consisting of a catalytic subunit, p110, constitutively associated with a regulatory subunit (for review see (60)). When activated, PI3K catalyzes the conversion of phosphatidylinositol-4,5-biphosphate (PIP₂) to phosphatidylinositol-3,4,5-triphosphate (PIP₃) (61, 62). PIP₂ and PIP₃ bind the PH domain of the serine/threonine kinase proteinkinase B, also termed Akt. This results in the recruitment of Akt from the cytosol to the membrane and a conformational change, which converts Akt into a substrate for the phosphoinositide-dependent kinase (Pdk)-1 (for review see (63)). Activation of Akt controls a broad variety of biological functions such as the regulation of glycogen and protein synthesis, protection from apoptosis,

stimulation of glucose transport and the regulation of gene transcription (for review see (64)).

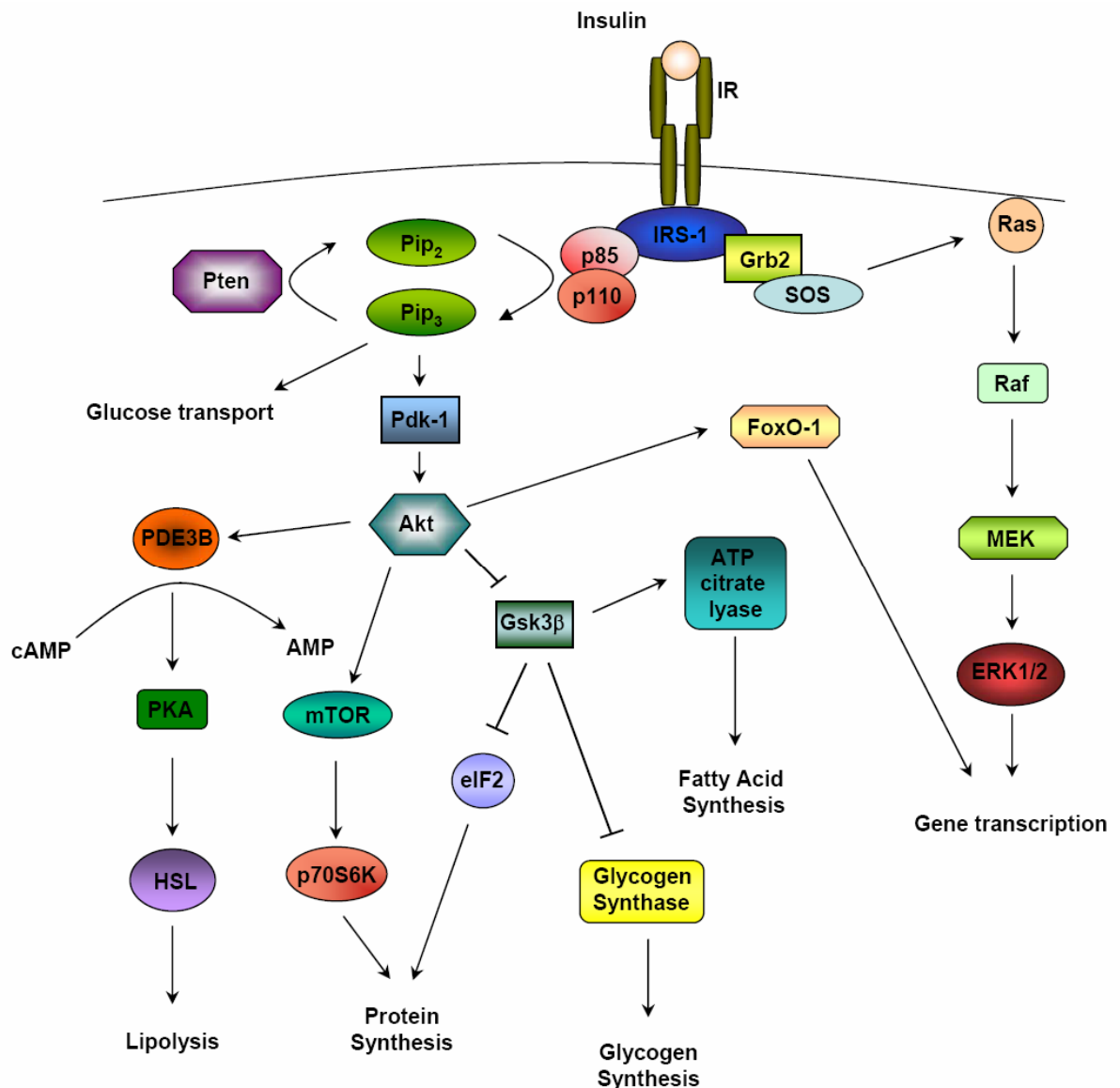


Fig. 2: Insulin signal transduction pathway.

Binding of insulin to the insulin receptor results in receptor trans-phosphorylation and activation leading to the recruitment and subsequent phosphorylation of insulin receptor substrates. This enables the binding of SH-2 domain containing proteins, which ultimately leads to the activation of downstream signaling pathways such as the PI3K or the MAPK signaling pathway. IR = insulin receptor, IRS = insulin receptor substrate, PI = Phosphatidylinositol, Pdk = phosphoinositide-dependent kinase, Akt = Proteinkinase B, FoxO1 = Forkhead transcription factor O1, Gsk3β = glycogen synthase kinase 3β, eIF2 = eukaryotic translation initiation factor 2, PDE3B = phosphodiesterase 3B, PKA = Proteinkinase A, HSL = hormone sensitive lipase = mTOR = mammalian target of rapamycin, p70S6K = p70 S6 kinase, Grb2 = growth factor receptor binding protein, SOS = son of sevenless, Ras = rat sarcoma, Raf = v-raf-leukemia viral oncogene, MEK = Mitogen-activated protein kinase kinase, ERK = extracellular signal-regulated kinase

1.4 Conditional Gene Targeting

Manipulating the mouse genome using homologous recombination in embryonic stem cells has now been recognized as a technique so valuable for the analysis of gene function that its discoverers Mario R. Capecchi, Sir Martin J. Evans and Oliver Smithies were awarded the Nobel Prize in Physiology or Medicine 2007 ((65-67), for review see (68)). However, since this process involves the manipulation of the murine germline, conventional gene targeting results in the loss of gene function in all cells during pre- and postnatal development. Consequences to be considered are the occurrence of embryonic lethality, compensatory effects by redundant genes and side effects caused by the inserted selection marker. To circumvent these potential drawbacks, gene inactivation in a spatially and temporally controlled manner can be achieved by conditional gene targeting, a more sophisticated method based on sequence-specific DNA recombinases as tools for genetic engineering (for review see (69, 70). One of these site-specific DNA recombinases, the Cre (causes recombination) recombinase, is a 38 kDa protein of the bacteriophage P1 that recognizes specific 34 bp palindromic sequences, termed *loxP* (locus of crossing (x) over in P1) sites (71, 72). Depending on the orientation of the loxP sites the Cre recombinase mediates the inversion, excision or translocation of the DNA sequence that is flanked by the two loxP sequences (73-76). DNA sequences flanked by directly repeating loxP sites are excised as a circular molecule, leaving a single loxP sequence at the site of recombination (73, 77).

1.4.1 Generation of loxP-flanked Alleles

Whereas conventional gene targeting results in the inactivation of a gene already in embryonic stem (ES) cells, the strategy of conditional mutagenesis is based on the flanking of an essential region in a gene of interest by loxP sequences in ES cells without interfering with the original gene function (70, 78). This approach requires the construction of a gene targeting vector, in which two loxP sites are flanking an indispensable gene segment, in most cases one or more exons. The loxP sites are placed within non-coding sequences to preserve gene integrity. Insertion of a selection marker is necessary for subsequent selection of homologous recombinants. The selection marker in turn is flanked by so-called FRT sequences, to later enable its excision from the genome of the ES cells by a transient transfection of the cells with a Flp recombinase-coding plasmid (79). Alternatively, mice still containing the selection

marker within their DNA can be crossed to mice expressing the Flp recombinase in their germline. The Flp/FRT system is the eukaryotic homolog of the Cre/loxP system, originating from the yeast *Saccharomyces cerevisiae*. FRT sites consist of two 13 bp long sequences immediately flanking an 8 bp long asymmetrical core sequence (80). Hence, the final gene targeting construct consists of, from 5' to 3', a sequence homologous to the target gene sequence, a loxP site, an FRT-flanked selection marker cassette, a second homologous sequence that contains essential regions of the targeted gene, a second loxP site, and a third homologous gene sequence.

The construct is introduced into murine ES cells via electroporation. Cells that have integrated the construct through homologous recombination can be selected for with the help of the selection marker and determined by Southern blot and PCR analyses (81, 82). The construct is integrated only into one of the two alleles of a gene, rendering ES cells heterozygous for the desired mutation. A homologous recombinant ES cell clone is injected into a murine embryo at the blastocyst stage, where it integrates into the inner cell mass of the embryo and participates in the continuing embryonic development (83-85). The blastocysts are implanted into the uterus of pseudopregnant mice. Since the injected ES cell clones can partake in the development of all organs, they can also differentiate into germ cells. All tissues of the resulting offspring, so-called chimeras, consist of two cell types of different origin. When mutated ES cells make up the chimeras germline, the mutation is passed on to its offspring. Further intercrosses yield mice homozygous for the recombinant locus (83, 84, 86, 87).

1.4.2 Cre-transgenic Mice

Cre-transgenic mouse strains are generated either by conventional random transgenics, targeted insertion into a gene (knock-in) or by generating bacterial artificial chromosome (BAC)-transgenic mice (88, 89). Regardless of the strategy, the promotor which drives Cre expression determines onset and cell type-specificity of the Cre-mediated recombination. By crossing mice carrying a loxP-flanked mutation of the gene of interest with mice expressing the Cre recombinase restricted to specific tissues, a conditional mouse mutant is generated that lacks the target gene only in the cells in which Cre is expressed.

To analyze gene function at a certain developmental stage, Cre expression can be temporally controlled either in a transcriptional or in a post-translational manner (for

review see (90)). Post-translational control of Cre expression involves the use of steroid hormone receptors. In the absence of their respective hormone ligands, these intracellular receptors are retained in the cytoplasm by the heatshock protein hsp90 (91). Binding of the respective hormones to the ligand binding domain (LBD) of the receptor leads to a conformational change, resulting in the dissociation of the multiprotein complex, thereby unmasking a nuclear localization sequence (NLS) which leads to the nuclear import of the receptor. In the nucleus, the receptor homodimerizes and binds specific hormone response elements (HRE) in the promoter of the target genes, thus either activating or repressing their transcription (92-94).

Temporally controlled Cre expression can be achieved by fusing the Cre recombinase to the mutated LBD of a steroid hormone receptor. This fusion protein can be expressed from any cell type-specific promoter. Mutations in the LBD prevent binding and activation of the fusion protein by endogenous steroids (95-97). Upon binding of a synthetic ligand specific for the mutated ligand binding domain of the CreLBD fusion protein, heatshock proteins detach and the fusion protein is transported into the nucleus, where the Cre recombinase mediates the deletion of all loxP-flanked alleles (Fig. 3) (for review see (98)).

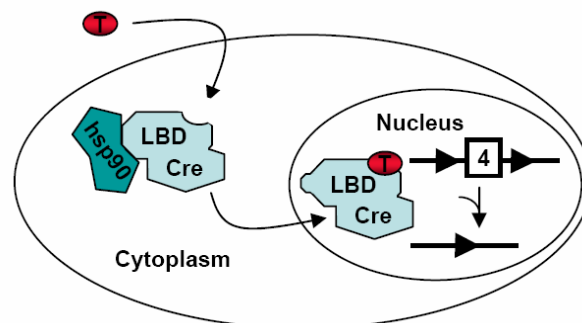


Fig. 3: General scheme of the ligand-activated CreLBD fusion protein.

The CreLBD fusion protein is sequestered by heatshock protein hsp90 in the cytoplasm. Binding of a synthetic ligand (T) to the mutated LBD promotes dissociation of hsp90 and nuclear import of the fusion protein, where the Cre recombinase (Cre) mediates recombination of the loxP (triangle) sites flanking an exon (4) of the gene of interest.

A mutant LBD of the human estrogen receptor (ER), ER^{T2}, has been generated, containing three amino acid substitutions, resulting in the inability of the estrogen receptor to be activated by its endogenous ligand, 17- β -estradiol (E₂). The result is a 10-fold higher affinity to synthetic ligands, such as the estrogen antagonists tamoxifen or 4-

hydroxy-tamoxifen, compared to former single mutants of the ER-LBD (99). Numerous transgenic mouse strains carrying a chimeric protein consisting of the Cre recombinase and the triple mutant ER^{T2} (CreER^{T2}) have been generated. Cre activity can be modulated in these mice by per os (p.o.) or intraperitoneal (i.p.) administration of tamoxifen, resulting in the highly efficient recombination of loxP-flanked target genes either ubiquitously or restricted to specific tissues (100-103). One of these mouse strains uses the ubiquitously expressed Rosa26 locus to drive expression of the CreER^{T2} fusion protein (RosaCreER^{T2}). As previously described for the RosaCreER^{T2} mice, upon tamoxifen administration, recombination occurs with high efficiency only in peripheral tissues, due to a lower local concentration of tamoxifen in the brain (100).

1.5 RNA interference

RNA interference (RNAi) is based on gene silencing using doublestranded RNA (dsRNA) (104). RNAi is mediated by short interfering RNAs (siRNAs), consisting of two 21 nucleotide single-stranded RNAs that form a 19 bp duplex with a 2 nucleotide 3' overhang on each strand (105). dsRNA is cleaved by the enzyme Dicer to form siRNAs (106). Dicer is a highly conserved protein, consisting of two RNase III domains, a double-stranded RNA binding domain and a long N-terminal region containing a DEAD-Box RNA helicase domain and a Piwi Argonaute Zwiille (PAZ) domain (106-108). The PAZ domain has been shown to bind the 3' overhang of small RNA molecules (109, 110). One protein family, after which the PAZ domain was named, consists of the Argonaute proteins. These are, together with Dicer, part of the RNA-induced silencing complex (RISC), which binds the antisense strand of the siRNA and uses it to guide mRNA cleavage, resulting in mRNA degradation (111) (Fig. 4).

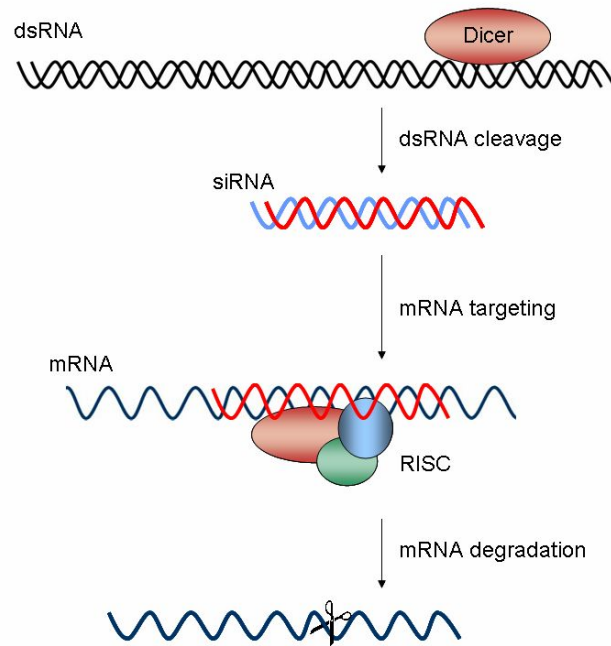


Fig. 4: RNA interference.

dsRNA is cleaved by Dicer into siRNAs. These bind to RISC and mediate mRNA degradation (adapted from (112)).

1.5.1 Small hairpin RNAs

In mammals, injection of long dsRNA to induce gene silencing leads to the activation of an antiviral response, resulting in translational repression and apoptosis in somatic cells (113, 114). These nonspecific dsRNA responses can be prevented by creating dsRNA triggers of less than 30 bp. *In vivo* expression constructs have been developed for so-called short hairpin RNAs (shRNAs), which resemble endogenously expressed hairpin RNAs and mediate sequence-specific gene silencing in mammalian cells without activating antiviral responses (115, 116). This approach uses small inverted repeats of 19 – 29 nt expressed under the control of an RNA polymerase III promoter to create shRNAs that are then processed by Dicer and shunted into the RNAi pathway. Conditional shRNA-mediated gene silencing in mice has been achieved by employing the Cre/loxP-System to induce tissue-specific control of shRNA expression (117-119). Temporal modulation of ubiquitous shRNA expression has been demonstrated in mice expressing a shRNA against the mRNA of the insulin receptor under the control of a modified RNA polymerase III-dependent promoter containing operator sequences from the *E. coli* tetracycline resistance operon from the ubiquitously expressed Rosa26 locus (120).

1.6 Mouse Mutants of Insulin and IGF-1 Receptor Signaling

Many insights into the molecular mechanisms of insulin action and its role in individual tissues of the mammalian organism have been gained from the *in vivo* inactivation of genes pivotal for insulin action, such as insulin, the insulin receptor, as well as downstream signaling molecules such as the IRS proteins, Gab-1, glucose transporter (GLUT)-2 and -4 and metabolic effector molecules like glucokinase (GK). Genes encoding insulin- like growth factors (IGF-1 and IGF-2) and their type I receptor (IGF-1R) have also been disrupted. A brief summary of the phenotypes is given in Table 1.

Mutation	Viable	DM	Phenotype	Reference
Insulin	-	+	intrauterine growth retardation, death within 2 days of diabetic ketoacidosis and liver steatosis	(121)
IR	-	+	normal intrauterine growth and development, death within 3 days of diabetic ketoacidosis	(122)
IRS-1	+	-	insulin resistance, hypertension, hypertriglyceridemia, impaired vascular relaxation	(123-125)
IRS-2	+	+	intrauterine and postnatal growth retardation	(126)
IRS-3	+	n.d.	normal glucose tolerance and growth	(127)
IRS-4	+	-	mild defects in growth, reproduction and glucose homeostasis	(128)
Gab-1	-	-	intrauterine death, developmental defects in heart, placenta, and skin	(129)
LGKO	+	-	improved hepatic insulin sensitivity, reduced glycemia, improved glucose tolerance	(130)
β IRKO	+	+	impaired insulin secretion	(131)
FIRKO	+	+	reduced fat mass, protection against obesity and glucose intolerance, altered adipose tissue morphology	(132)
MIRKO	+	-	increased adiposity	(133)
NIRKO	+	-	normal brain development, mild insulin resistance, diet-sensitive obesity	(134)
LIRKO	+	+	progressive liver failure	(135)
IRS-1, GK	+	+	growth retardation	(136)
FoxO1, IRS-1	+	-	improved insulin sensitivity	(137)
GLUT-2	-	mild	death within 2-3 weeks, postnatal growth retardation	(138)
GLUT-4	+	-	reduced fat mass, growth retardation, mild impairment of glucose homeostasis	(139)
IR, IRS-1	+	+	hyperinsulinemia, β cell hyperplasia	(140)

IGF-1	+/-	-	viability depends on background, dwarfism	(141, 142)
IGF-1R	-	-	death within 2-3 hours of respiratory failure, dwarfism, developmental defects of skin, bone, CNS	(141, 143)

Table 1: Excerpt of transgenic and knockout mouse models involving genes of the insulin or IGF-1 receptor signaling pathway.

DM = Diabetes mellitus, n.d. = not determined, IR = insulin receptor, IRS = insulin receptor substrate, KO = knockout, β = β cell-specific, F = fat-specific, M = muscle-specific, N = neuron-specific, L = liver-specific, G = Gab-1, GK = Glucokinase, FoxO1 = Forkhead transcription factor O1, GLUT = Glucose transporter, IGF = insulin-like growth factor.

Most signaling molecules downstream of the insulin receptor exist in more than one isoform, such as Akt or Pdk, or can be composed of different subunits, like PI3K, rendering the inactivation of these proteins difficult. Consequently, a prominent amount of studies have focused on the inactivation of the insulin receptor gene in mice, either in a conventional fashion (122, 144) or by conditional inactivation of the insulin receptor in selected murine tissues (131-134, 145). These experiments have yielded unexpected findings with respect to the role of insulin action in classical insulin target tissues such as skeletal muscle, liver and adipose tissue (132, 133, 135), but also in tissues previously viewed as non-insulin responsive, such as brain, pancreatic β cells, macrophages and blood vessels (131, 134, 146, 147). Nevertheless, analyses of tissue- or cell type-specific insulin receptor knockout mice are limited by the lack of insulin receptor throughout development. Abnormalities arising from impaired insulin action can therefore be partly compensated for by adaptive processes or arise from developmental defects influencing the differentiation of respective tissues.

1.7 Insulin and IGF-1 Receptor Signaling Redundancy

The insulin receptor and the IGF-1 receptor are present on the surface of almost all cells, although their relative proportion varies depending on the target tissue. Although these two receptors represent two separate gene products, they exhibit up to 85% homology in their amino acid sequence in different domains. Thus, while both insulin and IGF-1 exhibit the highest affinity to their innate receptors, insulin can also bind to and activate the IGF-1 receptor and IGF-1 is capable of binding to and activating the insulin receptor (for review see (148)). After binding of the ligand to its receptor, the same intracellular mechanisms modulate the activation of the PI3K or

MAPK signaling pathways (for review see (149)). Moreover, both receptors can form heterodimers, capable of effectively initiating the downstream signaling machinery (150, 151). Both the ligand binding characteristics as well as the formation of hybrid receptors raise the question of a possible redundancy between the two receptor tyrosine kinases.

In experiments using insulin receptor-deficient hepatocytes, no metabolic effects, such as an increase in glycogen synthesis or inhibition of glucose production, could be detected after insulin stimulation, whereas phosphorylation of insulin receptor substrates IRS-1 and Gab-1 and their binding of the PI3K was unaffected due to a compensatory activation via binding of insulin to the IGF-1 receptor (152). Also, the stimulation of muscle cells and fibroblasts of insulin receptor-deficient mice with IGF-1 or high concentrations of insulin results in an increase in glucose uptake, glycogen synthesis, IRS-1 phosphorylation and activation of PI3K and MAPK (153, 154). These experiments clearly indicate the ability of the IGF-1 receptor to function as an alternative receptor to the insulin receptor in the metabolic signal transduction of insulin receptor-deficient muscle cells. The IGF-1 receptor-stimulated glucose uptake into the skeletal muscle is also partially responsible for the hypoglycemic effect detectable after injection of insulin receptor-deficient mice with IGF-1 (155). Mice with a muscle-specific inactivation of the insulin receptor (MIRKO) maintain euglycemia with normal plasma insulin concentrations over months (133), indicating that a 95% reduction in insulin receptor protein and the resulting insulin resistance can be almost completely compensated for in MIRKO mice. Another example of IGF-1 receptor-mediated compensation for insulin receptor deficiency is provided by transgenic mice expressing a dominant-negative IGF-1 receptor in skeletal muscle. Transgene expression results in the formation of hybrid receptors between the mutant IGF-1 receptor and the endogenous IGF-1 and insulin receptor, leading to the inactivation of the endogenous receptors. This leads to insulin resistance and pancreatic β cell dysfunction, resulting in a diabetes-like phenotype (156).

In conclusion, increasing evidence suggests an important role for the IGF-1 receptor in insulin action, thus defining its signaling pathway as a possible candidate for the development of insulin resistance in the pathogenesis of Diabetes mellitus.

1.7.1 Insulin and IGF-1 Signaling in the CNS

Both the insulin receptor and the IGF-1 receptor are widely expressed throughout the central nervous system, both on neurons and glia cells (157, 158). Data from cultured neurons as well as animals lacking the insulin receptor or IGF-1 have established a role for the insulin/IGF-1 signaling machinery in the regulation of neuronal survival (159-162).

Insulin and IGF-1 have been demonstrated to regulate phosphorylation of the microtubule associated protein Tau. Hyperphosphorylated Tau represents a hallmark of neurodegenerative diseases such as Alzheimer's disease (AD) as it constitutes the major protein of neurofibrillary tangles (for review see (163)). Moreover, increasing evidence indicates a direct effect of insulin and IGF-1 on the metabolism and clearance of β -amyloid ($A\beta$) (164, 165), the deposition of which leads to the formation of neuritic plaques, a second key player in the pathogenesis of AD. Along this line, it could be demonstrated that IGF-1 treatment rescues neuronal apoptosis caused by a mutant form of the amyloid precursor protein (166). Mice with neuron-specific deletion of the insulin receptor gene exhibit hyperphosphorylation of Tau, presumably due to reduced activity of the AKT serine threonine kinase, resulting in disinhibition of glycogen synthase kinase (GSK)-3 β , a well-characterized Tau kinase (160). Nevertheless, brain-specific insulin receptor knockout mice fail to develop progression towards overt neurodegeneration and impaired learning.

Clinically, epidemiological studies clearly indicate the link of systemic insulin resistance, type 2 diabetes mellitus and AD. Therefore, neuronal insulin resistance might represent a risk factor, resulting in at least one of the biochemical hallmarks of Alzheimer's disease. On the other hand, given the ability of insulin to bind to the IGF-1 receptor and unaltered IGF-1 receptor signaling in brain-specific insulin receptor knockout mice, these experiments have left the question unaddressed, whether or not IGF-1 receptor signaling provides a compensatory mechanism in the presence of brain-specific deletion of the insulin receptor gene.

Beside the regulation of neuronal growth and survival, insulin has been demonstrated to modulate energy homeostasis, presumably through its signaling in the hypothalamus, particularly in the arcuate nucleus of the hypothalamus (for review see (167)). Mice with brain-specific deletion of the insulin receptor exhibit an increased bodyweight (134). Nevertheless, the contribution of neuronal IGF-1 receptor signaling in the regulation of these processes has so far not been analyzed.

In conclusion, there is strong evidence for the contribution of insulin and IGF-1 signaling in the regulation of neuronal growth and survival as well as the regulation of food intake and peripheral glucose metabolism. The proposed analysis of IGF-1 receptor signaling in mediating these effects will therefore reveal novel insights into the pathogenesis of neurodegenerative diseases as well as obesity and type 2 diabetes mellitus.

1.7.2 IGF-1 Signaling in Learning and Memory Formation

Many clinical syndromes including Alzheimer's disease, semantic dementia, schizophrenia or cerebral trauma, among others, are associated with disorders of learning and memory. One of the major structures involved in learning and memory formation is the hippocampus. It is required for the formation of declarative memory, meaning facts or events that can be consciously verbalized, as well as spatial memory, which is responsible for retaining information on surroundings and spatial orientation.

The integrity of the hippocampus has been shown to decline with age (168, 169). More frequent and more intense stimuli are then required to induce long-term potentiation (LTP), the molecular basis of memory formation. Cognitive deficits arising with old age appear to be the result of dysfunctions in neuronal circuits and synaptic plasticity, whereas neuronal cell death is apparently not influenced.

Throughout adulthood, new neurons are continuously generated in the brain, specifically in the subventricular zone and the dentate gyrus of the hippocampus (for review see (170)). Hippocampal neurogenesis can be modulated by various factors including hormones, neurotransmitters or environment (171) and, like memory formation, has been demonstrated to decline with age (172). Several studies have linked neurogenesis with the formation of some types of hippocampus-dependent memories (173). IGF-1 has been implicated in synaptic plasticity and neurogenesis and, like memory formation and adult neurogenesis, is downregulated in an age-dependent manner (for review see (174)). Intracerebroventricular infusion of IGF-1 in aging animals ameliorates the decline in neurogenesis observed with senescence (175). In line with these studies, Ames dwarf mice, which display increased hippocampal IGF-1 protein expression, live longer than normal animals and do not suffer from age-induced decline in cognitive function (176), revealing IGF-1 as a promising candidate in the regulation of conventional hippocampal neurogenesis.

1.8 Objectives

To study central insulin action and insulin resistance in the pathogenesis of type 2 diabetes mellitus in adult mice and to circumvent the problem of compensatory changes in the presence of insulin resistance during development, we opted for a time-controlled approach to gene inactivation. To this end, mice were generated with an inducible whole body insulin receptor deficiency and an inducible insulin receptor knockout restricted to peripheral tissues of adult mice. The comparison of the phenotypes of both models allows the observation of consequences of acutely induced insulin resistance for the first time in adult mice and serves as a model for discerning the effects of peripheral versus whole body insulin resistance in the adult mouse.

An additional aim of the current project was to address the contribution of the insulin-like growth factor 1 receptor signaling in the regulation of energy homeostasis and peripheral glucose metabolism, neuronal survival and learning and memory formation by generating and analyzing mice with a neuron-specific inactivation of the IGF-1 receptor gene by conditional mutagenesis.

2 Material and Methods

2.1 Chemicals

Size markers for agarose gel electrophoresis (Gene Ruler DNA Ladder Mix) and for SDS-PAGE (Prestained Protein Ladder Mix) were obtained from MBI Fermentas, St. Leon-Rot, Germany. RedTaq DNA Polymerase and 10 x RedTaq buffer were purchased from Sigma-Aldrich, Seelze, Germany.

Chemical	Supplier
α -[³² P]-dCTP	Amersham, Freiburg, Germany
ϵ -aminocaproic acid	Sigma-Aldrich, Seelze, Germany
2-Deoxy-D-[1- ¹⁴ C]-Glucose	Amersham, Freiburg, Germany
Acetone	KMF Laborchemie, Lohmar, Germany
Acrylamide	Roth, Karlsruhe, Germany
Agarose (Ultra Pure)	Invitrogen, Karlsruhe, Germany
Amyloglucosidase	Roche, Mannheim, Germany
Aprotinin	Sigma-Aldrich, Seelze, Germany
Benzamidine	Sigma-Aldrich, Seelze, Germany
β -Mercaptoethanol (β -ME)	AppliChem, Darmstadt, Germany
Bovine serum albumin (BSA)	Sigma-Aldrich, Seelze, Germany
Bradford reagent	Bio-Rad, Munich, Germany
Bromphenol blue	Merck, Darmstadt, Germany
Chloroform	Merck, Darmstadt, Germany
D-[3- ³ H]-Glucose	Amersham, Freiburg, Germany
Desoxy-Ribonucleotid-Triphosphates (dNTPs)	Amersham, Freiburg, Germany
Dextran sulfate	AppliChem, Darmstadt, Germany
Dimethylsulfoxide (DMSO)	Merck, Darmstadt, Germany
Dithiothreitol (DTT)	Boehringer, Mannheim, Germany
Doxycycline Hyclate	Sigma-Aldrich, Seelze, Germany
Enhanced Chemiluminescence (ECL) Kit	Perbio Science, Bonn, Germany
Ethanol, absolute	AppliChem, Darmstadt, Germany
Ethidium bromide	Sigma-Aldrich, Seelze, Germany
Ethylendiamine tetraacetate (EDTA)	AppliChem, Darmstadt, Germany
Fetal Calf Serum (FCS)	Gibco BRL, Eggenstein, Germany

Materials and Methods

Ganciclovir	Sigma-Aldrich, Seelze, Germany
Gelatine	Sigma-Aldrich, Seelze, Germany
Geneticin (G418)	Gibco BRL, Eggenstein, Germany
Glacial acetic acid	Roth, Karlsruhe, Germany
Glucose	DeltaSelect, Pfullingen, Germany
Glycerol	Serva, Heidelberg, Germany
Hydrochloric acid (37 %)	KMF Laborchemie, Lohmar, Germany
Insulin	Novo Nordisk, Bagsværd, Denmark
Isopropanol	Roth, Karlsruhe, Germany
Ladderman TM DNA Labeling Kit	Cambrex Bio Science, Verviers, Belgium
Leptin	Sigma-Aldrich, Seelze, Germany
Methanol	Roth, Karlsruhe, Germany
Non-essential amino acids	Gibco BRL, Eggenstein, Germany
Penicillin/Streptomycin Solution	Gibco BRL, Eggenstein, Germany
Phenol-Chloroform-Isoamyl alcohol	AppliChem, Darmstadt, Germany
Phenylmethylsulfonylfluoride (PMSF)	Sigma-Aldrich, Seelze, Germany
Phosphate buffered saline (PBS)	Gibco BRL, Eggenstein, Germany
Potassium hydroxide	Merck, Darmstadt, Germany
Proteinase K	Roche, Mannheim, Germany
RPMI 1640 w/out phenol red	Gibco BRL, Eggenstein, Germany
Salmon sperm DNA	Sigma-Aldrich, Seelze, Germany
Sodium acetate	AppliChem, Darmstadt, Germany
Sodium chloride	AppliChem, Darmstadt, Germany
Sodium dodecyl sulfate	AppliChem, Darmstadt, Germany
Sodium hydroxide	AppliChem, Darmstadt, Germany
Sodium fluoride	Merck, Darmstadt, Germany
Sodium orthovanadate	Sigma-Aldrich, Seelze, Germany
Sodium pyruvate	Gibco BRL, Eggenstein, Germany
Sucrose	AppliChem, Darmstadt, Germany
Tamoxifen	Sigma-Aldrich, Seelze, Germany
Tetramethylethylenediamine	Sigma-Aldrich, Seelze, Germany
Avertin	Sigma-Aldrich, Seelze, Germany
Trishydroxymethylaminomethane (Tris)	AppliChem, Darmstadt, Germany
Triton X-100	Appllichem, Darmstadt, Germany
Tween 20	Appllichem, Darmstadt, Germany

Table 2: Chemicals

2.2 Molecular Biology

Standard methods of molecular biology were performed according to Sambrook and Russell (177), unless stated otherwise.

2.2.1 Isolation of Genomic DNA

Mouse tail biopsies were incubated 1 hour (h) in lysis buffer (100 mM Tris-HCl (pH 8.5), 5 mM EDTA, 0.2% (w/v) SDS, 0.2 M NaCl, 500 mg/ml proteinase K) in a thermomixer (Eppendorf, Hamburg, Germany) at 56°C. Embryonic stem (ES) cells were incubated in lysis buffer at 60°C over night. DNA was then precipitated from the solution by adding an equivalent of isopropanol. After centrifugation, the DNA pellet was dried at 60°C for 10 minutes and resuspended in doubly distilled water (ddH₂O).

For Southern blot analysis, 100 mg of murine tissue DNA were digested in lysis buffer containing 1 g/ml of proteinase K over night in a thermomixer at 56°C. Samples were centrifuged to discard debris and an equal volume of phenol-chloroform-isoamyl alcohol mixture ((v/v/v) 25:24:1, saturated with 100 mM Tris (pH 8.0)) was added to the supernatant. Following centrifugation, the aqueous phase was transferred to a fresh vial and mixed with an equivalent of chloroform. After centrifugation, DNA was precipitated from the supernatant as described above and resuspended in TE buffer (10 mM Tris-HCl (pH 8), 1 mM EDTA) containing 50 µg/ml RNaseI.

2.2.2 Quantification of Nucleic Acids

DNA and RNA concentrations were assessed by measuring the sample absorption at 260 nm with a NanoDrop[®] ND-1000 UV-Vis Spectrophotometer (Peqlab, Erlangen, Germany). An optical density of 1 corresponds to approximately 50 µg/ml of double-stranded DNA and to 38 µg/ml of RNA.

2.2.3 Polymerase Chain Reaction (PCR)

The PCR method (178, 179) was used to genotype mice for the presence of floxed alleles or transgenes with customized primers listed in Table 3. Reactions were performed in a Thermocycler iCycler PCR machine (Bio-Rad, Munich, Germany) or in a Peltier Thermal Cycler PTC-200 (MJ Research, Waltham, USA). All amplifications were performed in a total reaction volume of 25 μ l, containing a minimum of 50 ng template DNA, 25 pmol of each primer, 25 μ M dNTP Mix, 10 x RedTaq reaction buffer and 1 unit of RedTaq DNA Polymerase. Standard PCR programs started with 4 minutes (min) denaturation at 95°C, followed by 30 cycles consisting of denaturation at 95°C for 45 seconds (sec), annealing at oligonucleotide-specific temperatures for 30 sec and elongation at 72°C for 30 sec and a final elongation step at 72°C for 7 min.

Primer	Sequence (5'-3')	T _{Annealing} [°C]	Orientation
<i>Cre5'</i>	ACCTGAAGATGTTTCGCGATTATCT	57	sense
<i>Cre3'</i>	ACCGTCAGTACGTGAGATATCTT	57	antisense
<i>IR5'</i>	GATGTGCACCCCATGTCTG	58	sense
<i>IR3'</i>	CTGAATAGCTGAGACCACAG	58	antisense
<i>shRNA5'</i>	CCATGGAATTCGAACGCTGACGTC	60	sense
<i>shRNA3'</i>	TATGGGCTATGAACTAATGACCC	60	antisense
<i>IGF1R5'</i>	TCC CTC AGG CTT CAT CCG CAA	59	sense
<i>IGF1R3'</i>	CTT CAG CTT TGC AGG TGC ACG	59	antisense

Table 3: Oligonucleotides used for genotyping.

All primer sequences are displayed in 5'-3' order. Primer orientation is designated "sense" when coinciding with transcriptional direction. All primers were purchased from Eurogentec, Cologne, Germany.

PCR-amplified DNA fragments were applied to 1% - 3% (w/v) agarose gels (1 x TAE, 0.5 mg/ml ethidium bromide) and electrophoresed at 120 V.

2.2.4 Southern Blot Analysis

10 μ g of phenol-chloroform-extracted DNA were digested over night at 37°C with 50 U of either NcoI or BamHI restriction enzyme (MBI Fermentas GmbH, St. Leon-Rot, Germany) and separated electrophoretically on a 0.8% agarose gel at 60 V.

The DNA was subsequently transferred to a HybondTM-N+ nylon membrane (Amersham, Braunschweig, Germany) by an alkaline capillary transfer (180) and crosslinked to the membrane by baking at 80°C for 20 min. A probe was PCR-amplified using customized primers (Table 4) and labelled with [³²P]-dCTP using the LaddermanTM DNA Labeling Kit (TaKaRa; Cambrex Bio Science, Verviers, Belgium). Membranes were equilibrated in 2 x SSC and then prehybridized at 65°C over 4 h in hybridization solution (1 M NaCl, 1% (w/v) SDS, 10% (w/v) dextran sulfate, 50 mM Tris-HCl (pH 7.5), 250 µg/ml sonicated salmon sperm DNA). The radioactively labeled probe was then added to the prehybridization solution. Hybridization of the probe to its corresponding sequence on the nylon membrane was performed over night at 68°C in a rotating cylinder. Unspecifically bound probe was removed by washing the membrane initially with 2 x SSC / 0.1 % (w/v) SDS, followed by 1 x SSC / 0.1% (w/v) SDS, if necessary. All washes were performed at 68°C under gentle shaking for 10-20 min. After each wash, the membrane was monitored with a Geiger counter and the washes were stopped when radioactivity reached 50 to 200 cps. The membrane was then sealed in a plastic bag and exposed to X-ray film (Kodak XAR-5 or BioMAX MS; Eastman Kodak) at -80°C. Films were developed in an automatic developer (Agfa, Cologne, Germany).

Probe	Primer	Sequence (5'-3')	Orientation
IR	<i>NcoI</i> 5'	CCATGGGTCCATAAGCTATC	sense
IR	<i>NcoI</i> 3'	AGTGATGAGATGGCTCATTAG	antisense
IGF-1R	<i>BamHI</i> 5'	ACTTTGTGAGTTGAGCCACAG	sense
IGF-1R	<i>BamHI</i> 3'	ACATTATGTTTGCCTGGGAA	antisense

Table 4: Oligonucleotides used to amplify the Southern blot probes.

All primer sequences are displayed in 5'-3' order. Primer orientation is designated "sense" when coinciding with transcriptional direction. All primers were purchased from Eurogentec, Cologne, Germany.

2.2.5 RNA Extraction, RT PCR and Quantitative Realtime PCR

Total hepatic RNA was extracted using the Qiagen RNeasy Kit (Qiagen, Hilden, Germany). 200 ng of each RNA sample were reversely transcribed using the Eurogentec RT Kit (Eurogentec, Cologne, Germany) according to manufacturer's protocols. The

cDNA was subsequently amplified using TaqMan Principles ABI Prism 7700 Sequence Detection System (Applied Biosystems, Foster City, USA). Relative expression of ObRb and IL-6 mRNA was determined using standard curves based on hepatic cDNA. Relative expression of LPL mRNA was determined using standard curves based on white adipose tissue cDNA. Samples were adjusted for total RNA content by Glucuronidase beta (Gusb) and hypoxanthine guanine phosphoribosyl transferase (Hprt-1) RNA quantitative Realtime-PCR. Calculations were performed by a comparative method ($2^{-\delta\delta CT}$).

Probe	Catalogue N°
Gusb	Mm00446953_m1
Hprt-1	Mm00446968_m1
ObRb	Mm01265583_m1
IL-6	Mm00446190_m1
LPL	Mm00434764_m1

Table 5: Probes used for Realtime PCR.

All probes were purchased from Applied Biosystems, Foster City, USA.

2.2.6 ELISA

Mouse serum insulin (Mouse/Rat Insulin ELISA; Crystal Chem, Downers Grove, IL, USA), leptin (ACTIVE[®] Murine Leptin ELISA; Diagnostics Systems Laboratories, Webster, TX, USA) and adiponectin (Quantikine Mouse Adiponectin/Acrp30 ELISA; R&D Systems, Wiesbaden, Germany) concentrations were determined using mouse standards according to manufacturer's guidelines and measured on a Precision Microplate Reader (Emax; Molecular Devices GmbH, Munich, Germany).

2.3 Cell Biology

2.3.1 Gene Targeting and Generation of IGF-1R^{ΔSyn} Mice

A targeting vector was constructed as previously described (181) by inserting a 600 bp sequence containing exon 3 of the murine IGF-1 receptor gene into the gene replacement vector pEasyfloxGK12 (Artemis Pharmaceuticals, Cologne, Germany). A 4.5 kbp sequence homologous to the target gene sequence upstream of exon 3 and a 1.3 kbp gene sequence homologous to the downstream region of exon 3 were inserted to be used as long and short arm of homology, respectively. The vector was purified by agarose gel electrophoresis following NotI digestion to remove plasmid sequences prior to electroporation.

Gene targeting was performed in Bruce4 ES cells (182). Culturing and transfection of ES cells was performed according to previously described protocols (181). For transfection, 1×10^7 ES cells were transfected with 40 μ g DNA as previously described (133). 48 hours after transfection, ES cells were placed under selection with the neomycin-analog G418 (180 μ g/ml, 71% active). G418 inhibits the 80S ribosome, thereby blocking protein synthesis. Integration of the neomycin resistance gene (*neo*^r) into the genome via recombination enables the ES cells to grow in G418-containing medium. To select against randomly integrated gene constructs that still contain the thymidine kinase cassette of the *Herpes simplex* virus (*HSV-tk*), the medium was supplemented with 2 mM ganciclovir 5 days after transfection. The *HSV-tk* gene lies 3' of the short homology arm of the gene targeting vector and thus outside of the recombination region. Hence, it is only integrated into the genome upon non-homologous recombination (183). *HSV-tk* phosphorylates ganciclovir, thereby converting it to a triphosphate which is inserted into the DNA instead of guanine, resulting in the disruption of DNA replication. Approximately 9 days after transfection, G418/Ganciclovir double-resistant colonies were picked and expanded on 96-well tissue culture dishes. Genomic DNA was extracted from each clone and analysed by Southern blot and PCR analysis. Recovery, microinjection and transfer of 3.5 day-old embryos were performed according to standard procedures. Chimeric animals (80-90% chimerism based on coat color) were bred with FlpE deleter on a pure C57BL/6 background.

2.3.2 Histological Analysis and Immunohistochemistry

Pancreatic tissue of IR^{Aper} and IR^{Awb} mice was excised and snap-frozen in Jung Tissue Freezing Medium[®] (Leica Microsystems Nussloch GmbH, Nussloch, Germany), transferred to a cryostat (Leica Microsystems Nussloch GmbH, Nussloch, Germany) and cut into 7 μ m thin sections. Specimens were collected on clean poly-L-lysine-coated glass slides (Menzel GmbH, Braunschweig, Germany), dried at room temperature overnight and then stained using hematoxylin and eosin (H&E) for general histology. H&E (Sigma-Aldrich, Seelze, Germany) staining was performed according to standard protocols. Pancreatic tissues were also stained for insulin (DakoCytomation, Hamburg, Germany) and glucagon (DakoCytomation, Hamburg, Germany) using a 1:20 and 1:75 dilution, respectively. Slides had been previously fixed in acetone at 4°C for 10 min and air-dried. Both stainings were incubated with a secondary antibody consisting of a 1:100 dilution of horseradish peroxidase-coupled anti-rabbit IgG (Vector Laboratories/Linaris GmbH, Wertheim-Bettingen, Germany). Tissues were counterstained 2 minutes with Mayers Hematoxylin then washed in tepid water for 5 minutes. Stainings were analyzed with a Zeiss Axioskop 40 microscope (Carl Zeiss MicroImaging GmbH, Cologne, Germany) and β cell mass was determined using the microscopy software AxioVision (Carl Zeiss MicroImaging GmbH, Cologne, Germany).

White adipose tissue of C57BL/6 mice was dissected, fixed overnight in 7% formaldehyde and then embedded for paraffin sections. Subsequently, 7 μ m thin sections were deparaffinized and stained with H&E for general histology.

For staining against IGF-1 receptor and β -galactosidase, IGF-1R ^{Δ Syn} mice were bred with RosaArte1 reporter mice (100). IGF-1R ^{Δ Syn}-LacZ and wildtype reporter (SynCre-LacZ) mice were anesthetized and transcardially perfused with 0.9% saline solution. Brains were then excised and frozen in tissue freezing medium. 7 μ m cryostat sections were stained with a 1:50 dilution of IGF-1R α (Upstate, Billerica, USA) and a 1:200 dilution of β -galactosidase antibody (Cappel, Cochranville, USA). The IGF-1R staining was subsequently incubated with 1:500 dilution of a FITC-labeled goat anti-chicken secondary antibody (Invitrogen, Karlsruhe, Germany). β -galactosidase stainings were stained with a 1:200 dilution of a multifluorescent anti-rabbit IgG (Mabtec GmbH, Göttingen, Germany). Slides were analyzed and photographed using a Zeiss Axioskop 40 microscope.

2.4 Biochemistry

2.4.1 Protein Extraction

Snap-frozen tissues were thawed and homogenized in lysis buffer (50 mM HEPES (pH 7.4), 1% Triton X-100, 0.1 M sodium fluoride, 10 mM EDTA, 50 mM sodium chloride, 10 mM sodium orthovanadate, 0,1% SDS, 10 µg/ml Aprotinin, 2 mM Benzamidine, 2 mM PMSF) using a polytron homogenizer (IKA Werke, Staufen, Germany). Particulate matter was removed by centrifugation for 1 h at 4°C. The supernatant was transferred to a fresh vial and protein concentrations were determined using a Bradford assay. Protein extracts were diluted to 1 mg/ml with lysis buffer and 4 x SDS sample buffer (125 mM Tris-HCl (pH 6.8), 5% SDS, 43.5% glycerol, 100 mM DTT, and 0.02% bromphenol blue), incubated at 95°C over 5 min and stored at -80°C.

2.4.2 Western Blot Analysis

Frozen protein extracts were thawed at 95°C for 5 min, then separated on 8-10% (v/v) SDS polyacrylamide gels (184) and blotted onto PVDF membranes (Bio-Rad, Munich, Germany). Membranes were then incubated with 1% blocking reagent (Roche, Mannheim, Germany) for 1 h at RT or over night at 4°C. Subsequently, primary antibodies (Table 6) diluted in 0.5% blocking solution were applied for 1 h at RT or over night at 4°C. PVDF membranes were then washed twice for 10 min with 1 x TBS/Tween and incubated twice for 10 min with 0.5% blocking solution. After 1 h incubation at RT with the respective secondary antibodies, membranes were washed 4 times for 5 min with 1 x TBS/Tween, incubated for 1 min in Pierce ECL Western Blotting Substrate (Perbio Science, Bonn, Germany), sealed in a plastic bag and exposed to chemiluminescence film (Amersham, Braunschweig, Germany) at -80°C. Films were developed in an automatic developer.

Antibody	Catalogue N°	Distributor	Dilution
Akt	#9272	Cell Signaling, Danvers, MA, USA	1:1000
pAkt (Ser473)	#9271	Cell Signaling, Danvers, MA, USA	1:1000
IRβ (C-19)	sc-711	Santa Cruz, Heidelberg, Germany	1:200
ObR (M-18)	sc-1834	Santa Cruz, Heidelberg, Germany	1:400

Stat-3 (C-20)	sc-482	Santa Cruz, Heidelberg, Germany	1:400
pStat-3 (B7)	sc-8059	Santa Cruz, Heidelberg, Germany	1:200
IGF-1R β	#3027	Cell Signaling, Danvers, MA, USA	1:200
Actin	A5441	Sigma Aldrich, Seelze, Germany	1:2000

Table 6: Primary antibodies used for Western blot analysis.

All respective secondary antibodies were purchased from Sigma Aldrich, Seelze, Germany, and used in a 1:1000 dilution.

2.5 Mouse Experiments

General animal handling was performed as described by Hogan (185) and Silver (186).

2.5.1 Animals

Mice were housed in a virus-free facility at 22-24°C on a 12 h light/ 12 h dark cycle with the light on at 6 a.m. and were fed standard rodent chow (Teklad Global Rodent 2018; Harlan Winkelmann GmbH, Borcheln, Germany) containing 53.5% carbohydrates, 18.5% protein and 5.5% fat. All animals had access to water *ad libitum*. Food was only withdrawn if required for an experiment. At the end of the study period, animals were sacrificed by CO₂ anesthesia or cervical dislocation. All animal procedures and euthanasia were reviewed by the animal care committee of the University of Cologne, approved by local government authorities (Bezirksregierung Cologne) and were in accordance with National Institutes of Health guidelines.

2.5.1.1 IR ^{Δ per} mice

Mice homozygous for the loxP-flanked insulin receptor allele (IR^{flox/flox}) (133) were bred with mice heterozygous for the Rosa26CreER^{T2} transgene (100). Rosa26CreER^{T2+/-}IR^{flox/wt} mice were further crossed with IR^{flox/flox} mice to achieve homozygosity for the loxP-flanked allele. Breeding colonies were maintained by mating IR^{flox/flox} mice and Rosa26CreER^{T2+/-}IR^{flox/flox} mice (IR ^{Δ per}).

2.5.1.2 IR^{Δwb} mice

Breeding colonies were maintained for C57BL/6 mice and mice expressing an insulin receptor-specific shRNA from the *Rosa26* locus (120).

2.5.1.3 IGF-1R^{ΔSyn} mice

A correctly integrated homologous recombinant ES cell clone was injected into a CB-20 blastocyst and implanted into the uterus of a pseudopregnant mouse. Resulting chimeras were crossed with C57BL/6 mice. IGF-1R^{flox/wt} mice, which had received the mutation by germline transmission, were crossed with FlpE deleter mice to insure deletion of the selection marker cassette. Intercrosses of IGF-1R^{flox/wt} mice yielded mice homozygous for the recombinant locus IGF-1R^{flox/flox}. IGF-1R^{flox/flox} were crossed with mice expressing the Cre recombinase under the control of the rat Synapsin-1 promoter (187) to delete the IGF-1 receptor specifically in neurons.

2.5.2 Experimental Setup

2.5.2.1 Tamoxifen administration

An aliquot of 50 mg tamoxifen-free base (Sigma Aldrich, Seelze, Germany) was suspended in 50 μl ethanol and dissolved in 500 μl peanut oil (Sigma Aldrich, Seelze, Germany). This 5 mg/50 μl tamoxifen solution was sonicated for 1 minute and then stored at -20°C. On five consecutive days at the age of 9-12 weeks, the tamoxifen solution was thawed at 60°C and administered to IR^{Δper} mice by oral gavage using a 22 gauge feeding needle (Fine Science Tools, Heidelberg, Germany).

2.5.2.2 Doxycycline administration

At 10-13 weeks of age, IR^{Δwb} mice were administered drinking water supplemented with 10% sucrose and 2 mg/ml doxycycline hyclate over a period of 30 days to induce shRNA-expression under control of the H1/U6 promoter. Doxycycline-supplemented water was changed every 2-3 days.

2.5.3 Body Weight and Blood Glucose Levels

Body weight and blood glucose levels were monitored daily. Blood glucose values were determined from whole venous blood using an automatic glucose monitor (GlucoMen[®] GlycÓ; A. Menarini Diagnostics, Neuss, Germany).

2.5.4 Food Intake

Food Intake was measured over a period of 30 days and daily food intake was calculated as the average intake of chow over the time stated.

2.5.5 Glucose and Insulin Tolerance Test

Glucose tolerance tests (GTT) were performed on animals that had been fasted over night for 16 hours. Insulin tolerance test (ITT) was performed on random fed mice. Animals were injected with either 2 g/kg body weight of glucose or 0.75 U/kg body weight of human regular insulin into the peritoneal cavity. Glucose levels were determined in blood collected from the tail tip immediately before and 15, 30 and 60 minutes after the injection, with an additional value determined after 120 minutes for the GTT.

2.5.6 Glucose-stimulated Insulin Secretion

All animals were fasted over night for 16 hours. Blood samples were collected from mice prior to an intravenous injection of 2g/kg body weight of glucose. Further blood samples were amassed 2, 5, 15, 30 and 60 min after the injection and serum insulin levels were determined.

2.5.7 Insulin Signaling

Mice were anesthetized by intraperitoneal (i.p.) injection of avertin and adequacy of the anesthesia was ensured by loss of pedal reflexes. The abdominal cavity of the mice was opened and 125 µl samples containing 5 units regular human insulin diluted in 0.9% saline were injected into the *Vena cava inferior*. Sham injections were performed with 125 µl of 0.9% saline. Samples of liver tissue and skeletal muscle tissue

were harvested two and five minutes after injection, respectively. Proteins were extracted from tissues for Western blot analysis.

2.5.8 Intracerebroventricular Insulin Infusion

For intracerebroventricular (icv) cannula implantation, 11-week old male C57BL/6 mice were anesthetized as previously described and placed in a stereotactic device (Stoelting, Foehr Medical Instruments GmbH, Seeheim, Germany). A sterile osmotic pump connector cannula (Alzet[®] Brain Infusion Kit 3, Charles River, Sulzfeld, Germany) was implanted into the left lateral brain ventricle (-0.2 mm anterior, 1.0 mm lateral relative to Bregma, 2.3 mm below the surface of the skull). The pedestal of the cannula was attached to the skull with super glue. The cannula was connected to an Alzet[®] mini-osmotic pump (Model 1002; Charles River, Sulzfeld, Germany), which secreted 200 μ U insulin per day over a period of 7 days. After 7 days, animals were sacrificed and correct positioning of the icv cannula was verified in each animal by injection of 1% methylene blue. White adipose tissue mass was removed, weighed and processed for histological analysis and RNA extraction as described.

2.5.9 Leptin Restoration

16 days after start of administration of doxycycline-supplemented water, 5 IR^{Δwb} mice and 5 respective controls were anesthetized by i.p. avertin injection and subcutaneously implanted Alzet[®] mini-osmotic pumps (Model 2001; Charles River, Sulzfeld, Germany), which secrete 0.5 μ g leptin per μ l per h over a period of 7 days. Food intake, body weight and blood glucose were measured daily over the entire period of the experiment, starting two days prior to pump implant. Serum blood samples were taken 2, 4 and 7 days after the operation to monitor leptin levels. 7 days after pump implant, mice were sacrificed and hepatic Stat-3 phosphorylation was assessed by Western blot analysis.

2.5.10 Kainic Acid-induced Seizures

To evaluate potential neurotoxicity caused by kainic acid, 16-week-old IGF-1R^{ΔSyn} mice and littermate controls received an i.p. injection of 30 mg/kg kainic acid

(KA; Sigma Aldrich, Seelze, Germany) before noon, in order to minimize interactions with circadian patterns of endogenous substances such as hormones and neurotransmitters. KA-induced seizures were scored for 2 h post-injection based on the following criteria: 0 = no abnormality; 1 = mice become motionless; 2 = forelimb and/or tail extension (appearance of rigid posture); 3 = myoclonic jerks of head and neck, w/ brief twitching movements, or repetitive movements w/ head bobbing or "wet-dog-shakes"; 4 = forelimb clonus and partial rearing or rearing and falling; 5 = forelimb clonus, continuous rearing and falling; 6 = generalized tonic-clonic activity w/ loss of postural tone, often resulting in death. Time of seizure initiation was measured from time of KA injection to more than or equal to stage 3. In addition, maximum seizure intensity and seizure scores at various time points were analyzed. 3 days after KA injection, mice were anesthetized with avertin and perfused intracardially with saline. Brains were removed and cut into 7 μm thin sections that were subjected to Nissl staining with 0.1% cresyl violet (Sigma Aldrich, Seelze, Germany) for assessment of neuronal damage. Slides were analyzed and photographed using a Zeiss Axioskop 40 microscope.

2.5.11 Analysis of Body Composition

Nuclear magnetic resonance (NMR) was employed to determine whole body composition of live animals using the NMR Analyzer minispec mq7.5 (Bruker Optik, Ettlingen, Germany). Radiofrequency (RF) pulse sequences are transmitted into the tissue. In response, RF signals are generated by the hydrogen in the tissue, which are detected by the minispec. The amplitude and duration of these signals are related to properties of the material.

2.5.12 Behavioral Analysis

2.5.12.1 Morris Water Maze

This test was performed according to standard procedures (188) with minor modifications previously described (189, 190). In summary, after a 1 day habituation trial (day 0), in which preferences of IGF-1R ^{Δ Syn} mice and littermate controls for a specific quadrant were ruled out, the animals learned to find a hidden platform over the following 6 days, performing 4 trials per day, each trial lasting 60 seconds plus 20

seconds on the platform. If an animal failed to reach the platform, it was placed on it after 60 seconds. On the 7th day, the animals were subjected to an extinction trial, in which the platform had been removed to assess preference for the platform quadrant.

2.5.12.2 Rotarod

Motor coordination of IGF-1R^{ΔSyn} mice and littermate controls was determined by placing the animals in a rotarod apparatus with constant acceleration in 6 consecutive trials of 5 minutes each (191). The apparatus consisted of a horizontal motor-driven rotating rod in which the animals were placed perpendicular to the long axis of the rod, with the head directed against the direction of rotation so that the mouse has to progress forward to avoid falling. Animals were familiarized with the procedure under constant rod speed 1 day earlier. The trial was stopped when the animal fell down or after a maximum of 5 min. The time spent in the rotating rod was recorded for each animal and trial.

2.5.12.3 Elevated Plus-Maze

IGF-1R^{ΔSyn} mice and littermate controls were exposed to an elevated plus-maze, consisting of two open and two enclosed arms, to study anxiety-like behavior (192, 193). Each rat was placed on the central platform facing a closed arm, and allowed to freely explore the maze for 5 min. Exploration was recorded through an automated tracking system. Percentage of time spent exploring the open arms were calculated as an index of anxiety-like behavior.

2.5.12.4 Object Recognition

IGF-1R^{ΔSyn} mice and littermate controls were individually habituated to an open-field box for 3 days. During training sessions, two novel objects were placed into the open field and the animal was allowed to explore for 5 min. The time spent exploring each object was recorded. During retention tests, the animals were placed back into the same box, in which one of the familiar objects used during training was replaced by a novel object, and allowed to explore freely for 5 min. A preference index was determined from the amount of time spent exploring the novel object over the total time spent exploring both objects to measure visual recognition memory.

2.5.12.5 Activity Cage

Exploratory activity levels were determined using photocell detection, based on a computer-based system which registers an animal's horizontal and vertical movements within a plexiglas box equipped with ultrared beams. Activity was defined as the interruption of a photocell beam and the number of interruptions was recorded.

2.6 Computer Analysis

2.6.1 Densitometrical Analysis

Protein expression was assessed by Western blot analysis and bands were measured in intensity per mm² using the Quantity One Software (Bio-Rad, Munich, Germany). After background subtraction, each sample was normalized to an internal loading control. Average protein expression of control mice was set to 100% and compared to protein expression of knockout animals unless stated otherwise.

2.6.2 Statistical Methods

Data sets were analyzed for statistical significance using a two-tailed unpaired student's t test. All *p* values below 0.05 were considered significant.

3 Results

3.1 Inducible inactivation of the insulin receptor gene in peripheral tissues of adult mice

Mice homozygous for the loxP-flanked insulin receptor allele ($IR^{lox/lox}$) were crossed with mice expressing a Cre recombinase fused to the mutated ligand binding domain of the estrogen receptor from the ubiquitous Rosa26 locus ($Rosa26CreER^{T2}$) (Fig. 5). The Cre recombinase is inactive as long as it is retained in the cytoplasm by heatshock proteins. Administration of tamoxifen results in the detachment of the heatshock proteins, thereby uncovering a nuclear localization signal that leads to the nuclear import of the fusion protein. In the nucleus, Cre mediates recombination of all loxP-flanked alleles. When expressed from the Rosa26 locus, Cre-mediated recombination of loxP-flanked alleles occurs in all tissues except the central nervous system, due to a lower local concentration of tamoxifen in the brain (103, 194).

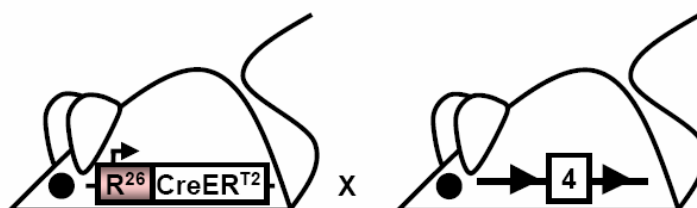


Fig. 5: General scheme of the inducible peripheral insulin receptor knockout mouse ($IR^{\Delta per}$).

Mice, expressing the $CreER^{T2}$ fusion protein under the control of the Rosa26 promoter ($Rosa26CreER^{T2}$) were crossed with mice homozygous for a loxP-flanked exon 4 of the insulin receptor allele ($IR^{lox/lox}$). Only one loxP-flanked allele is depicted here. Each loxP site is here and hereafter depicted as a triangle.

To inactivate the insulin receptor gene in peripheral tissues of adult mice in an inducible manner and to control for the metabolic effects of tamoxifen treatment, $IR^{\Delta per}$ and $IR^{lox/lox}$ $Rosa26CreER^{T2}$ -negative littermates ($Control^{\Delta per}$) were treated daily by oral administrations of 5 mg tamoxifen on 5 consecutive days. At various time points during and after the feeding period, tissues were removed from the animals and recombination of the loxP-flanked insulin receptor gene was assessed by Southern blot analysis (Fig. 6, Fig. 7). Just two days after the start of tamoxifen administration, partial recombination of the loxP-flanked insulin receptor gene was detectable in heart, skeletal muscle, liver, pancreas and white adipose tissue of $IR^{\Delta per}$ mice. Recombination was

almost complete on the first day after the last feeding (day 6) (Fig. 7). While deletion was variable in heart, ranging between 70 and 80%, more than 90% of the recombined loxP-flanked insulin receptor gene was detectable in skeletal muscle and liver. The most efficient recombination occurred in pancreas and white adipose tissue (Fig. 7), while, as expected, less than 15% recombination was found in the CNS.

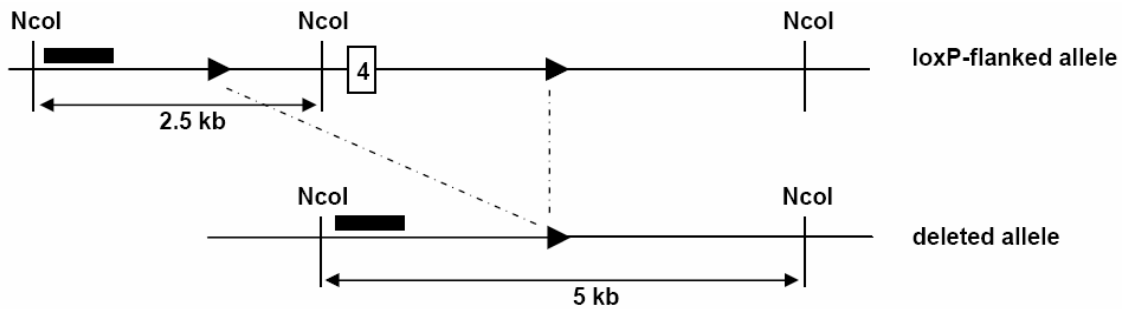


Fig. 6: Genomic map of the mouse insulin receptor locus surrounding exon 4.

Location of the probe used for Southern blot analysis is indicated by a black bar. NcoI = restriction enzyme sites, 4 = exon 4 of the insulin receptor gene, 2.5 kb = size of loxP-flanked allele band, 5 kb = size of deleted allele band.

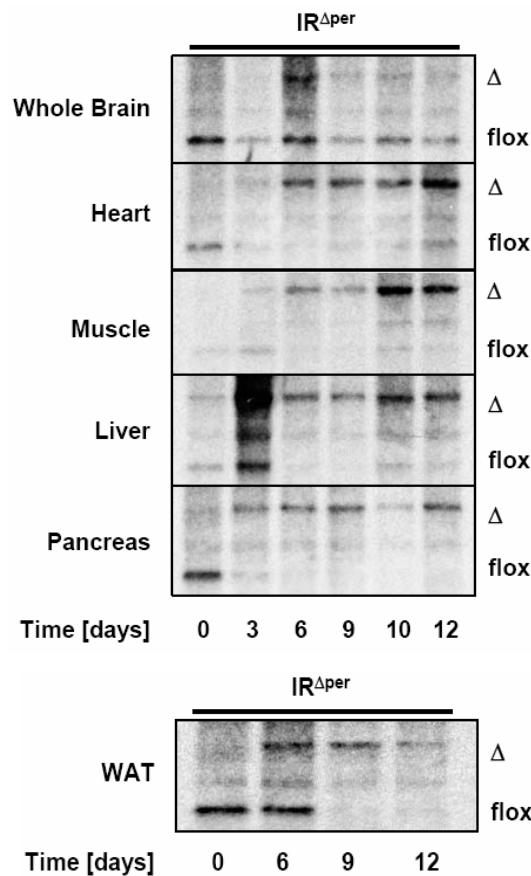
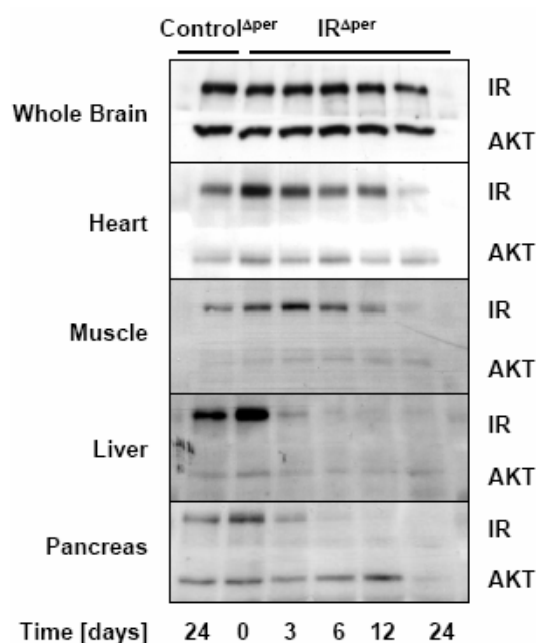


Fig. 7: Southern blot analysis of insulin receptor recombination.

Tissues analyzed were whole brain, heart, skeletal muscle, liver, pancreas and white adipose tissue (WAT) of IR^{Δper} mice over a period of 12 days. Mice were administered tamoxifen from day 1 until day 5. Δ = 5 kb band of the deleted allele, flox = 2.5 kb band of the loxP-flanked allele.

In conclusion, efficient tamoxifen-induced recombination of the loxP-flanked insulin receptor alleles in IR^{Δper} mice was achieved in metabolically relevant peripheral tissues such as heart, skeletal muscle, liver, pancreas and white adipose tissue without significant recombination occurring in the CNS.

To investigate the impact of Cre-mediated recombination on insulin receptor protein expression, Western blot analyses were performed on tissue lysates obtained from IR^{Δper} mice during and after tamoxifen treatment. As expected, the level of immunoreactive insulin receptor protein paralleled that of the loxP-flanked insulin receptor allele recombination (Fig. 8). Hence, while there was a visible decline of insulin receptor expression in heart and skeletal muscle over the course of 24 days after the beginning of tamoxifen administration, the maximum reduction of insulin receptor expression observed on day 30 was approximately 50% in the former and 90% in the latter, consistent with the presence of unrecombined loxP-flanked insulin receptor alleles in these tissues (Fig. 8). Similarly, insulin receptor protein expression was abolished in liver, pancreas and white adipose tissue of IR^{Δper} mice after completion of tamoxifen treatment (Fig. 9), whereas protein extracts prepared from whole brain revealed no alteration in immunodetectable insulin receptor protein (Fig. 8).



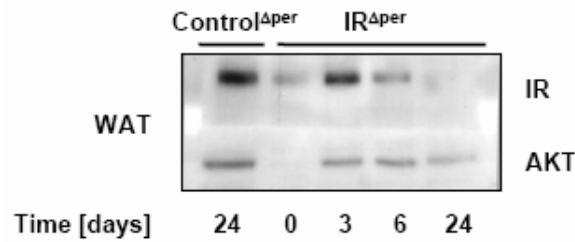
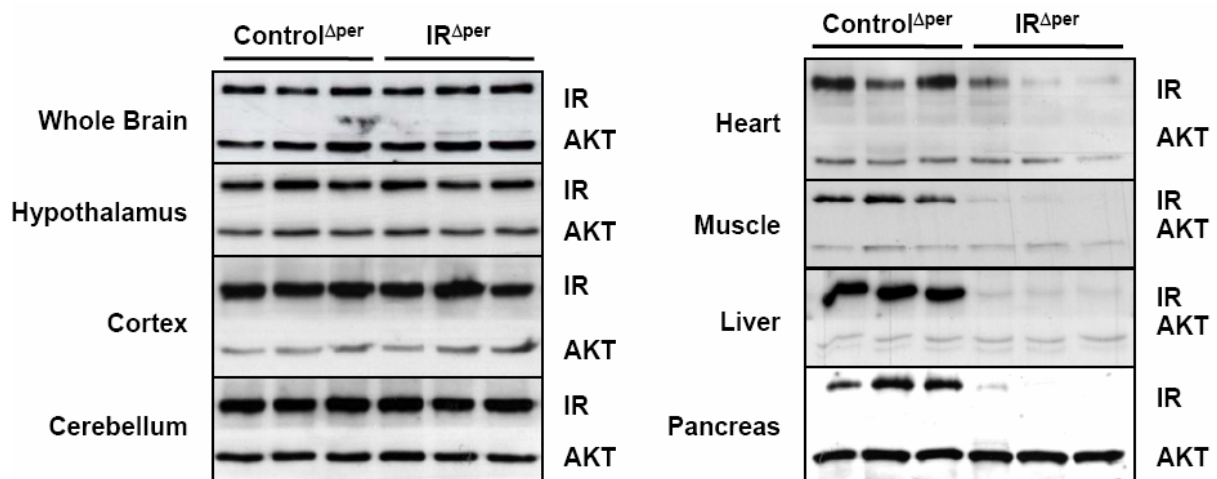


Fig. 8: Western blot analysis of insulin receptor expression.

Western blot analysis of insulin receptor (IR) and protein kinase B (AKT, loading control) expression. Proteins were extracted from whole brain, heart, skeletal muscle, liver, pancreas and WAT of tamoxifen-treated IR^{Δper} mice and Control^{Δper} mice over a period of 24 days. Tamoxifen administration lasted from day 1 until day 5.

To rule out the possibility that the modest amount of Cre-mediated recombination detectable in whole brain extracts of IR^{Δper} mice (Fig. 7) was due to complete recombination in a certain area of the brain rather than a modest degree of recombination throughout, individual brain regions were probed for immunodetectable insulin receptor protein. This analysis revealed unaltered insulin receptor expression in hypothalamus, cortex and cerebellum of tamoxifen-treated IR^{Δper} mice (Fig. 9). Thus, consistent with the pattern of DNA recombination, insulin receptor protein expression was efficiently reduced in peripheral tissues of IR^{Δper} mice without significant alterations in the CNS.



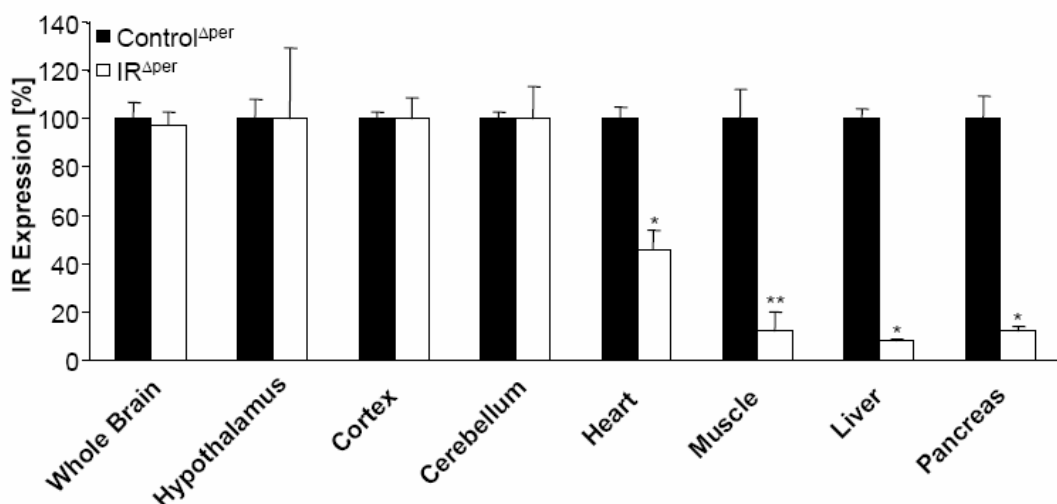


Fig. 9: Insulin receptor deficiency in peripheral organs of IR^{Aper} mice.

(A) Western blot analysis of insulin receptor (IR) and proteinkinase B (AKT, loading control) expression in whole brain, hypothalamus, cortex, cerebellum, heart, skeletal muscle, liver and pancreas of tamoxifen-treated Control^{Aper} and IR^{Aper} mice. Indicated tissues were dissected 25 days after the last day of tamoxifen administration. (B) Relative IR expression of Control^{Aper} (black bars) and IR^{Aper} mice (white bars) as assessed by Western blot analysis. Values are mean \pm SEM. * $P \leq 0.05$; ** $P \leq 0.01$ versus control.

Next, insulin's ability to activate signaling in skeletal muscle and liver of control and IR^{Aper} mice was assessed. Consistent with abrogated insulin action as a consequence of insulin receptor deficiency, insulin failed to activate phosphorylation of proteinkinase B (Akt) in skeletal muscle of IR^{Aper} mice following *in vivo* insulin stimulation (Fig. 10). Similarly, insulin-stimulated Akt phosphorylation was reduced by $\sim 80\%$ in liver of IR^{Aper} mice (Fig. 10).

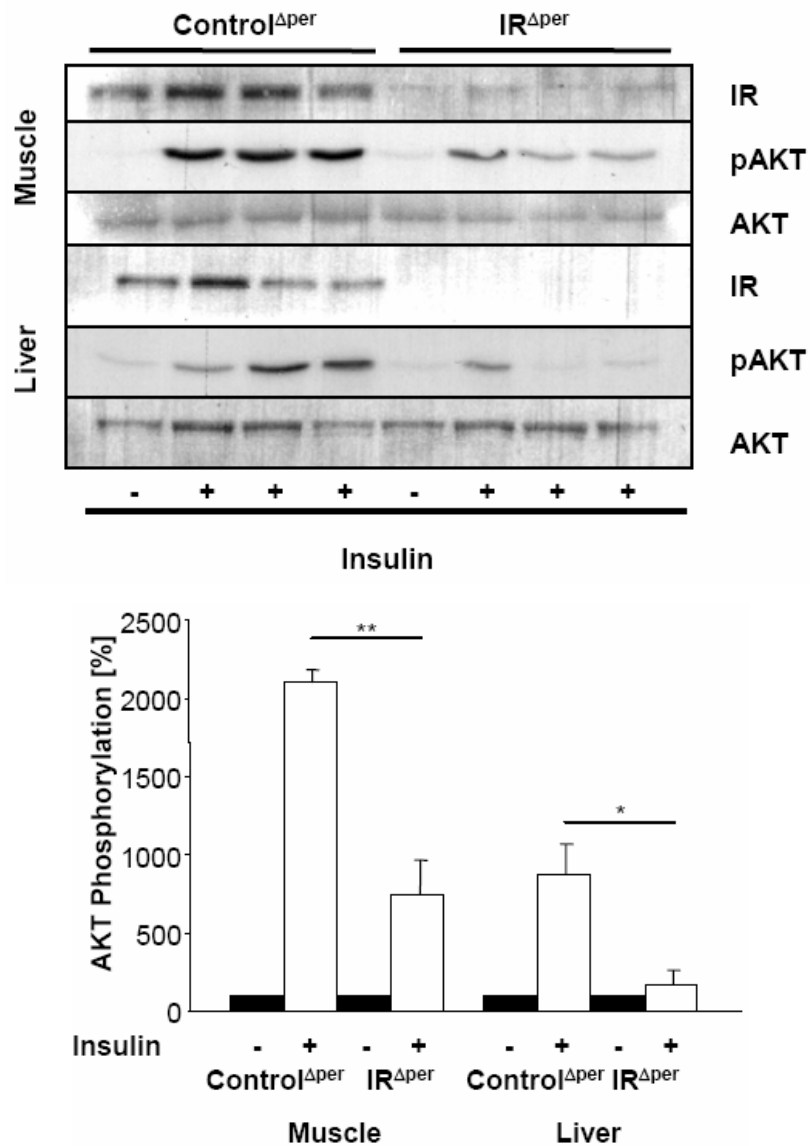


Fig. 10: Abrogated insulin signaling in peripheral organs of IR^{Δper} mice.

(A) Western blot analysis of IR, phosphorylated AKT (pAKT) and AKT (loading control) in skeletal muscle and liver of Control^{Δper} and IR^{Δper} mice after injection of either saline (-) or insulin (+) into the *Vena cava inferior*. (B) Relative phosphorylation of AKT in skeletal muscle and liver of Control^{Δper} and IR^{Δper} mice as assessed in (A). pAKT protein amount was normalized to AKT protein expression. pAKT expression of saline injected mice was set to 100%. Values are mean ± SEM. *P ≤ 0.05, **P ≤ 0.01 versus control. Black bars = saline; white bars = insulin.

3.2 Inducible inactivation of the insulin receptor in peripheral tissues and the central nervous system of adult mice

To investigate the relative contribution of insulin resistance in the CNS in an inducible fashion in addition to peripheral insulin resistance, a second mouse model was employed in which transcription of a small hairpin RNA (shRNA) is directed against the insulin receptor. This shRNA is under transcriptional control of the human H1/U6 promoter, which contains a tetracycline-operated sequence (tetO). In the presence of the tet repressor (tetR), transcription of the shRNA is silenced. Upon doxycycline administration, the tet repressor is sequestered from the promoter, thus allowing for ubiquitous transcription of the insulin receptor shRNA (Fig. 11) (120, 195).

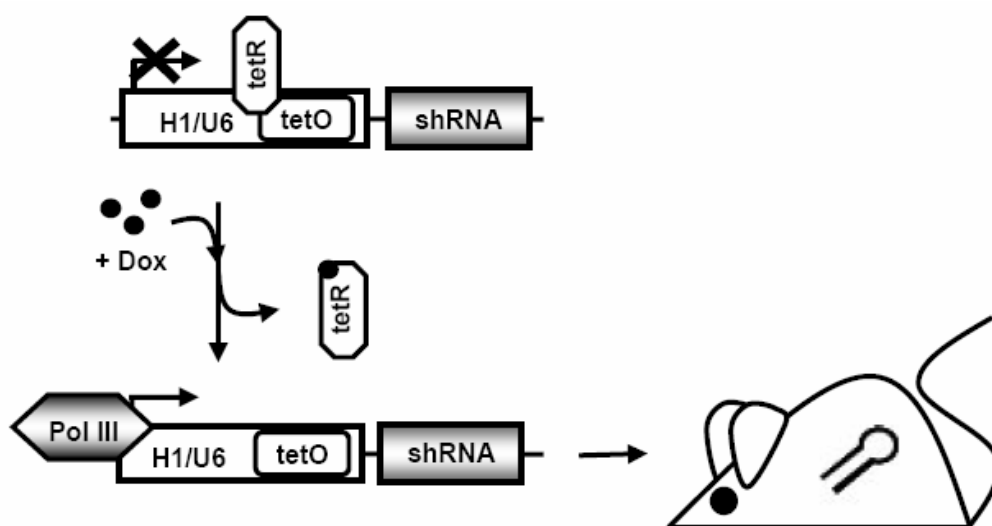


Fig. 11: General scheme of the inducible whole body insulin receptor knockout mouse ($IR^{\Delta wb}$).

Expression of an insulin receptor-specific short hairpin RNA (shRNA) is dependent on the RNA-Polymerase III (Pol III)-dependent promoters H1/U6, containing the operator sequences (tetO) of the *E. coli* tetracycline resistance operon. Binding of the tetracycline resistance operon repressor (tetR) to tetO prevents transcription. Doxycycline (Dox) sequesters tetR and enables the binding of Pol III to the H1/U6 promoter, which results in transcription of the shRNA. The shRNA is processed to a siRNA, which binds to its complementary mRNA sequence, leading to the degradation of the insulin receptor mRNA.

Adult mice carrying this transgene ($IR^{\Delta wb}$) and wildtype littermates ($Control^{\Delta wb}$) were given doxycycline-supplemented water for 30 days and expression of the insulin receptor was analyzed in various tissues. Upon doxycycline-mediated induction of shRNA transcription, there was a similar decrease in insulin receptor expression in

skeletal muscle and liver compared to $IR^{\Delta per}$ mice, but additionally there was a significant reduction of insulin receptor expression in the CNS (Fig. 12).

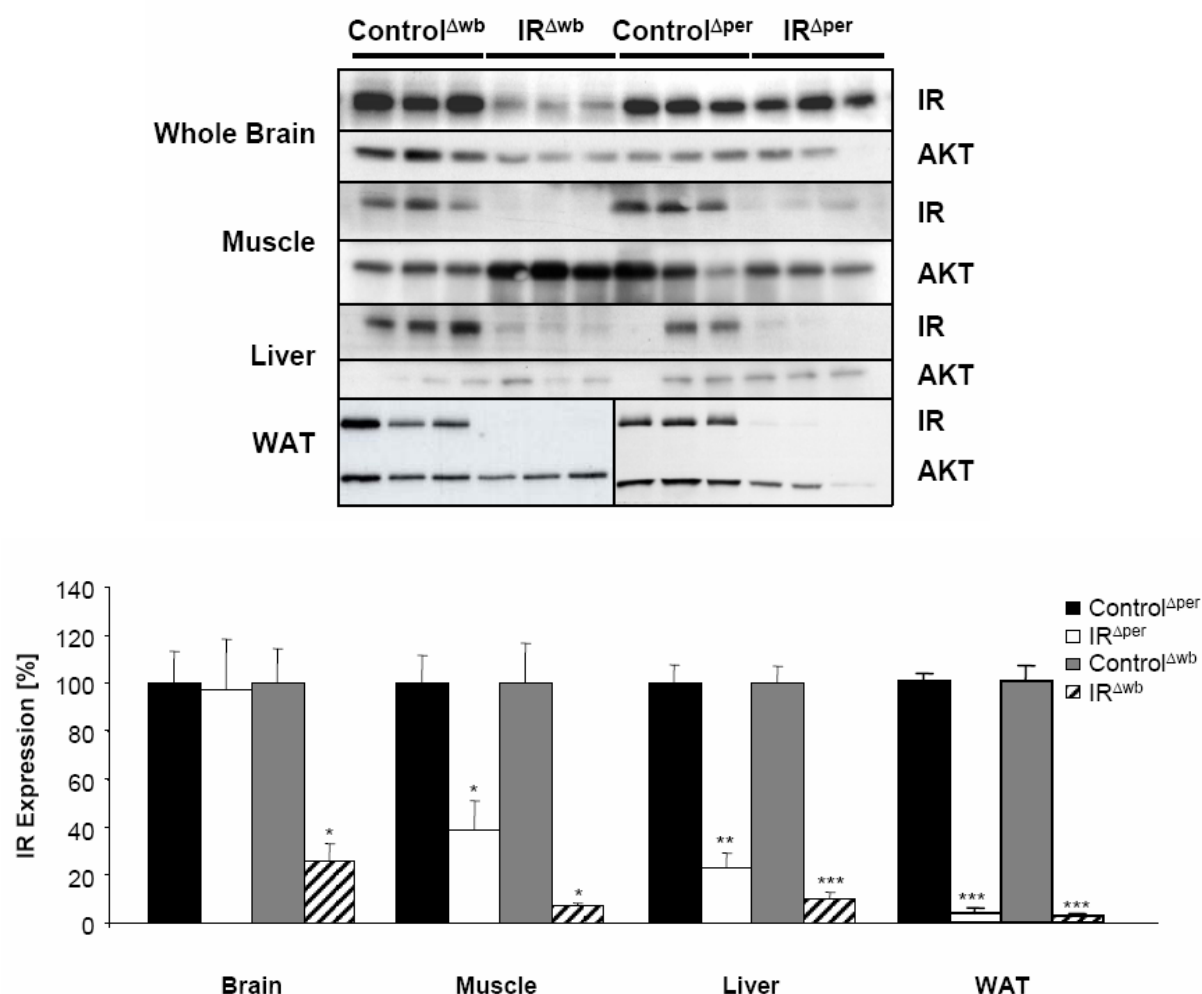


Fig. 12: Insulin receptor deficiency in central and peripheral organs of $IR^{\Delta wb}$ mice.

(A) Western blot analysis of IR and AKT (loading control) in whole brain, skeletal muscle, liver and white adipose tissue (WAT) of Control Δwb , IR Δwb , Control Δper and IR Δper mice. Indicated tissues were dissected 30 days after the start of inducer administration, except WAT of Control Δwb and IR Δwb mice, which was extracted 7 days after start of doxycycline administration. (B) Relative insulin receptor expression of Control Δper (black bars), IR Δper mice (white bars), Control Δwb (grey bars) and IR Δwb mice (striped bars) as assessed in (A). Values are mean \pm SEM. * $P \leq 0.05$; ** $P \leq 0.01$; *** $P \leq 0.001$ versus control.

In conclusion, the two inducible insulin resistance mouse models here described display a similar degree of insulin receptor inactivation in peripheral tissues, while the doxycycline-regulated shRNA expression in IR Δwb mice also results in the significant reduction of insulin receptor expression in the CNS. Thus, a comparative analysis of

these two mouse strains allows insights into the additional effect of neuronal insulin resistance in comparison to peripheral insulin resistance.

3.3 Combined central and peripheral insulin resistance leads to a more severe lipodystrophy than peripheral insulin resistance

Analysis of body weight upon insulin receptor inactivation in $IR^{\Delta\text{per}}$ and $IR^{\Delta\text{wb}}$ mice revealed that acute inactivation of the insulin receptor in peripheral tissues of adult mice has only a modest effect on the regulation of body weight. Only a transient decrease in body weight was observed between day 6 and 18 after tamoxifen treatment of $IR^{\Delta\text{per}}$ mice (Fig. 13). In contrast, $IR^{\Delta\text{wb}}$ mice exhibited a continuous decrease in body weight upon induction of the insulin receptor shRNA (Fig. 13).

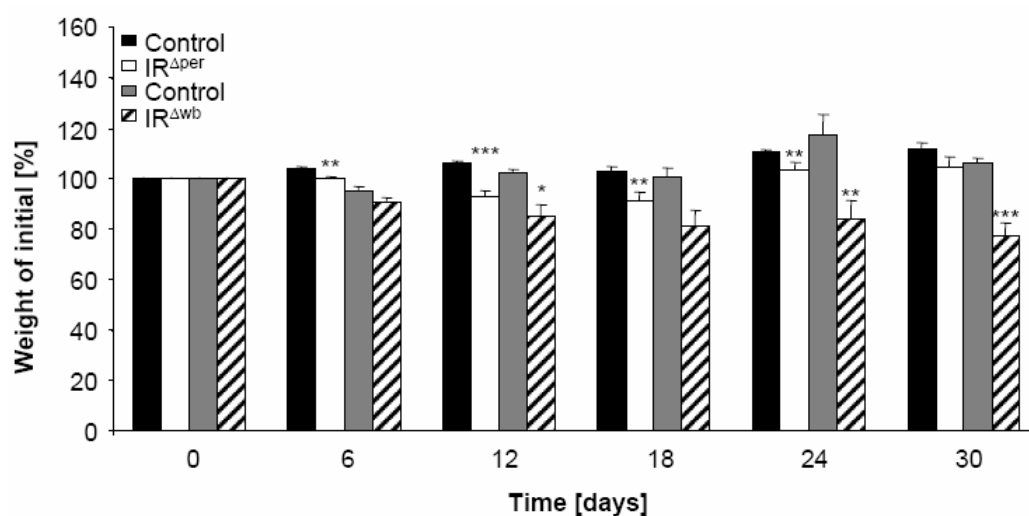


Fig. 13 Changes in body weight in insulin receptor deficient mice.

Body weight as percentage of initial body weight of Control $^{\Delta\text{per}}$ (black bars, n = 24-44), $IR^{\Delta\text{per}}$ (white bars, n = 12-42), Control $^{\Delta\text{wb}}$ (grey bars, n = 4-28) and $IR^{\Delta\text{wb}}$ mice (striped bars, n = 6-17) mice, over 30 days after start of either tamoxifen or doxycycline administration. Values are mean \pm SEM. * $P \leq 0.05$; *** $P \leq 0.001$ versus respective controls.

Although both mouse models displayed the same degree of insulin receptor deficiency in white adipose tissue as determined by Western blot analysis (Fig. 12), almost no residual white adipose tissue was detectable in $IR^{\Delta\text{wb}}$ mice 30 days after start

of treatment, while $IR^{\Delta per}$ mice exhibited a reduction in white adipose tissue mass of 40% (Fig. 14).

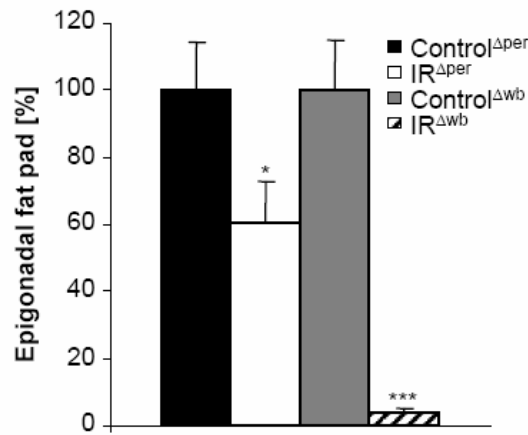


Fig. 14: Reduction of white adipose tissue mass in insulin receptor deficient mice.

Average weight of epigonadal fat pads of Control^{Δper} (black bars, n = 19), IR^{Δper} (white bars, n = 18), Control^{Δwb} (grey bars, n = 18) and IR^{Δwb} mice (striped bars, n = 13) mice, 30 days start of inducer administration. Values are mean ± SEM. *P ≤ 0.05 versus Control^{Δper}, ***P ≤ 0.001 versus Control^{Δwb}.

In accordance, assessment of body composition using nuclear magnetic resonance revealed a highly significant reduction in whole body fat mass of IR^{Δwb} mice, while the differences in fat mass detected between tamoxifen-treated IR^{Δper} mice and littermate controls did not reach significance (Fig. 15).

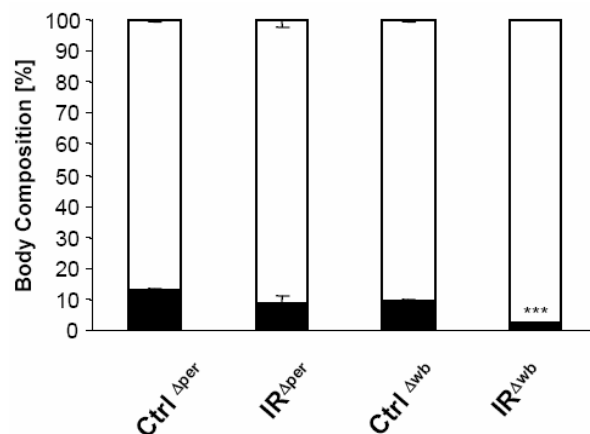


Fig. 15: Body composition in insulin receptor deficient mice.

Total lean mass (white bars) and total fat mass (black bars) of Control^{Δper} (n = 9), IR^{Δper} mice (n = 5), Control^{Δwb} (n = 8) and IR^{Δwb} mice (n = 12) measured by nuclear magnetic resonance. Values are mean ± SEM. ***P ≤ 0.001 versus Control^{Δwb}.

To establish whether the reduction in adipose tissue represented a tissue-specific phenomenon or was also detectable in other organs of IR^{Δwb} mice, organ weight of liver, skeletal muscle, brain, kidney, lung and heart of IR^{Δwb} mice was determined. This analysis revealed a selectively reduced mass of white adipose tissue, while weights of the other organs tested remained unchanged in IR^{Δwb} mice compared to controls (Fig. 16).

In summary, these experiments reveal that combined insulin resistance in the CNS and peripheral organs leads to a much more pronounced lipodystrophic phenotype than insulin resistance restricted to the periphery, including white adipose tissue.

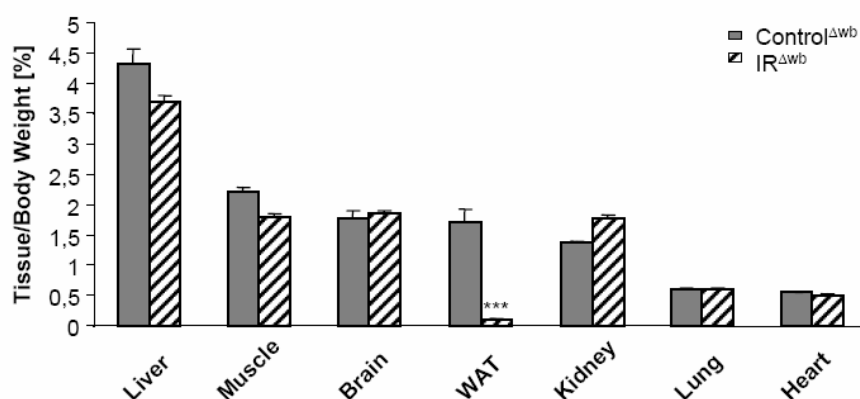


Fig. 16: Adipose tissue-specific hypoplasia in IR^{Δwb} mice.

Tissue weight of liver, muscle, brain, white adipose tissue (WAT), kidney, lung and heart, correlated to body weight, of Control^{Δwb} (n = 8-13) and IR^{Δwb} mice (n = 8-16) 30 days after start of doxycycline administration. Values are mean ± SEM. ***P ≤ 0.001 versus Control^{Δwb}.

3.4 Intracerebroventricular infusion of insulin leads to increased lipogenesis

It is well documented that insulin inhibits lipolysis in adipocytes via activation of the insulin receptor expressed on these cells (196-198). In light of the more pronounced lipodystrophy detected in IR^{Δwb} mice, it was addressed whether insulin acting via the CNS has additional effects on adipocyte function. To this end, C57BL/6 mice received a chronic intracerebroventricular infusion of either insulin or carrier solution over a period of 7 days. Peripheral insulin levels were determined on the first and last day of insulin infusion and were found to be unchanged between insulin and

carrier infused mice, thereby ruling out the possibility of insulin leaking from the brain into the periphery and directly acting on peripheral tissues (Fig. 17).

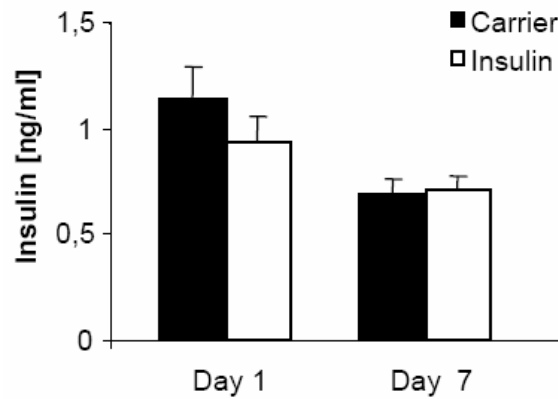
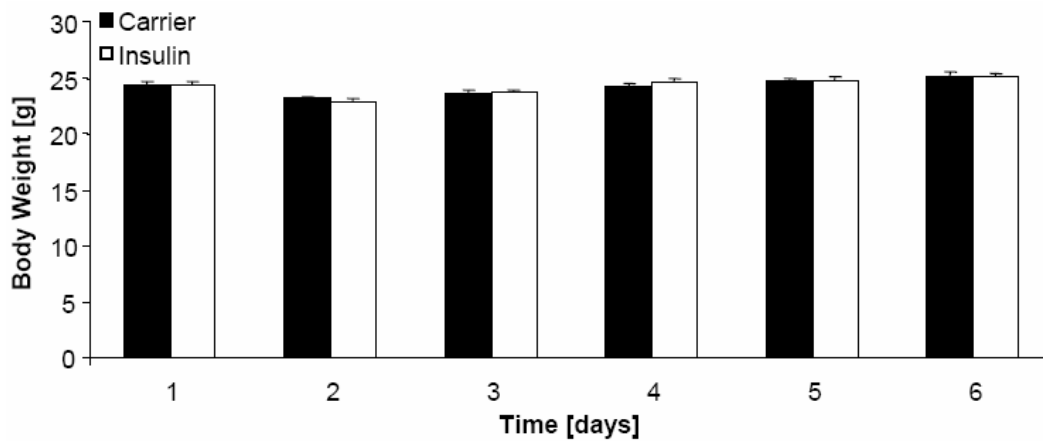


Fig. 17: Chronic icv infusion of insulin has no effect on peripheral insulin concentrations in C57BL/6 mice.

Serum insulin concentrations of C57BL/6 mice receiving chronic intracerebroventricular infusion of carrier (black bars, n = 5) or insulin solution (white bars, n = 5) at a rate of 200 μ U per day over 7 days. Day 0 = day of icv cannula and insulin osmotic mini-pump implant. Values are mean \pm SEM.

While insulin administration into the right lateral ventricle did not affect food intake or overall body weight, white adipose tissue mass of mice receiving intracerebroventricular insulin infusions was slightly but significantly elevated (Fig. 18).



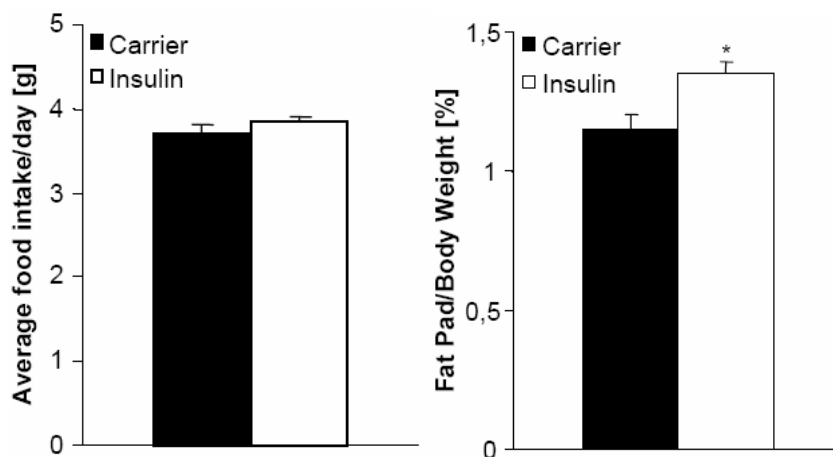
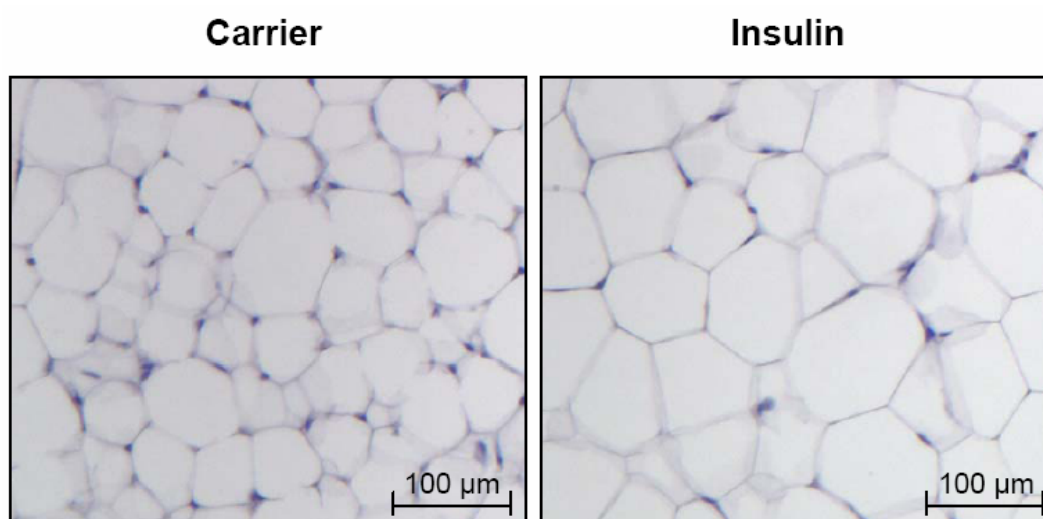


Fig. 18: Chronic icv infusion of insulin increases adipose tissue mass without changes in body weight or food intake in C57BL/6 mice.

(A) Mean body weight, (B) average daily food intake and (C) epigonadal fat pad weight corrected for body weight of C57BL/6 mice receiving chronic intracerebroventricular infusion of carrier (black bars, $n = 5$) or insulin solution (white bars, $n = 5$) at a rate of $200 \mu\text{U}$ per day over 7 days. Day 0 = day of icv cannula and insulin osmotic mini-pump implant. Values are mean \pm SEM. * $P \leq 0.05$ versus control.

The increase in adipose tissue mass was also reflected in an augmented adipocyte size as determined by histological and computational analysis (Fig. 19). In addition, mRNA analysis revealed an increase of the lipogenesis-promoting enzyme lipoprotein lipase in white adipose tissue (Fig. 19). These data directly indicate that insulin action in the CNS, in addition to its fat-cell-autonomous inhibition of lipolysis, promotes lipogenesis.



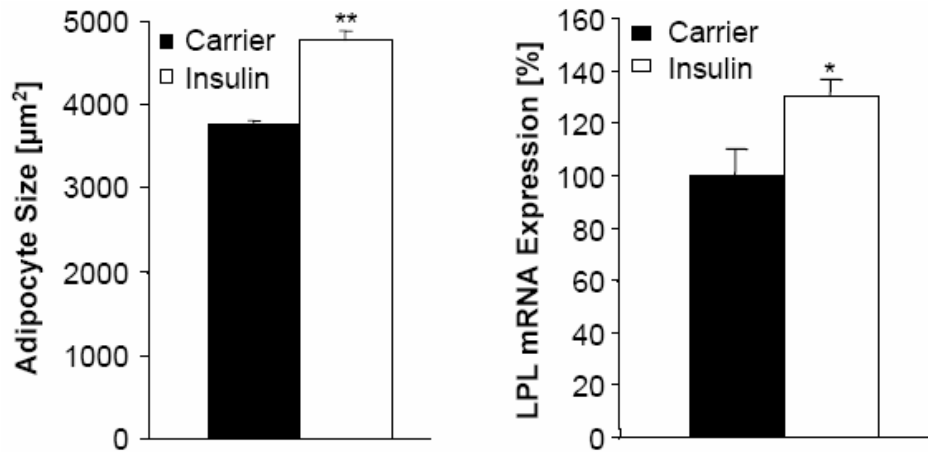


Fig. 19: Chronic icv infusion of insulin increases lipogenesis in C57BL/6 mice.

(A) H&E staining of white adipose tissue (magnification: 100x), (B) mean adipocyte size and (C) relative mRNA expression of lipoprotein lipase (LPL) in white adipose tissue of C57BL/6 mice after 7 days of chronic intracerebroventricular infusion of carrier (black bars, n = 5) or insulin (white bars, n = 5) at a rate of 200 µU per day. Values are mean ± SEM. *P ≤ 0.05, **P ≤ 0.01 versus control.

3.5 Insulin inhibits adipocyte-autonomous leptin secretion

Given the differential regulation of white adipose tissue mass, the concentrations of different adipokines were measured at several time points after induction of insulin receptor deficiency in IR^{Δper} mice and IR^{Δwb} mice. Analysis of circulating serum leptin concentrations revealed a constant increase in plasma leptin levels in IR^{Δper} mice compared to control animals after induction of insulin receptor deletion in peripheral tissues (Fig. 20).

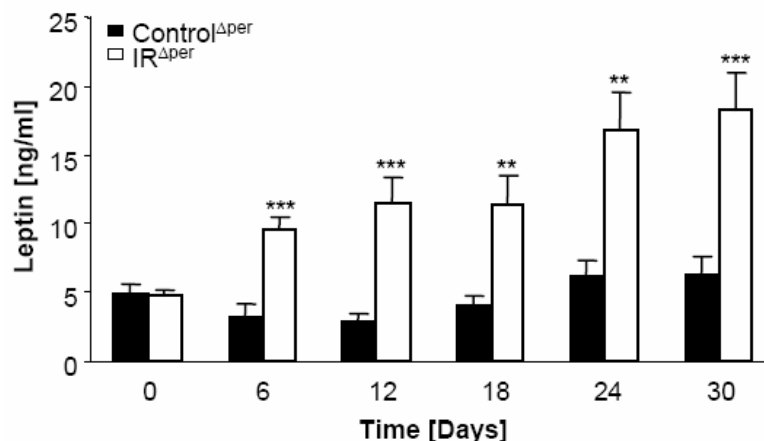


Fig. 20: Peripheral insulin resistance results in an increase in total serum leptin concentrations.

Total serum leptin levels of Control^{Δper} (n = 18) and IR^{Δper} mice (n = 18) over a period of 30 days. Mice were administered tamoxifen from day 1 until day 5. Values are mean ± SEM. **P ≤ 0.01, ***P ≤ 0.001 versus Control^{Δper}.

In contrast, deleting the insulin receptor additionally in the CNS of $IR^{\Delta wb}$ mice led to a progressive decline in circulating serum leptin concentrations (Fig. 21).

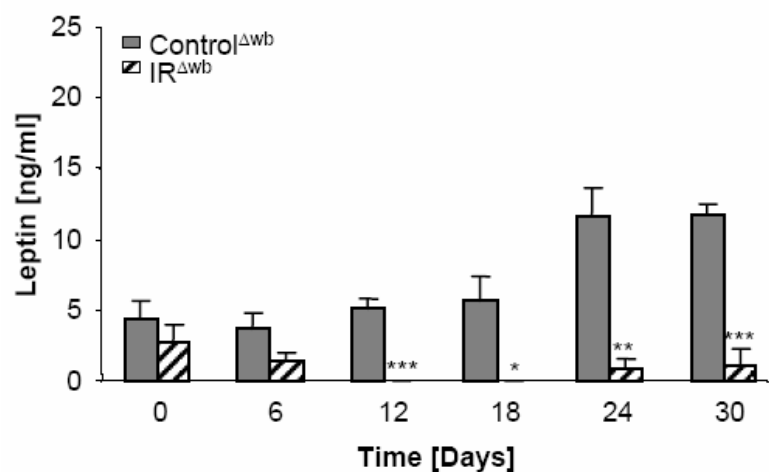


Fig. 21: Whole body insulin resistance results in a decrease in total serum leptin concentrations.

Total serum leptin levels of Control^{Δwb} (n = 5) and IR^{Δwb} mice (n = 5) over the course of 30 days. Mice were administered doxycycline from day 1 onwards. Values are mean ± SEM. *P ≤ 0.05, **P ≤ 0.01, ***P ≤ 0.001 versus Control^{Δwb}.

However, when leptin concentrations were corrected for epigonadal fat pad weight, both IR^{Δper} and IR^{Δwb} mice exhibited a staggering increase in leptin levels compared to their tamoxifen- or doxycycline-treated littermate controls (Fig. 22). In the same manner, serum adiponectin levels were found to be significantly increased in IR^{Δper} and IR^{Δwb} mice when correlated with white adipose tissue mass (Fig. 22).

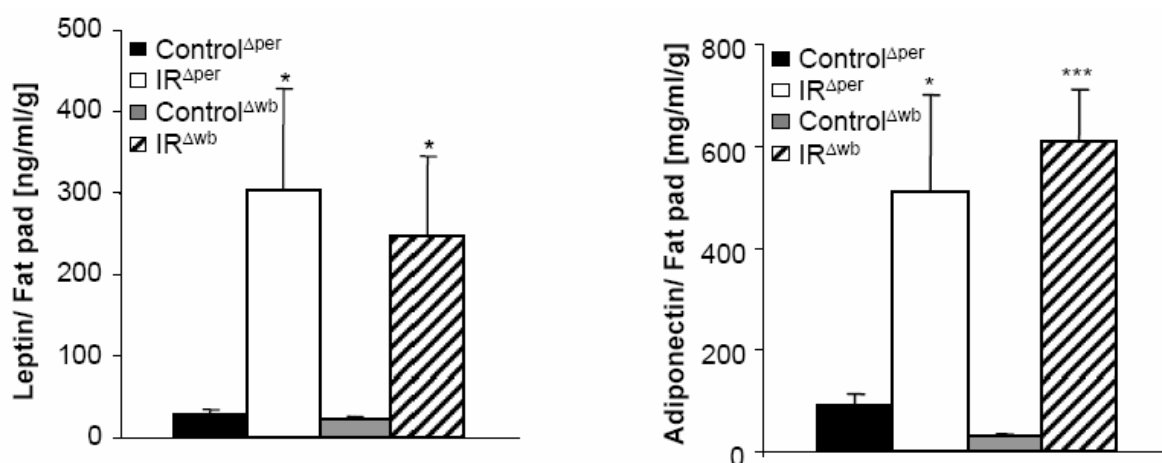


Fig. 22: Serum adipokine levels correlated with white adipose tissue mass in insulin receptor deficient mice.

(A) Serum leptin levels correlated to epigonadal fat pads of Control^{Δper} (black bars; n = 17), IR^{Δper} (white bars; n = 13), Control^{Δwb} (grey bars; n = 13) and IR^{Δwb} mice (striped bars; n = 6). (B) Serum adiponectin levels correlated to epigonadal fat pad weight of Control^{Δper} (black bars; n = 13), IR^{Δwb} (white bars; n = 10), Control^{Δwb} (grey bars; n = 13) and IR^{Δwb} mice (striped bars; n = 16). Serum samples were measured 30 days after start of tamoxifen or doxycycline administration. Values are mean ± SEM. *P ≤ 0.05, ***P ≤ 0.001 versus respective controls.

In conclusion, lack of insulin receptor expression in adipocytes results in an increase in leptin secretion from the adipose tissue. In the case of the IR^{Δwb} mice, this effect is masked by the more predominant phenotype of reduced adipose tissue mass, whereas the rise in serum leptin levels remains detectable in the IR^{Δper} mice, due to the smaller reduction of absolute fat mass in these mice.

3.6 Peripheral and central insulin action regulate hepatic ObRb expression

Next, the potential impact of increased leptin concentrations on leptin signal transduction in peripheral tissues was analyzed, by determining the expression of the long form of the leptin receptor (ObRb) in liver of IR^{Δper} and IR^{Δwb} mice. This analysis revealed a 76-fold increase in ObRb mRNA expression in IR^{Δper} compared to control mice (Fig. 7a). In IR^{Δwb} mice, a significant increase in hepatic ObRb mRNA expression could also be detected, although to a lesser extent than in IR^{Δper} mice (Fig. 23).

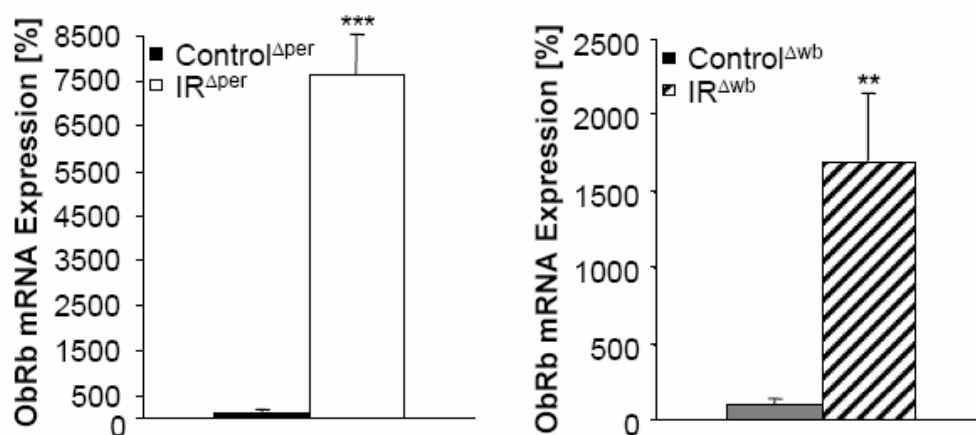


Fig. 23: Peripheral and central insulin receptor deficiency increases hepatic ObRb mRNA expression.

(A) Relative mRNA expression of hepatic ObRb of Control^{Δper} (black bars; n = 8) and IR^{Δper} (white bars; n = 7) mice 30 days after start of tamoxifen administration. Values are mean ± SEM. ***P ≤ 0.001 versus control. (B) Relative mRNA expression of hepatic ObRb of Control^{Δwb} (black bars; n = 5) and IR^{Δwb} (striped bars; n = 4) mice 30 days after start of doxycycline administration. Values are mean ± SEM. **P ≤ 0.01 versus control.

In both mouse models, the rise in ObRb mRNA was reflected by a rise in ObRb protein expression as shown by Western blot analysis, while almost no immunoreactive ObRb was present in the liver of tamoxifen- or doxycycline-treated control mice (Fig. 24).

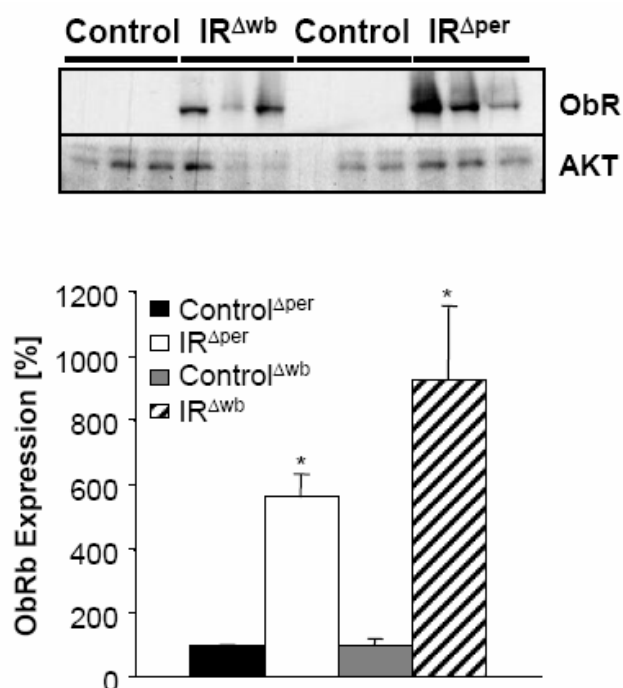


Fig. 24: Peripheral and central insulin receptor deficiency increases hepatic ObRb protein expression.

Western blot analysis of ObRb and AKT (loading control) in liver of Control^{Δwb}, IR^{Δwb}, Control^{Δper} and IR^{Δper} mice. Tissues were excised 30 days after the start of inducer administration. ObRb expression is also visualized as a comparative densitometric analysis with the average of ObRb expression of respective controls set to 100%. Values are mean ± SEM. *P ≤ 0.05 versus control.

To determine whether the increment in hepatic ObRb expression in the presence of elevated leptin concentrations resulted in an increased leptin receptor signaling, the expression and tyrosine phosphorylation of the downstream target of leptin signaling signal transducer and activator of transcription (Stat)-3 was determined. While hepatic Stat-3 protein expression remained indistinguishable between control and IR^{Δper} mice, a

significant increase in tyrosine phosphorylated Stat-3 could be detected in IR^{Δper} mice (Fig. 25). In contrast, both expression and tyrosine phosphorylation of Stat-3 were unaltered in IR^{Δwb} mice compared to control mice (Fig. 25), indicating that both acute selective peripheral and whole body insulin resistance lead to ObRb upregulation in liver, but central insulin action is needed for hepatic Stat-3 activation.

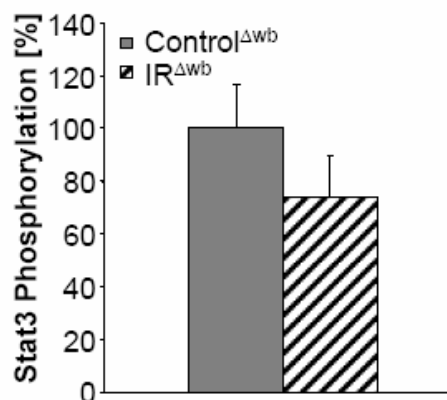
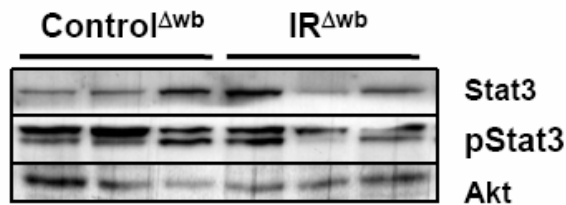
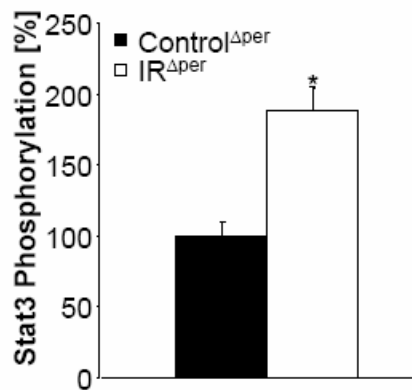
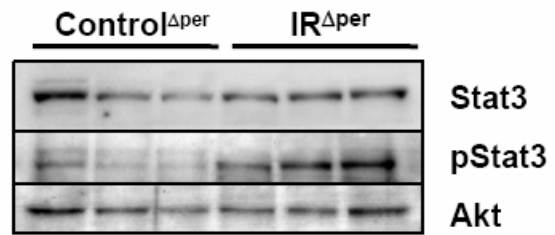


Fig. 25: Peripheral but not central insulin receptor deficiency results in an increase in hepatic Stat-3 phosphorylation.

(A) Western blot analysis of Stat-3, phosphorylated Stat-3 (pStat-3) and AKT (loading control) in liver of Control^{Δper} and IR^{Δper} mice. The tissue was excised 30 days after the start of the tamoxifen administration. (B) Western blot analysis of Stat-3, pStat-3 and AKT (loading control) in liver of Control^{Δwb} and IR^{Δwb} mice. The tissue was excised 30 days after the start of doxycycline administration. (C) Stat-3 phosphorylation of Control^{Δper} (black bars) and IR^{Δper} mice (white bars) was quantified via comparative densitometric analysis with the average of phosphorylated Stat-3 in Control^{Δper} mice set to 100%. Values are mean ± SEM. *P ≤ 0.05 versus control. (D) Stat-3 phosphorylation of Control^{Δwb} (grey bars) and IR^{Δwb} mice (striped bars) was quantified via comparative densitometric analysis with the average of phosphorylated Stat-3 in Control^{Δwb} mice set to 100%. Values are mean ± SEM.

3.7 Central insulin action regulates hepatic IL-6 mRNA levels

Recently, insulin was demonstrated to activate hypothalamic insulin signaling leading to increased hepatic interleukin (IL)-6 mRNA expression resulting in Stat-3 phosphorylation in hepatocytes (199), a process specifically regulated via AgRP neurons (200). As insulin receptor expression in the brain is unaltered in IR^{Δper} mice and since these mice exhibit increased circulating serum insulin concentrations, intact neuronal insulin signal transduction may lead to upregulation of hepatic IL-6 mRNA expression. Indeed, we observed a significant 2.5-fold upregulation of IL-6 mRNA expression in the liver of IR^{Δper} mice (Fig. 26).

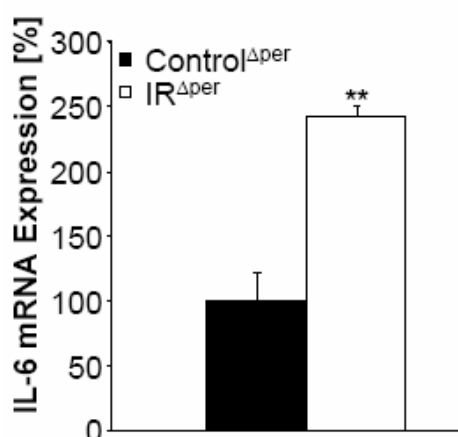


Fig. 26: Peripheral insulin receptor deficiency results in an increase in hepatic IL-6 mRNA expression.

Relative mRNA expression of IL-6 in liver of Control^{Δper} (black bars; n = 8) and IR^{Δper} (white bars; n = 7) mice. Data was collected 25 days after the last tamoxifen administration. Values are mean ± SEM. **P ≤ 0.01 versus control.

Thus, the observed increased Stat-3 phosphorylation in the liver of IR^{Δper} mice may result either from signal transduction via the hepatic ObRb *or* via the hepatic IL-6 receptor, possibly as a consequence of increased hepatic IL-6 expression due to intact neuronal insulin signaling in the presence of elevated serum insulin concentrations. In contrast to IR^{Δper} mice, hepatic IL-6 mRNA expression remained unaltered in IR^{Δwb} mice (Fig. 27), indicating a role for central insulin in the regulation of hepatic IL-6 mRNA expression.

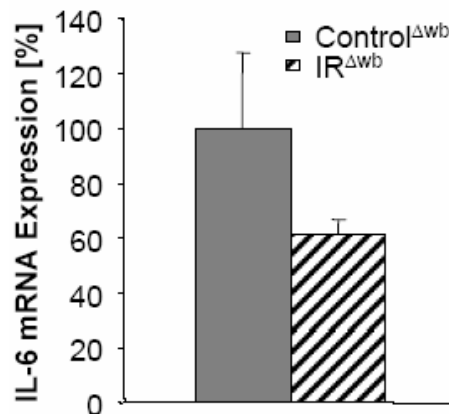


Fig. 27: Unaltered IL-6 mRNA expression in the liver of IR^{Δwb} mice.

Relative mRNA expression of interleukin 6 (IL-6) in liver of Control^{Δwb} (black bars; n = 7) and IR^{Δwb} (white bars; n = 7) mice. Data was collected 30 days after the start of doxycycline administration. Values are mean ± SEM. P = 0.06 versus Control^{Δwb}.

3.8 IR^{Δwb} mice display a higher degree of impaired peripheral glucose metabolism

To determine the regulation of peripheral glucose metabolism after acute induction of peripheral or whole body wide insulin resistance, blood glucose levels in randomly fed mice were assessed daily from the period of induction with either tamoxifen in IR^{Δper} or doxycycline in IR^{Δwb} mice. An early onset rise of blood glucose concentrations in IR^{Δwb} mice reaching 600 mg/dl 17 days after the beginning of doxycycline induction was observed (Fig. 28). IR^{Δper} mice also exhibited a clear increase in blood glucose concentrations after completion of tamoxifen treatment. Nevertheless, both the kinetics of hyperglycemia onset and the magnitude of hyperglycemia reached were significantly lower in IR^{Δper} mice (Fig. 28). Blood glucose concentration reached the maximum of approximately 400 mg/dl 17 days after start of

tamoxifen administration and stayed stable in this range during the following 2 weeks (Fig. 28).

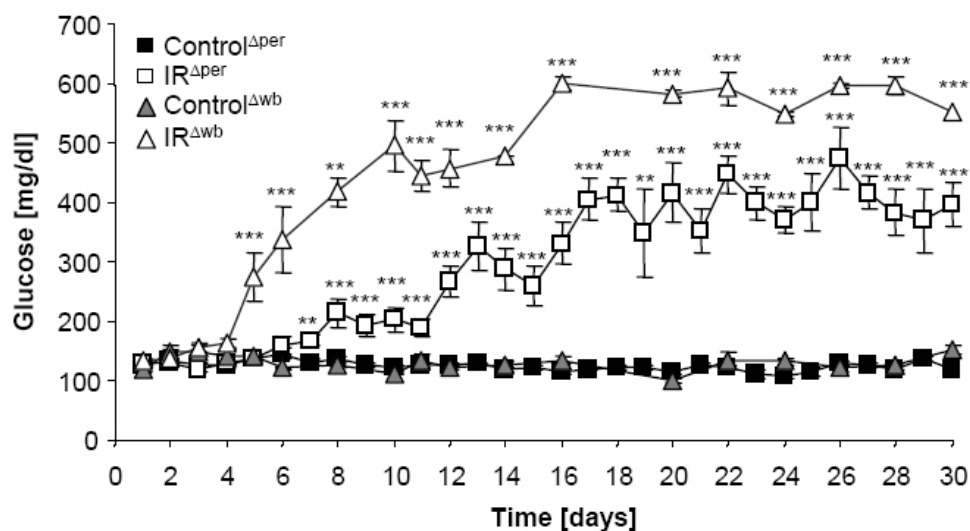


Fig. 28: Loss of central insulin receptor signaling results in more pronounced hyperglycemia.

Random fed blood glucose concentrations of Control^{Δper} (filled squares; n = 3-50), IR^{Δper} (open squares; n = 3-48), Control^{Δwb} (grey triangles; n = 5-27) and IR^{Δwb} mice (open triangles; n = 5-32) over 30 days. Data represent the mean ± SEM. **P ≤ 0.01, ***P ≤ 0.001 versus respective controls.

Accordingly, glucose tolerance tests performed at day 18 after induction of IR ablation in both mouse models disclosed a significant impairment of glucose tolerance in IR^{Δper} mice (Fig. 29). Fasting blood glucose concentrations remained unaltered at the same time point (Fig. 29).

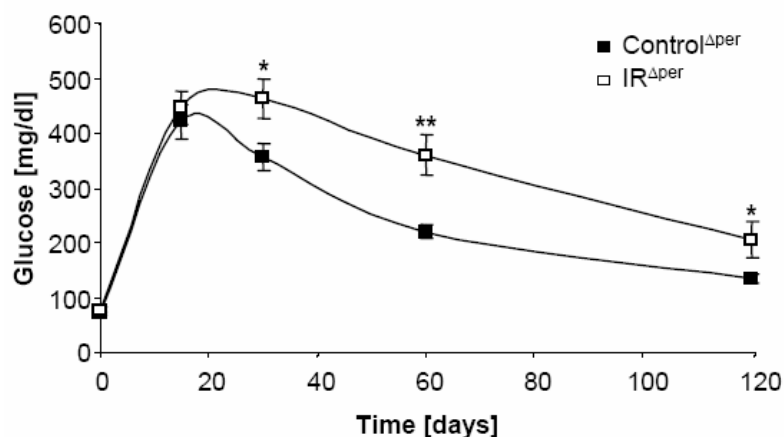


Fig. 29: Impaired glucose tolerance in IR^{Δper} mice.

Glucose tolerance tests in Control^{Δper} (filled squares, n = 18) and IR^{Δper} (open squares; n = 19) mice. Blood glucose concentrations were measured immediately before and 15, 30, 60 and 120 minutes after injection of 2 g/kg of glucose. Data represent the mean ± SEM. *P ≤ 0.05, **P ≤ 0.01 versus control.

IR^{Δwb} mice, on the other hand, exhibited a significant increase in fasting blood glucose concentrations, but also reacted with a significantly higher rise in blood glucose concentrations upon exogenous glucose administration (Fig. 30). Since IR deletion occurred to a similar extent in peripheral tissues of IR^{Δper} and IR^{Δwb} mice, this data indicates that lack of the insulin receptor in the CNS of IR^{Δwb} mice leads to a significantly more severe impairment of peripheral glucose homeostasis.

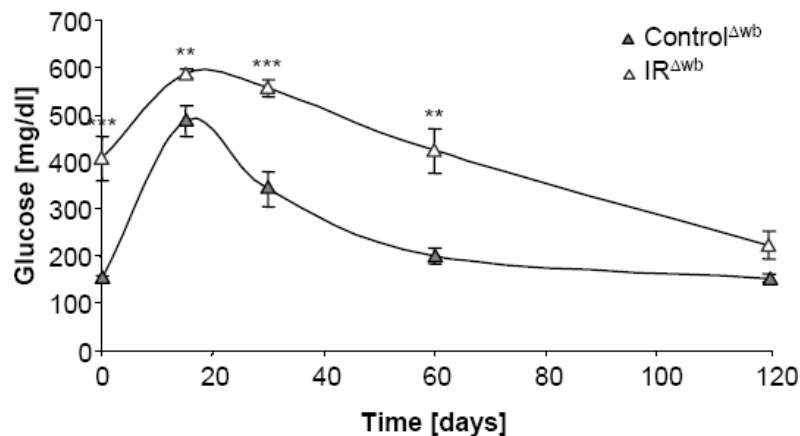


Fig. 30: Impaired glucose tolerance in IR^{Δwb} mice.

Glucose tolerance tests in Control^{Δwb} (grey triangles; n = 9) and IR^{Δwb} (open triangles; n = 13) mice. Blood glucose concentrations were measured immediately before and 15, 30, 60 and 120 minutes after injection of 2 g/kg of glucose. Data represent the mean ± SEM. **P ≤ 0.01, ***P ≤ 0.001 versus control.

3.9 Leptin administration improves glucose metabolism in IR^{Δwb} mice

To analyze whether loss of signaling via hepatic Stat-3 in IR^{Δwb} mice, either as a consequence of reduced hepatic IL-6 expression or due to the absence of leptin, contributes to the impairment of peripheral glucose homeostasis, doxycycline-treated IR^{Δwb} mice and littermate controls received a chronic leptin infusion over a period of 7 days via subcutaneously implanted osmotic mini-pumps. Serum leptin levels were measured at several time points during chronic administration of leptin. Leptin levels were significantly increased as early as two days after pump implant and remained elevated to a similar extent in IR^{Δwb} mice and littermate controls over the course of the experiment (Fig. 31).

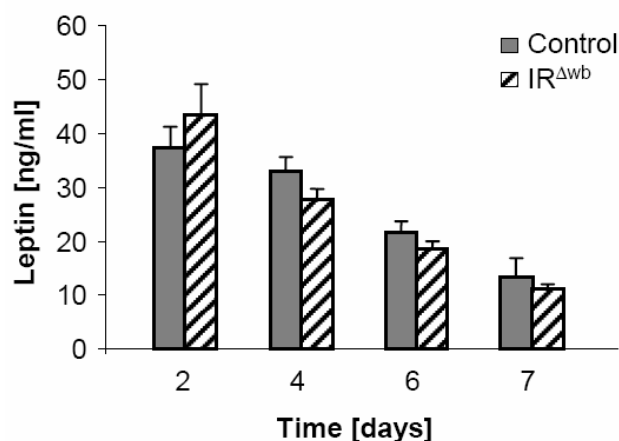


Fig. 31: Restoration of serum leptin concentrations of IR^{Δwb} mice.

Total serum leptin levels of Control^{Δwb} (grey bars; n = 5) and IR^{Δwb} mice (striped bars; n = 5) receiving a chronic infusion of leptin at a rate of 12 μg per day. Blood samples were taken, 2, 4, 6 and 7 days after the subcutaneous implantation of an osmotic mini-pump. Mice had been administered doxycycline for 16 days prior to pump implantation. Values are mean ± SEM.

Western blot analysis revealed an increase in hepatic Stat-3 tyrosine phosphorylation after leptin reconstitution in IR^{Δwb} mice, whereas no phosphorylated Stat-3 could be detected in controls receiving leptin infusions (Fig. 32).

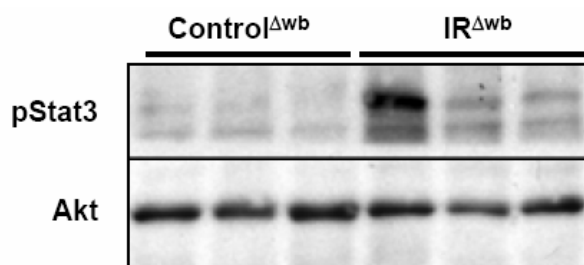


Fig. 32: Chronic infusion of leptin increases hepatic Stat-3 phosphorylation in IR^{Δwb} mice.

Western blot analysis of pStat-3 and AKT (loading control) in liver of Control^{Δwb} and IR^{Δwb} mice receiving a chronic infusion of leptin at a rate of 12 μg per day. Tissues were excised 7 days after the subcutaneous implantation of the osmotic mini-pump.

Strikingly, in parallel to increased hepatic Stat-3 phosphorylation in IR^{Δwb} mice receiving leptin infusion, blood glucose levels decreased dramatically two days after start of leptin infusion to levels comparable to those found in control mice (Fig. 33).

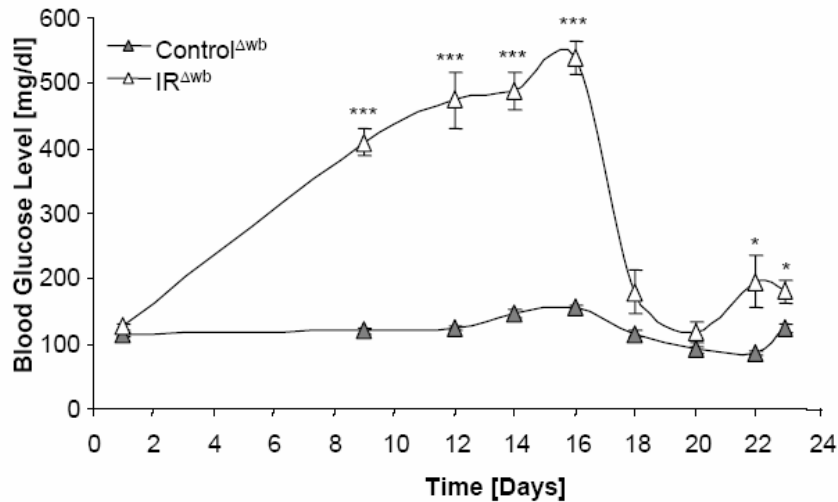


Fig. 33: Restoration of hepatic Stat-3 phosphorylation ameliorates blood glucose concentrations.

Random fed blood glucose concentrations of Control^{Δwb} (grey triangles; n = 5) and IR^{Δwb} mice (open triangles; n = 5) receiving a chronic infusion of leptin at a rate of 12 μg per day from day 16 onwards. Data represent the mean ± SEM. *P ≤ 0.05, ***P ≤ 0.001 versus control.

Taken together, the data show that increasing hepatic Stat-3 activation largely ameliorates dysregulated glucose metabolism in IR^{Δwb} mice.

3.10 Peripheral insulin resistance results in β cell hyperplasia but unaltered insulin secretion

As insulin resistance restricted to pancreatic β cells throughout development has been demonstrated to impair insulin secretion, serum insulin concentrations and the insulin secretory response to exogenously applied glucose in IR^{Δper} and IR^{Δwb} mice were determined. Assessment of serum insulin concentrations revealed that both IR^{Δper} and IR^{Δwb} mice suffer from severe hyperinsulinemia as an indirect measure of peripheral insulin resistance upon induction of insulin receptor ablation. IR^{Δper} mice reached a maximum 50-fold increase on day 18, while IR^{Δwb} mice displayed their maximum on day 12 following the induction of IR ablation, exhibiting a 54-fold increase of circulating plasma insulin concentrations (Fig. 34).

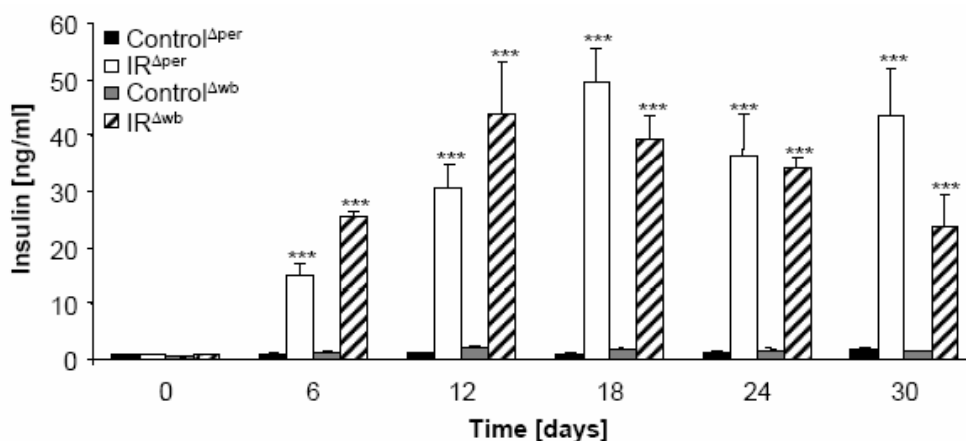


Fig. 34: Peripheral and whole body insulin receptor deficiency results in hyperinsulinemia.

Plasma insulin concentrations in Control^{Δper} (black bars; n = 14 – 24), IR^{Δper} (white bars; n = 13 - 23), Control^{Δwb} (grey bars; n = 5) and IR^{Δwb} (striped bars; n = 4 - 5) mice over 30 days. Data represent the mean ± SEM. ***P ≤ 0.001 versus respective controls.

Further analysis revealed a significant increase in fasting serum insulin concentrations in IR^{Δper} and even higher levels in IR^{Δwb} mice, consistent with the degree of insulin resistance in these mouse models (Fig. 35). Following an intravenous injection of glucose, serum insulin concentrations of IR^{Δper} mice were significantly elevated, both acutely within 2 to 5 minutes after glucose injections and in a prolonged fashion 30 minutes after injection (Fig. 35), whereas the typical diphasic pattern of glucose-stimulated insulin secretion was disrupted in IR^{Δwb} mice.

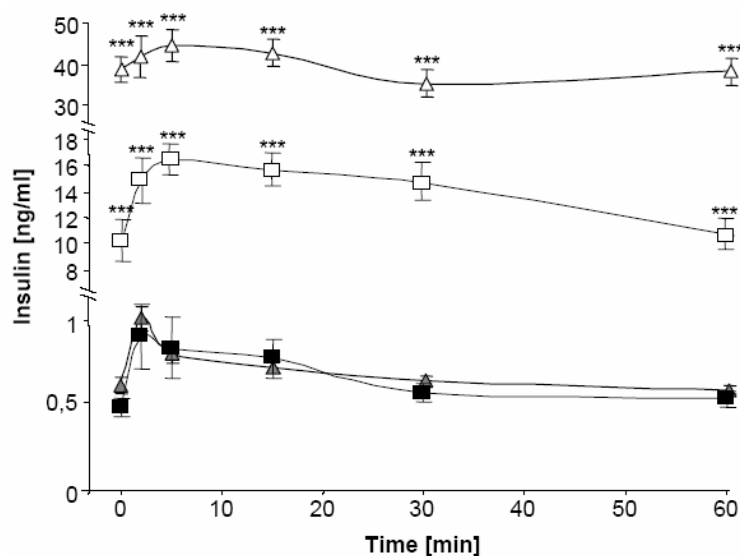


Fig. 35: Glucose-stimulated insulin secretion in IR^{Δper} and IR^{Δwb} mice.

Results

Insulin concentrations after administration of an exogenous glucose bolus in Control^{Δper} (filled squares; n = 8), IR^{Δper} (open squares; n = 5), Control^{Δwb} (grey triangles; n = 5) and IR^{Δwb} mice (open triangles; n = 8) on day 18. Values are mean ± SEM. ***P ≤ 0.001 versus control.

Histological analysis of pancreatic tissues revealed a clear β cell hyperplasia upon induced insulin receptor ablation in both mouse models, consistent with the β cell proliferative response to insulin resistance (Fig. 36). Despite a significant enlargement of pancreatic islets both in IR^{Δper} and IR^{Δwb} mice, their architecture appeared normal with unaltered distribution of insulin producing β cells and glucagon producing α cells (Fig. 36).

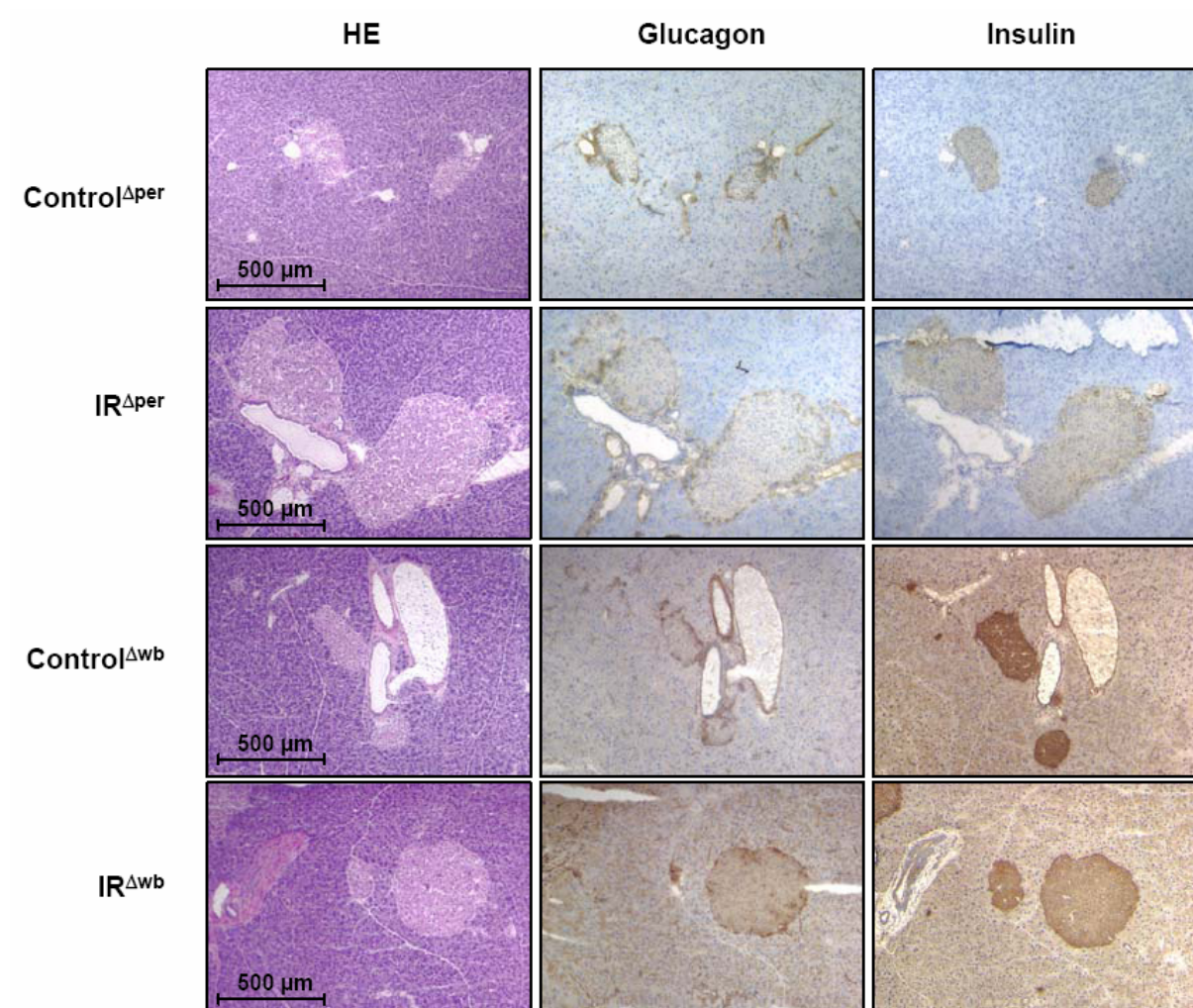


Fig. 36: Peripheral and central insulin resistance results in β cell hyperplasia.

Immunohistochemical stainings of pancreatic islets in Control^{Δper}, IR^{Δper}, Control^{Δwb} and IR^{Δwb} mice. Pancreatic tissues were stained for H&E, Insulin and Glucagon. Magnification: x100.

Quantitative assessment of β cell mass exhibited a significant increase in β cell mass 3 weeks after induction of insulin receptor deficiency indicating a fast hyperproliferative β cell response to peripheral insulin resistance (Fig. 37).

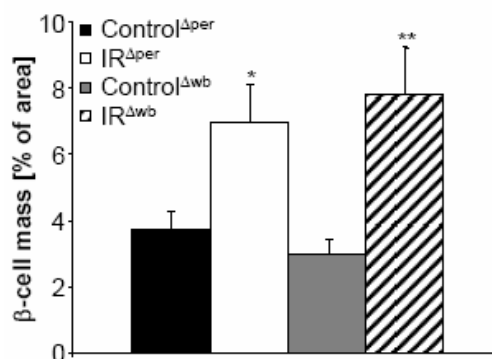


Fig. 37: Increased β cell mass in IR ^{Δ_{per}} and IR ^{Δ_{wb}} mice.

Percentage of β cell mass in Control ^{Δ_{per}} (black bars; n = 4) and IR ^{Δ_{per}} mice (white bars; n = 4), Control ^{Δ_{wb}} (grey bars; n = 3) and IR ^{Δ_{wb}} mice (striped bars; n = 3). Data was collected 30 days after starting the experiment. Values are mean \pm SEM. *P \leq 0.05, **P \leq 0.01 versus control.

These data indicate that in response to acutely induced insulin resistance in adult mice, even within pancreatic β cells themselves, β cell mass remains dynamic and still allows for the occurrence of β cell hyperplasia. If insulin resistance remains peripheral, the hyperproliferative β cells are still capable of secreting insulin acutely in response to exogenously administered glucose.

3.11 Targeted disruption of the IGF-1 receptor allele

Since there is strong evidence for a redundancy of insulin and IGF-1 signal transduction, and both signaling pathways contribute to the regulation of neuronal growth and survival, as well as the regulation of food intake and peripheral glucose metabolism, the IGF-1 receptor gene was specifically inactivated in the central nervous system of mice, by using a targeting construct to introduce two loxP-sites into the murine IGF-1 receptor gene (Fig. 38). Cre-mediated recombination and subsequent excision of exon 3 of the IGF-1 receptor gene results in a frame shift after 213 codons, with an appended sequence of 27 amino acids followed by a stop codon in exon 4.

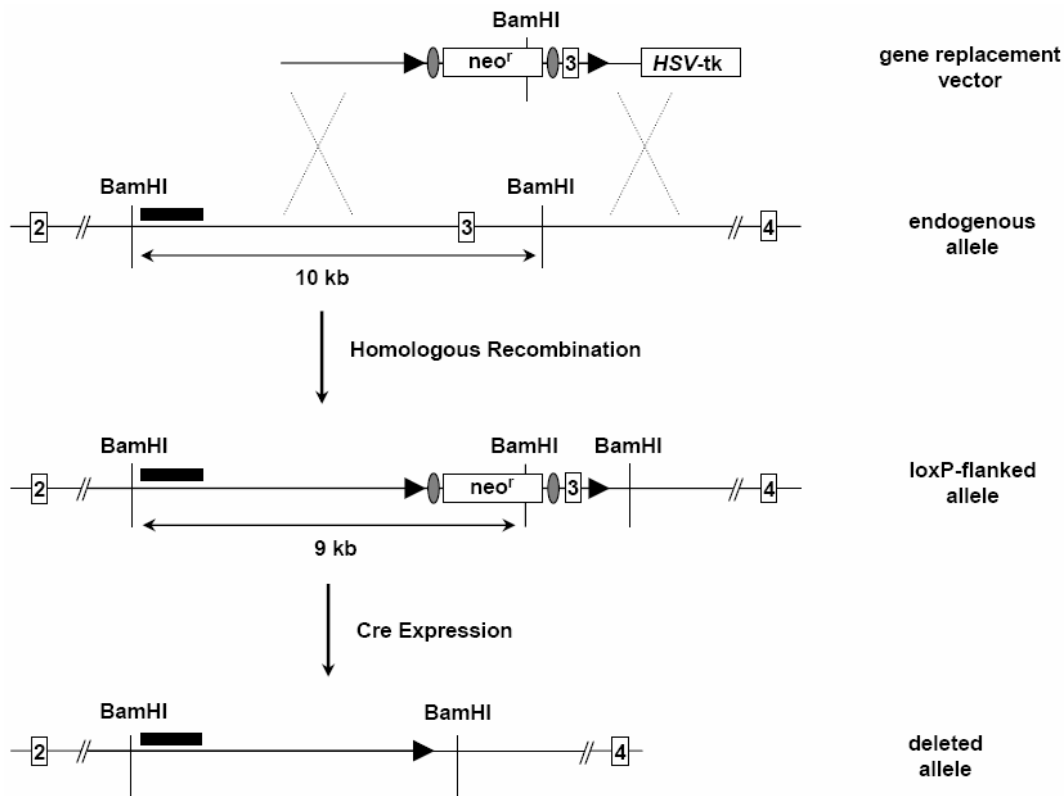


Fig. 38: Conditional gene targeting strategy.

Location of the probe used for Southern blot analysis is indicated by a black bar. BamHI = restriction enzyme sites, 2, 3, 4 = exon 2, 3 or 4 of the IGF-1 receptor gene, neo^r = neomycin resistance gene cassette, HSV-tk = Herpes simplex virus thymidine kinase gene cassette.

After transfection of Bruce4 ES cells with this construct, ES cell clones were identified in which the construct had been integrated in the endogenous IGF-1 receptor gene locus by homologous recombination. By combined Southern blot and PCR analysis, the integrity of the IGF-1 receptor gene surrounding the construct integration site was confirmed both at the 3' and 5'-end (Fig. 39).

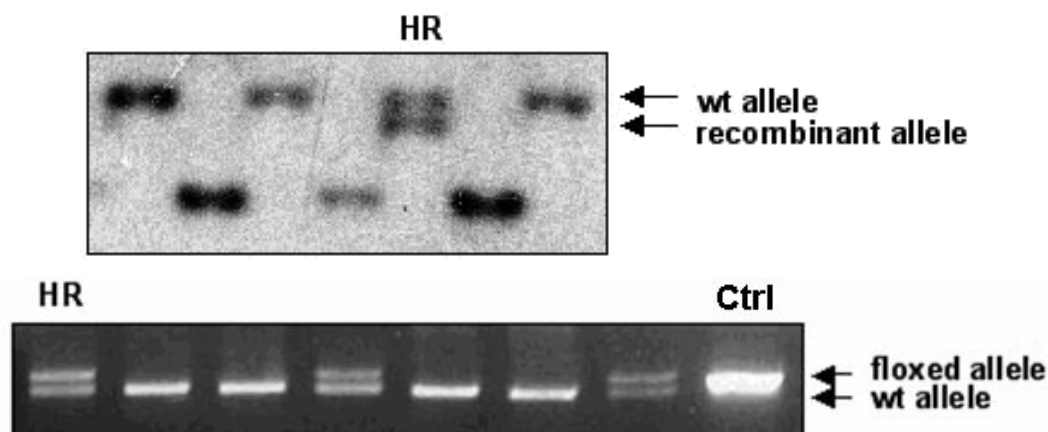


Fig. 39: Correct construct integration into the endogenous IGF-1 receptor locus.

Southern blot analysis using the 5'-probe and PCR analysis using primers flanking the 3'-loxP site of homologous ES cell clones isolated after transfection with the linearized targeting vector.

Taken together, successful integration of the loxP-sites surrounding exon 3 of the IGF-1 receptor gene was established. Deletion of exon 3 has been demonstrated to yield a functionally inactive IGF-1 receptor gene, lacking the extracellular ligand binding domain, the transmembrane region, as well as the intracellular tyrosine kinase domain (201). Injection of the homologous recombinant ES cell clone into blastocysts yielded chimeric mice, which consist of two cell types of different origin, as becomes visible when using donor mice of different coat colors for the ES cells and the blastocyst. Chimeric mice carrying the mutated IGF-1 receptor allele ranged between 30% and 90% chimerism according to coat color (Fig. 40).



Fig. 40: Chimeras heterozygous for the mutated IGF-1 receptor allele.

Picture of IGF1R^{fllox/+} chimeras generated by injection of a homologous recombinant Bruce4 ES cell clone into a CB-20 blastocyst.

Backcrossing the chimeric mice with C57BL/6 mice resulted in germline transmission of the mutation, as could be assessed by PCR analysis (Fig. 41).

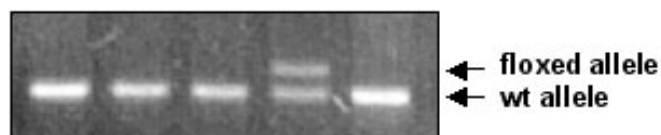


Fig. 41: Germline transmission of the mutated IGF-1 receptor allele.

PCR of the 3' loxP site performed on DNA of tail biopsies from mice born of an IGF1R^{fllox/+}-chimera/Flp deleter breeding.

Since the construct carries a neomycin resistance gene, which might interfere with the transcription and translation of the modified IGF-1 receptor allele, the resistance cassette was initially flanked by FRT recombination sites, allowing for excision by Flp recombinase-mediated recombination. To this end, backcrossing was performed into mice expressing the Flp recombinase in their germline (FlpE deleter). Since the FlpE deleter mice had previously been backcrossed onto a C57BL/6 background for eight generations, offspring from the chimeras carrying the IGF-1 receptor mutation on a pure C57BL/6 background and the FlpE deleter mice yielded double-transgenic animals without a neomycin resistance gene and a genetic background contributed by more than 99.9% from the C57BL/6 strain. These mice were bred to mice expressing the Cre recombinase under the control of the neuron-specific rat Synapsin 1 promoter (187, 202) to yield mice heterozygous for an IGF-1 receptor deficiency exclusively in neural tissues (hetIGF1R^{ΔSyn}). hetIGF1R^{ΔSyn}, in turn, were intercrossed to obtain mice homozygous for the loxP-flanked IGF-1 receptor allele either with Cre expression (IGF1R^{ΔSyn}) or without Cre expression (Control^{ΔSyn}) to be used as littermate controls.

3.12 Conditional inactivation of the IGF-1 receptor gene in the central nervous system

The efficiency of IGF-1 receptor gene recombination was assessed by Western blot analysis and immunohistochemistry. To this end, brain tissue was removed from IGF1R^{ΔSyn} mice and littermate controls and expression of the IGF-1 receptor protein was determined for a number of different brain regions. IGF-1 receptor protein expression was found to be significantly reduced by 90% in the hippocampus of IGF1R^{ΔSyn} mice, whereas expression levels were indistinguishable from that of control littermates for the region of the cerebellum. A reduction in IGF-1R protein expression of approximately 70% could also be detected in the parietal cortex of IGF1R^{ΔSyn} mice. However, these values did not reach significance.

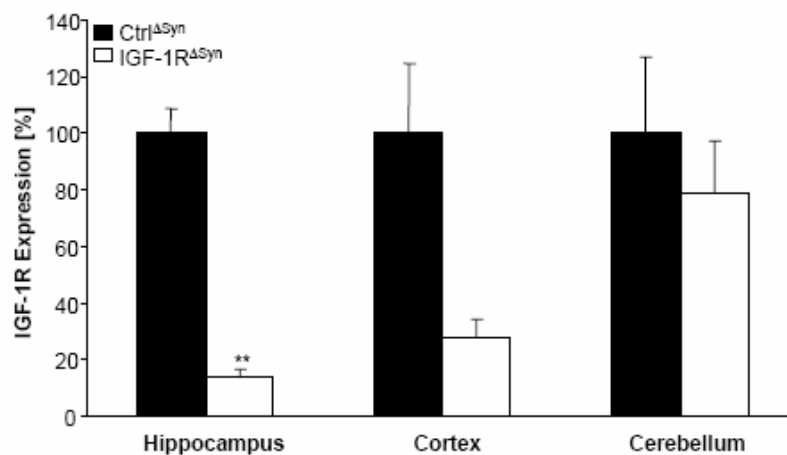
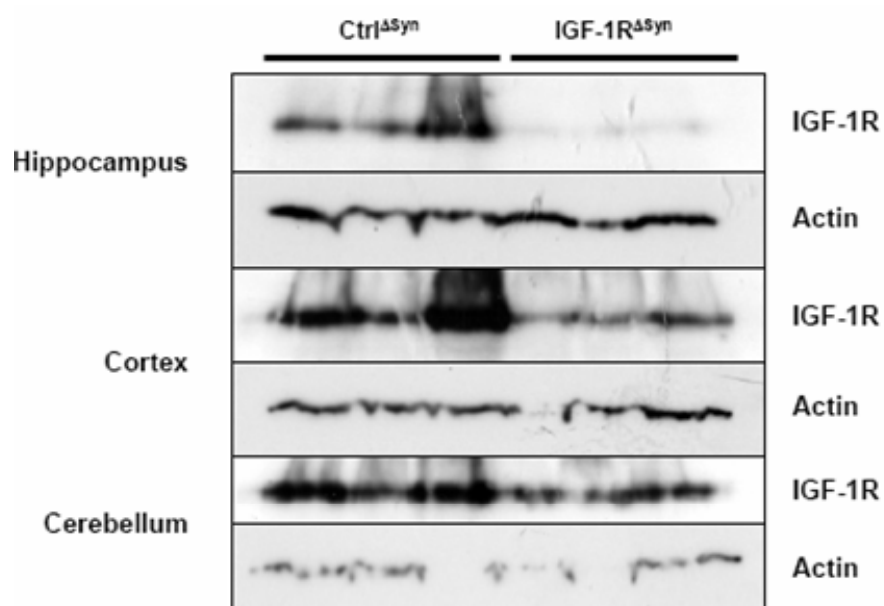


Fig. 42: Central IGF-1 receptor protein expression.

Western blot and densitometric analysis of IGF-1R and actin (loading control) expression in protein lysates from different brain regions such as hippocampus, parietal cortex and cerebellum of 12-week-old IGF1R^{ΔSyn} mice (white bars, n = 3) and littermate controls (black bars, n = 3). Values represent the mean ± SEM. **P ≤ 0.01 versus controls.

On the other hand, IGF-1 receptor protein expression in the periphery was found to be unchanged from that of littermate controls in tissues such as heart, skeletal muscle, pancreas and lung (Fig. 43).

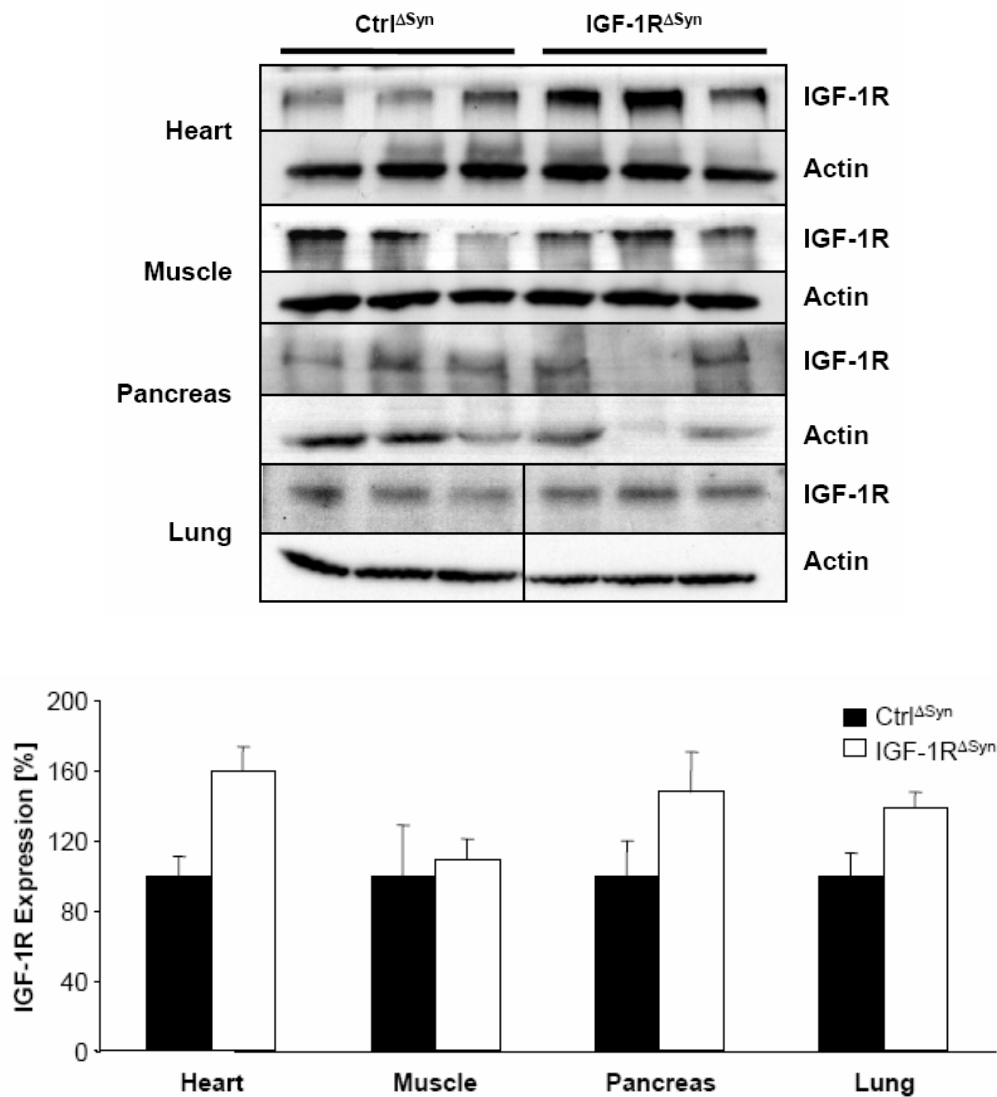


Fig. 43: Peripheral IGF-1 receptor protein expression.

Western blot and densitometric analysis of IGF-1R and actin (loading control) expression in protein lysates from heart, skeletal muscle, pancreas and lung of 28-week-old IGF1R Δ Syn mice (white bars, n = 3) and littermate controls (black bars, n = 3). Data represent the mean \pm SEM.

Cre-mediated recombination was also visualized using a reporter mouse strain in which transcription of the β -galactosidase gene (LacZ) under the control of the ubiquitously expressed Rosa26 promoter is prevented by a loxP-flanked hygromycin resistance gene (RosaArte1) (100). Expression of the Cre recombinase under the control of the Synapsin-1 promoter enables transcription of LacZ in Synapsin-1-expressing neurons, which can be visualized by immunofluorescent staining of brains of Synapsin Cre-expressing LacZ (SynCre-LacZ) mice. Cre expression under the control of the Synapsin-1 promoter was confirmed in the dentate gyrus (Fig. 44), a region of the hippocampus which has been implicated in neurogenesis (203-205), a process linked to

learning and memory, and to a lesser extent in the cortex of SynCre-LacZ mice, thereby paralleling the previous results found by Western blot analysis.

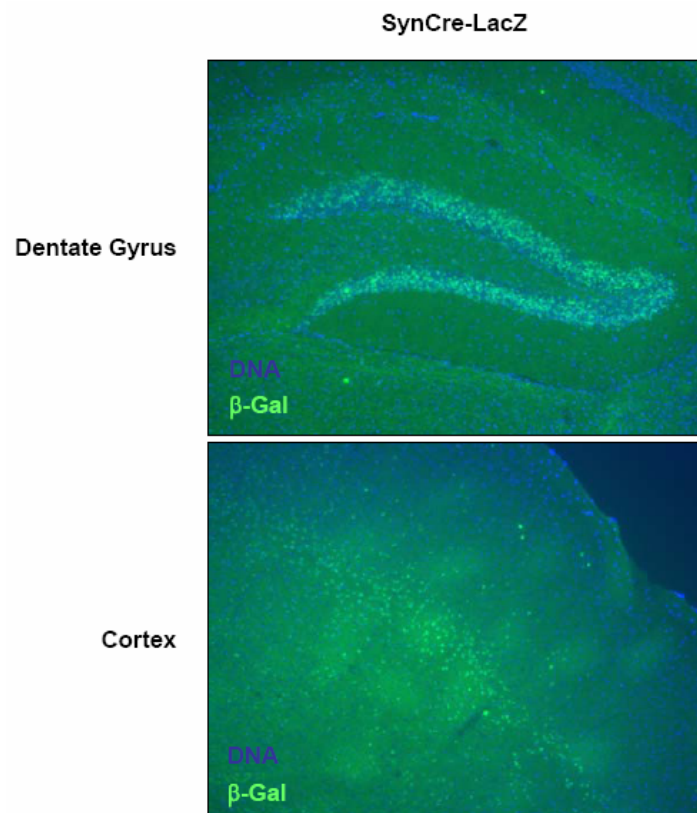


Fig. 44: Synapsin Cre expression in brain regions of SynCre-LacZ mice.

Fluorescence immunohistochemical stainings of the dentate gyrus and the cortex of a SynCre-LacZ mouse. Magnification: 200x. Blue = DAPI = DNA, green = FITC = β-Galactosidase = β-Gal.

Histological analysis of brain tissues of IGF1R^{ΔSyn} mice and littermate controls exhibited a significant reduction in IGF-1 receptor protein expression within the dentate gyrus (Fig. 45), co-localizing IGF-1 receptor deletion with those cells expressing the Cre recombinase.

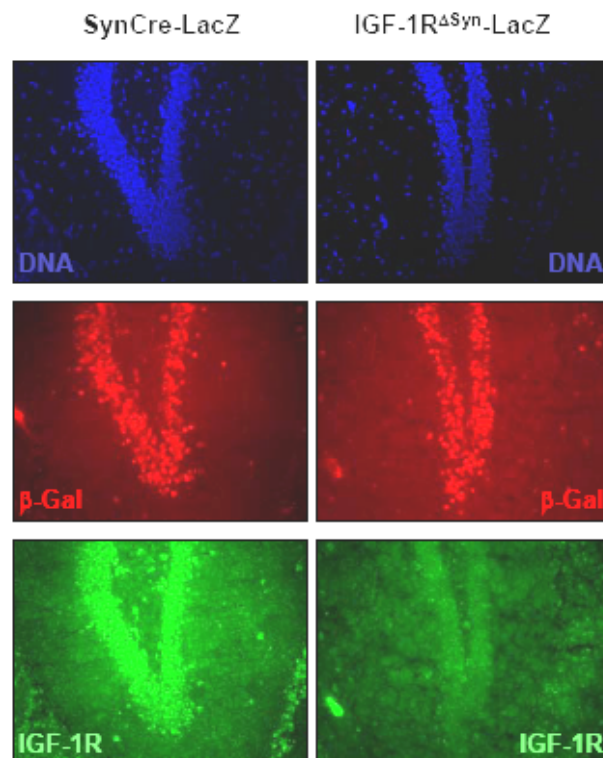


Fig. 45: Reduced IGF-1 receptor expression in the dentate gyrus of IGF1R^{ΔSyn} mice.

Fluorescence immunohistochemical stainings of brains of Control^{ΔSyn} and IGF1R^{ΔSyn} mice. Magnification: 200x. Blue = DAPI = DNA, red = Rhodamin = β-Galactosidase (β-Gal), green = FITC = IGF-1R.

In conclusion, these experiments demonstrate the generation of a central IGF-1 receptor deficiency in IGF-1R^{ΔSyn} mice without significant recombination occurring in the periphery.

3.13 Physiological characterization of IGF-1R^{ΔSyn} mice

3.13.1 Energy homeostasis

To assess the importance of central IGF-1 receptor action in the regulation of energy homeostasis, body weight of IGF-1R^{ΔSyn} and IGF-1R^{flox/flox} (Control^{ΔSyn}) mice was monitored from weaning, 3 weeks after birth, until 7 months of age. This analysis revealed a reduction in body weight of IGF-1R^{ΔSyn} mice compared to littermate controls on the day of weaning, which became indistinguishable from the age of 4 weeks on and remained thus (Fig. 46).

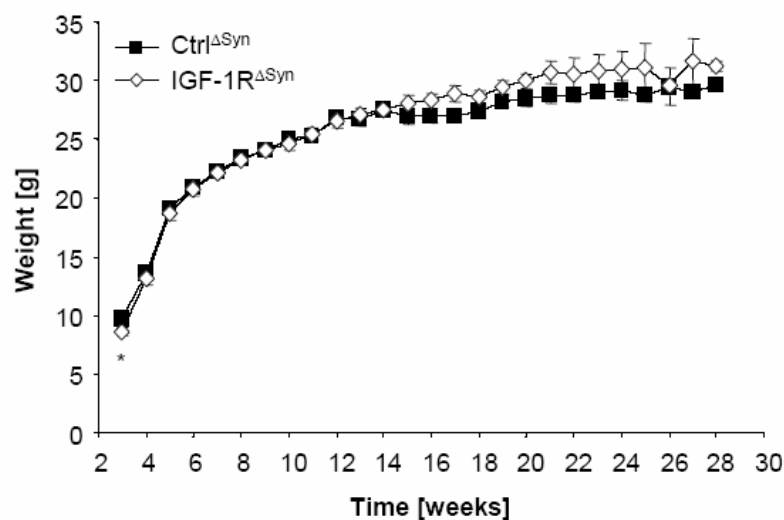


Fig. 46: Body weight of IGF-1R^{ΔSyn} mice.

Average body weight of Control^{ΔSyn} (black squares, n = 24) and IGF-1R^{ΔSyn} mice (white squares, n = 17), over 30 weeks. Litters were weaned at week 3. Values are mean ± SEM. *P ≤ 0.05 versus control.

Consistent with these findings, nuclear magnetic resonance analysis revealed no differences between fat or lean mass of adult IGF-1R^{ΔSyn} and littermate controls (Fig. 47).

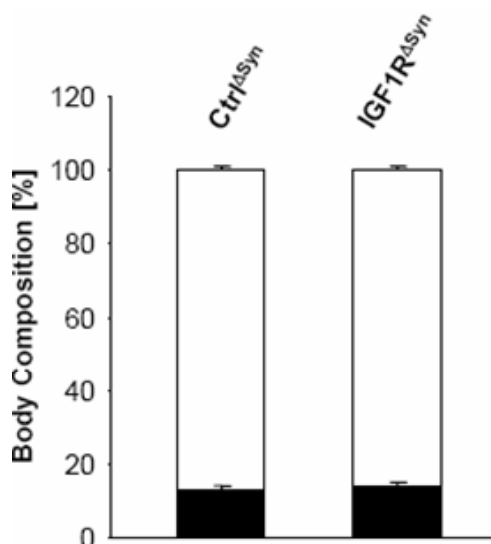


Fig. 47: Unaltered body composition of IGF-1R^{ΔSyn} mice.

Fat mass (black bars) and lean mass (white bars) of Control^{ΔSyn} (n = 6) and IGF-1R^{ΔSyn} mice (n = 3) at the age of 12 weeks. Values are mean ± SEM.

Accordingly, epigonadal fat pad weights were unaltered and no changes were detected in circulating serum leptin and insulin concentrations in adult IGF-1R^{ΔSyn} mice when compared to controls (Fig. 48).

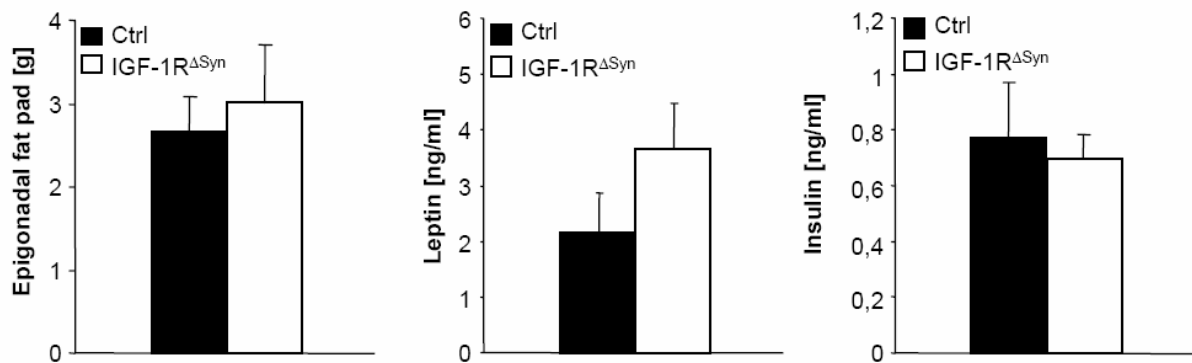


Fig. 48: Central IGF-1 receptor deficiency has no impact on adipose tissue mass or serum leptin and insulin concentrations.

(A) Average weight of epigonadal fat pad correlated to body weight of Control^{ΔSyn} (black bars, n = 3) and IGF-1R^{ΔSyn} mice (white bars, n = 5) at the age of 30 weeks. Values are mean ± SEM. (B) Total serum leptin levels of Control^{ΔSyn} (black bars, n = 12) and IGF-1R^{ΔSyn} mice (white bars, n = 20). Values are mean ± SEM. (C) Total serum insulin levels of Control^{ΔSyn} (black bars, n = 6) and IGF-1R^{ΔSyn} mice (white bars, n = 11). Values are mean ± SEM.

Taken together, these experiments indicate that energy homeostasis in adult mice is unaffected by the targeted disruption of the IGF-1 receptor gene in the central nervous system, at least in those neurons targeted by the Synapsin-1-Cre transgene.

3.13.2 Glucose homeostasis

To analyze the contribution of neuronal IGF-1 receptor signaling in Synapsin-1 positive neurons in the regulation of peripheral glucose homeostasis, glucose concentrations were determined in 18-week-old IGF-1R^{ΔSyn} mice. This analysis revealed that glucose concentrations were indistinguishable between IGF-1R^{ΔSyn} mice and littermate controls both in a random fed and in a fasted state (Fig. 49).

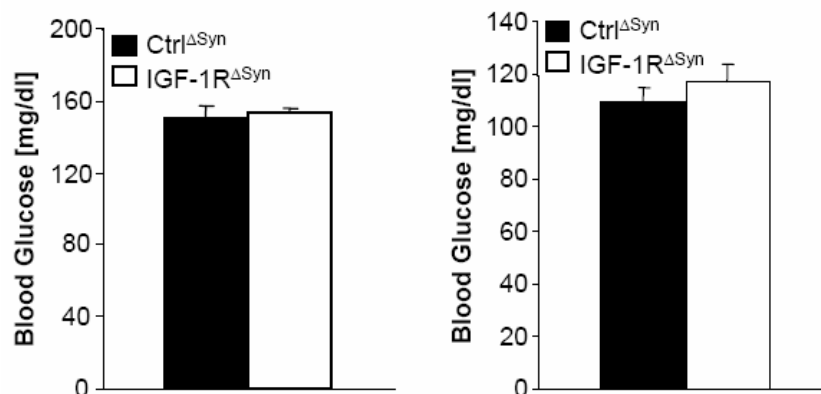


Fig. 49: Loss of central IGF-1 receptor signaling has no impact on blood glucose concentrations.

(A) Random fed blood glucose concentrations of 18-week old Control^{ΔSyn} (filled bars; n = 9) and IGF-1R^{ΔSyn} mice (white bars; n = 5). Data represent the mean ± SEM. (B) Fasted blood glucose concentrations of 18-week old Control^{ΔSyn} (filled bars; n = 9) and IGF-1R^{ΔSyn} mice (white bars; n = 5). Data represent the mean ± SEM.

In addition, no significant changes could be detected when assessing glucose tolerance through i.p. administration of an exogenous glucose challenge. Both IGF-1R^{ΔSyn} mice and littermate controls reacted with a similar increase in blood glucose concentrations and although glucose clearance from the blood appeared at first delayed in IGF-1R^{ΔSyn} mice, all animals returned to original concentrations after 120 minutes (Fig. 53).

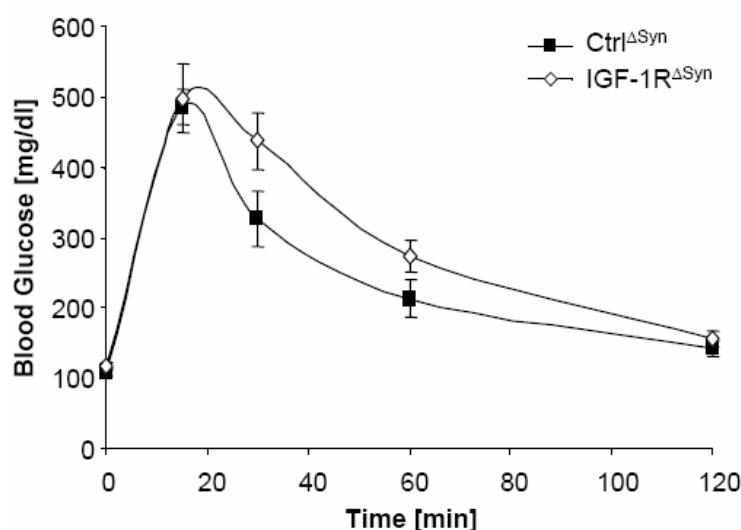


Fig. 50: Unaltered glucose tolerance in IGF-1R^{ΔSyn} mice.

Glucose tolerance test in 18-week-old Control^{ΔSyn} (filled squares, n = 9) and IGF-1R^{ΔSyn} mice (open diamonds; n = 5). Blood glucose concentrations were measured immediately before and 15, 30, 60 and 120 minutes after injection of 2 g/kg of glucose. Data represent the mean ± SEM.

To determine insulin sensitivity, IGF-1R^{ΔSyn} mice and littermate controls received an i.p. injection of insulin, to which all animals reacted with a 30-35% decrease in blood glucose concentrations within 30 minutes after insulin administration, before returning to initial levels 60 minutes after injection (Fig. 51). Again, no differences were noticeable between IGF-1R^{ΔSyn} mice and controls, indicating that loss of central IGF-1 signaling does not lead to insulin resistance.

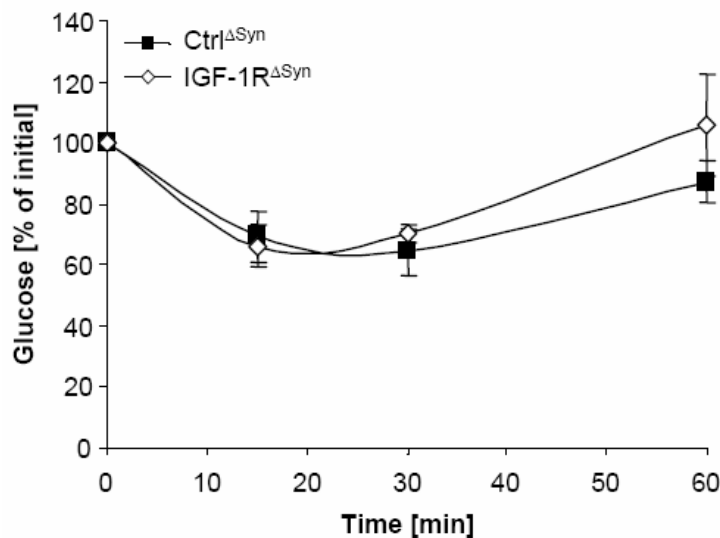


Fig. 51: Unaltered insulin sensitivity in IGF-1R^{ΔSyn} mice.

Insulin tolerance test in Control^{ΔSyn} (filled squares, n = 9) and IGF-1R^{ΔSyn} mice (open diamonds; n = 5) at the age of 18 weeks. Blood glucose concentrations were measured immediately before and 15, 30, and 60 minutes after injection of 0,75 U/kg of insulin. Data represent the mean ± SEM.

In conclusion, loss of signaling through the IGF-1 receptor in the CNS apparently has no consequence for peripheral glucose homeostasis in the presence of normal central insulin action.

3.14 Brain weight is unaffected by central IGF-1R deficiency

The so-called synRas mice express a constitutively active form of the small GTPase Ras in differentiated neurons (206). These animals display severe brain hypertrophy due to an increase in cell size, while the number of neurons remains unaltered (206). This effect could also be detected specifically in hippocampal neurons (207). Since IGF-1 receptor signaling is an important inducer of Ras activity, loss of central IGF-1 receptor signaling and thereby Ras activation could potentially lead to the

opposite effect, resulting in an atrophy of brain tissues. This holds true for IGF-1-deficient mice, which exhibit severe reductions in brain size, in particular a reduced dentate gyrus granule cell layer, as well as CNS hypomyelination (208). To analyze this, brain tissue of IGF-1R^{ΔSyn} and control mice was dissected and weighed. No significant alterations were detected between IGF-1R^{ΔSyn} mice and littermate controls (Fig. 52), indicating that loss of central IGF-1 receptor signaling has no visibly deleterious effect on the central nervous system.

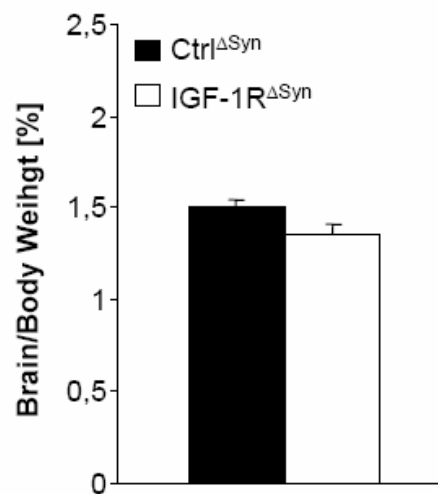


Fig. 52: Unaltered brain weight of IGF-1R^{ΔSyn} mice.

Average brain weight of Control^{ΔSyn} (black bars, n = 8) and IGF-1R^{ΔSyn} mice (white bars, n = 8) at the age of 19 weeks. Values are mean ± SEM.

3.15 Unaltered susceptibility to kainic acid of IGF-1R^{ΔSyn} mice

Systemic IGF-1 has been shown to increase adult neurogenesis and neuronal excitability and is considered a potent neuroprotective factor in the adult brain (189, 209, 210). The glutamate receptor agonist kainic acid (KA) is a potent excitotoxin that causes severe limbic motor seizures culminating in *status epilepticus* when binding to the non-N-methyl-D-aspartate (NMDA) receptors, a subtype of ionotropic glutamate receptors (for review see (211)). Administration of KA induces neuronal apoptosis, predominantly in the hippocampal subregions *cornu ammonis* (CA) 1 and CA3, as well as the dentate gyrus (DG), and increases production of reactive oxygen species (ROS) and mitochondrial dysfunction.

Upon i.p. administration of KA, IGF-1R^{ΔSyn} mice and littermate controls reacted with epileptic seizures starting at an average of 40 min and 57 min after injection,

respectively. The maximum seizure score did not differ between IGF-1R^{ΔSyn} and control mice (Fig. 53).

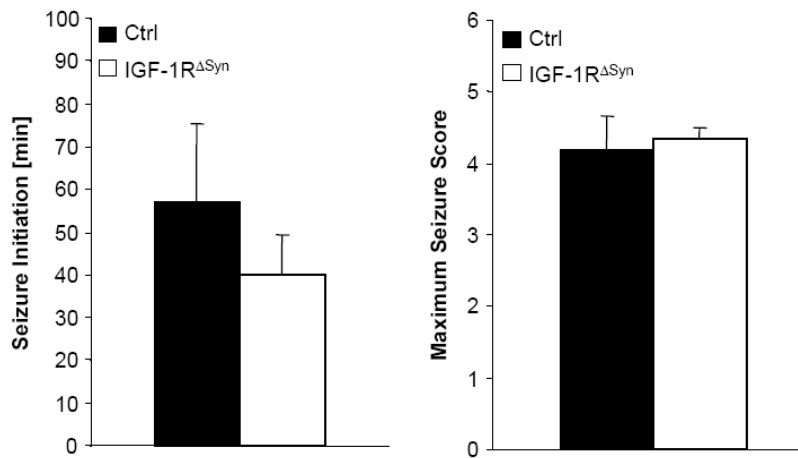
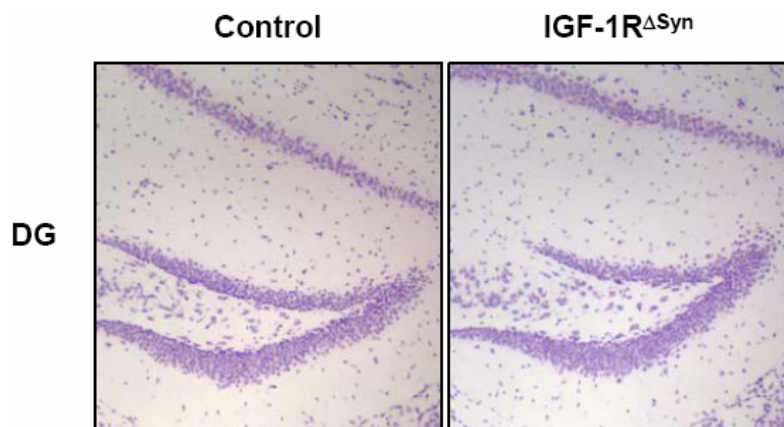


Fig. 53: Central IGF-1 receptor deficiency has no impact on kainic acid-induced seizures.

(A) Seizure initiation time of Control^{ΔSyn} (black bars, n = 6) and IGF-1R^{ΔSyn} mice (white bars, n = 11). Values are mean ± SEM. (B) Maximum seizure score of Control^{ΔSyn} (black bars, n = 6) and IGF-1R^{ΔSyn} mice (white bars, n = 11). Values are mean ± SEM.

Assessment of neuronal damage by Nissl staining revealed no significant differences in the brain regions targeted predominantly by KA, like the dentate gyrus and the CA1 region of the hippocampus (Fig. 54), indicating that loss of central IGF-1 receptor signaling has no consequence for KA-induced neuronal cell death.



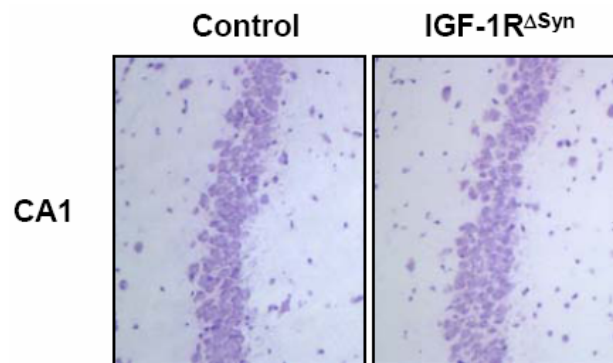


Fig. 54: Kainic acid-induced neuronal damage occurs to similar extent in IGF-1R^{ΔSyn} and control mice.

(A) Nissl staining of the dentate gyrus region of the hippocampus of Control^{ΔSyn} and IGF-1R^{ΔSyn} mice. Magnification: 100x. (B) Nissl staining of the CA1 region of the hippocampus of Control^{ΔSyn} and IGF-1R^{ΔSyn} mice. Magnification: 200x.

3.16 Central IGF-1 receptor deficiency results in loss of spatial memory formation and anxiety-like behavior

A plethora of neurodegenerative diseases, such as Alzheimer's disease, have been associated with altered circulating insulin and IGF-1 concentrations (163). Moreover, IGF-1 levels decline with age, a well-known risk factor in the formation of neurodegenerative conditions (212). Many of these clinical syndromes are associated with disorders of learning and memory, processes that have been linked to the hippocampus. To analyze whether loss of central IGF-1 receptor signaling has any effect on learning and/or memory formation, IGF-1R^{ΔSyn} mice were submitted to a series of behavioral analysis.

The Morris water maze is used to measure hippocampus-dependent learning, such as spatial memory. Spatial memories are formed after gathering and processing information about surroundings by vision and proprioception. Mice are placed in a basin filled with water and are trained in consecutive sessions to find a submerged platform. In a final session, the platform is removed and the time spent in each quadrant of the basin is recorded. Control^{ΔSyn} mice showed a marked preference for the quadrant in which the platform was placed during training, indicating that they memorized the location of the platform, whereas IGF-1R^{ΔSyn} mice were unable to form long-term spatial memories (Fig. 55).

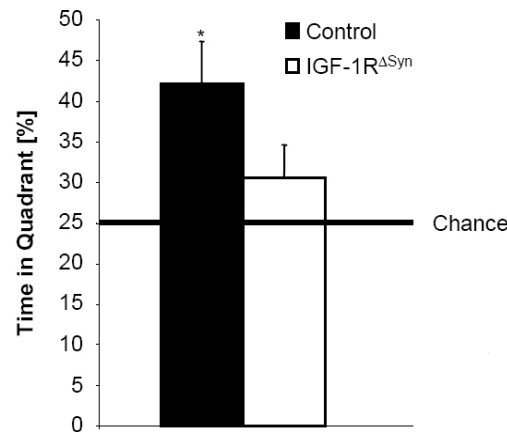


Fig. 55: Spatial navigation working memory is impaired in IGF-1R^{ΔSyn} mice.

Water maze test performed on 6-month-old Control^{ΔSyn} (black bars, n = 5) and IGF-1R^{ΔSyn} mice (white bars, n = 5) after acquisition training on day 7. Time spent in the quadrant previously containing the platform is depicted in %. Free exploration time lasted 60 s. Values are mean ± SEM. *P ≤ 0.05 versus time spent in other quadrants.

The elevated plus-maze task is used to measure anxiety-like behavior. It is based on the observation that rodents prefer the closed arms of a maze to those without walls (193). The open arms of the maze combine the fear of a brightly-lit open field and the fear of balancing on a raised, constricted platform. The closed arms, by contrast, have high walls forming a narrow alley providing possible protection from potential predators. IGF-1R^{ΔSyn} mice exhibited great endurance to anxiety by staying in the open arms of the maze for a longer period than littermate controls (Fig. 56), indicating that lack of central IGF-1 receptor has a tranquilizing, anxiolytic effect.

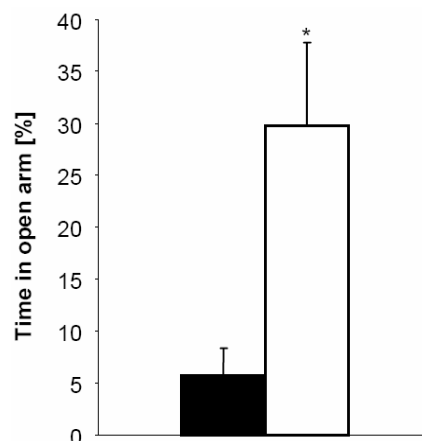


Fig. 56: IGF-1R^{ΔSyn} mice do not display signs of anxiety.

Elevated plus-maze test performed on 6-month-old Control^{ΔSyn} (black bars, n = 5) and IGF-1R^{ΔSyn} mice (white bars, n = 5). Time spent in the open arms is depicted in %. Values are mean ± SEM. *P ≤ 0.05 versus controls.

Motor coordination was assessed using a rotarod apparatus. In this experiment, mice were placed on a horizontal motor-driven rotating rod, with the head directed against the direction of rotation, so that the mouse has to progress forward to avoid falling for a period of 5 minutes. IGF-1R^{ΔSyn} mice performed as well as control littermates in this task and managed to stay on the rotarod for the entire duration of the experiment (Fig. 57).

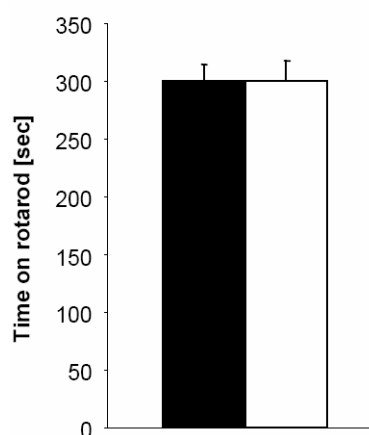


Fig. 57: Unaltered motor coordination in IGF-1R^{ΔSyn} mice.

Rotarod test performed on 6-month-old Control^{ΔSyn} (black bars, n = 5) and IGF-1R^{ΔSyn} mice (white bars, n = 5). Values are mean ± SEM.

The object recognition task is based on the spontaneous novelty-preference paradigm. Under normal circumstances mice will spend more time exploring a new object than a familiar one (213). No differences could be detected in the acquisition of visual recognition memory of IGF-1R^{ΔSyn} mice in comparison to littermate controls (Fig. 58), since both mouse strains exhibited similar preference towards the novel object, indicating that motivation and curiosity are unaltered. These findings were further confirmed using a photocell activity cage to determine exploratory behavior (Fig. 58).

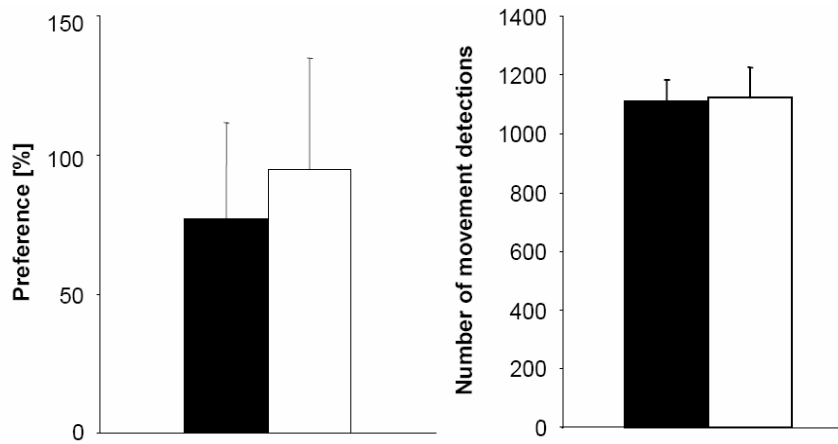


Fig. 58: Unaltered spontaneous novelty preference and exploratory activity in IGF-1R^{ΔSyn} mice.

(A) Preference assessed by object recognition task performed on 6-month-old Control^{ΔSyn} (black bars, n = 5) and IGF-1R^{ΔSyn} mice (white bars, n = 5). Values are mean ± SEM. (B) Number of movement detections during a 60-minute activity trial performed on 6-month-old Control^{ΔSyn} (black bars, n = 5) and IGF-1R^{ΔSyn} mice (white bars, n = 5). Values are mean ± SEM.

In conclusion, these behavioral analyses indicate that IGF-1R^{ΔSyn} mice display an impaired spatial memory acquisition and a loss of reaction to anxiety-inducing stimuli. Motor coordination, object recognition and exploratory behavior, on the other hand, appear to function normally.

4 Discussion

Resistance to the biological effects of the peptide hormone insulin represents one of the hallmarks during the development of type 2 diabetes (214, 215). Apart from the direct effect of impaired insulin action on the dysregulation of glucose and lipid homeostasis (23), insulin resistance predisposes to obesity, atherosclerosis and cardiovascular diseases (reviewed in (216-218)). Nevertheless, the exact molecular mechanisms leading to insulin resistance in patients suffering from type 2 diabetes are largely unknown and it remains unclear whether they are restricted to selective tissues or represent a more body wide phenomenon.

4.1 Inducible mouse models of insulin resistance

To elucidate the contribution of brain insulin signaling compared to peripheral insulin signaling with respect to the pathophysiology of insulin resistance, two novel, acutely inducible insulin receptor-deficient mouse models were employed: the IR^{Δwb} mice show a strong reduction of the insulin receptor in all tissues including the CNS, whereas the IR^{Δper} mice lack the insulin receptor only in the periphery.

The IR^{Δper} mouse model uses a Cre recombinase-steroid receptor fusion protein to acutely induce a peripheral insulin receptor knockout. These RosaCreER^{T2}-expressing mice show little or no recombination in brain, thought to be an effect of a lower local concentration of tamoxifen in the CNS (100). This is potentially attributable to low efficiency transport of tamoxifen through the blood-brain-barrier. Therefore, this model serves as a valuable tool for analyzing the effects of acutely induced peripheral insulin resistance.

The IR^{Δwb} mouse model employs the method of conditional RNAi-mediated gene knockdown through the expression of an ubiquitous insulin receptor-specific shRNA. In both models the onset of systemic insulin resistance can be modulated through administration of inducers, tamoxifen in the former and doxycycline in the latter. The successful generation of these two inducible insulin resistance models was demonstrated. They serve as an ideal model to study the role of insulin action and insulin resistance for the first time in the adult mouse devoid of any developmental compensation, thus bypassing any changes arising from deletion of the insulin receptor during embryonic development. As type 2 diabetes manifests itself during the later

stages of life in humans, the adult mouse model is likely to more accurately resemble human disease.

4.2 Peripheral versus central insulin signaling

Recent studies have provided increasing evidence for a role of neuronal insulin action in the maintenance of glucose homeostasis (219-223). Nevertheless, the debate continues whether insulin's direct or indirect effects on peripheral tissues are more important determinants in these mechanisms. On the one hand, Edgerton *et al.* have shown that insulin's direct effects on the liver regarding the control of hepatic glucose production prove dominant over indirect effects in conscious dogs (224). The importance of insulin's direct effects has also been elaborately described by the analysis of liver insulin receptor knockout mice (LIRKO), which exhibit increased plasma insulin levels and signs of hepatic insulin resistance (135, 145). In contrast, the neuron-specific insulin receptor knockout (NIRKO) mice show an increase in food intake and moderate signs of diet-dependent obesity but also impaired suppression of hepatic glucose production (134); evidence for a significant indirect effect of insulin signaling in the regulation of hepatic glucose production. This is supported by studies employing injections of antisense oligonucleotides (ASO) to impair insulin receptor signaling selectively in the mediobasal hypothalamus (219, 221). These controversial findings have been subject to extensive discussion and have been attributed to differences of glucose metabolism in different species (225). The present study reveals several novel aspects in understanding the consequences and particularly the relative contribution of CNS insulin action to metabolic regulation in adult mice.

4.2.1 The role of central insulin action in lipogenesis

Both IR^{Δper} and IR^{Δwb} mice display a significant reduction of white adipose tissue mass, which was to some extent expected due to the loss of inhibition of lipolysis by insulin as a result of the lack of adipocyte-autonomous insulin signal transduction. Surprisingly, the loss of epigonadal fat pads in IR^{Δwb} mice is much more pronounced compared to IR^{Δper} mice in the presence of the same degree of insulin receptor ablation in adipose tissue. Body composition analysis revealed a significantly more pronounced loss of fat mass in IR^{Δwb} mice, while the size of other organs remained unaltered.

Recent studies suggest the presence of a new neuroendocrine circuit in the CNS involving ghrelin, which is responsible for the regulation of metabolism in adipose tissue (226). Chronic intracerebroventricular administration of ghrelin resulted in an increase in glucose and triglyceride uptake in white adipocytes, inhibition of lipid oxidation and a rise in lipogenesis (226). Our findings suggest a novel role for central insulin in this CNS neuroendocrine network of adipose metabolism. Chronic intracerebroventricular infusion of insulin into the lateral ventricle of C57BL/6 mice resulted in a slightly increased epigonadal fat pad, larger adipocytes and an increase in the fat-storage promoting enzyme lipoprotein lipase compared to mice receiving carrier infusion. As previously mentioned, isolated neuronal insulin resistance, either via tissue-specific knockout mouse models (134) or through injection of ASOs directed against the insulin receptor (219, 221), has been shown to result in mild obesity. The increase in body weight as a consequence of central insulin resistance appears to result from hyperphagia. Lateral intracerebroventricular infusion of insulin as used in the present study, on the other hand, has been shown not to alter food intake in rodents (227), but apparently allows access of insulin to brain areas regulating lipogenesis in white adipose tissue (Fig. 59), indicating a novel role for central insulin in the neuronal control of lipogenesis in addition to the well-documented cell-autonomous inhibition of lipolysis. Taken together, these results reveal differential, partially counterbalancing actions of insulin in the CNS; a catabolic function via control of food intake and an anabolic function via indirect stimulation of lipogenesis. These data are in line with the notion that insulin acts as a primary hormone to control metabolism, while its overall energy homeostasis-regulating function appears to be minor compared to leptin.

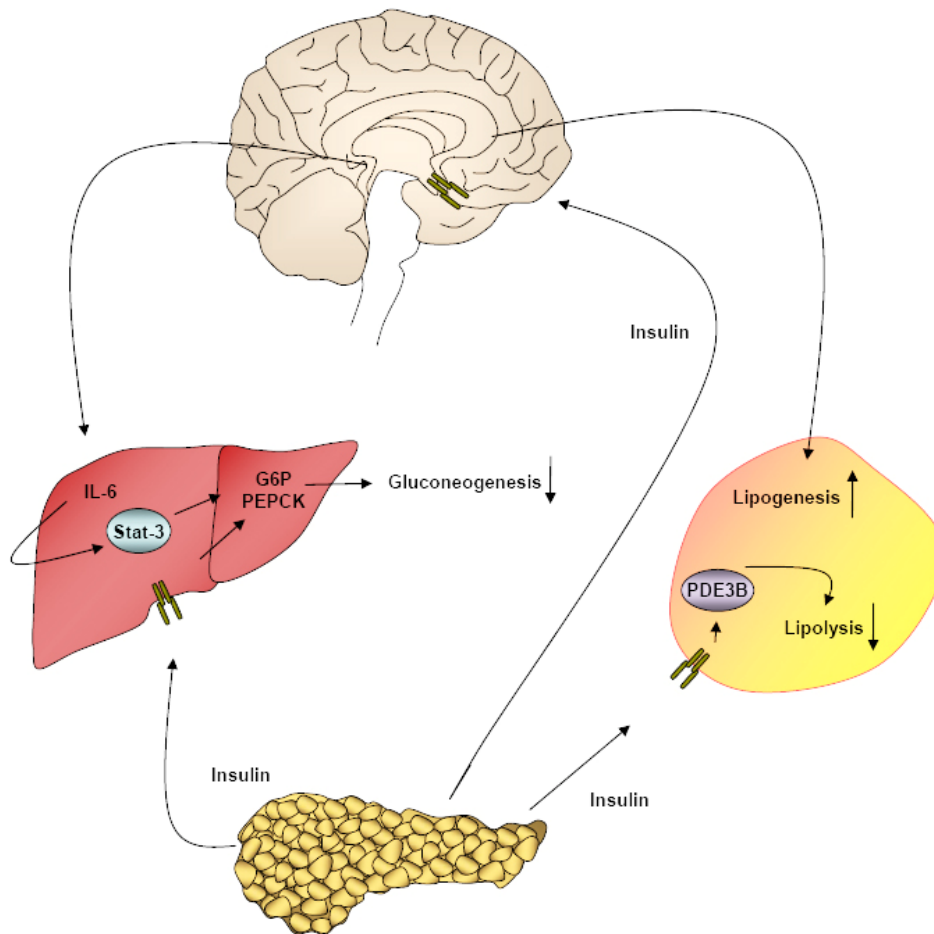


Fig. 59: Proposed model for insulin action in the CNS and in the periphery in the regulation of glucose and adipose tissue metabolism.

Insulin is secreted from the pancreas and binds directly to insulin receptors on peripheral organs such as liver and adipose tissue, thereby mediating signals leading to the downregulation of gluconeogenesis and lipolysis. By binding and activating insulin receptors in the central nervous system, insulin action ultimately leads to the activation of hepatic IL-6 and the upregulation of lipogenic genes in white adipose tissue.

4.2.2 Insulin-mediated inhibition of adipocyte-autonomous leptin secretion

Since adipokine secretion is tightly correlated with the amount of adipose tissue (for review see (228)), the differential regulation of white adipose tissue mass observed in $IR^{\Delta per}$ and $IR^{\Delta wb}$ mice implied consequences for circulating leptin and adiponectin levels. Leptin acts as an essential endocrine signal to the hypothalamus in the control of food intake and energy balance (229). Until today, the effects of insulin on leptin expression remain controversial. *In vitro*, while several studies could detect only mild or no effects of insulin on leptin expression (230-232), others have described a stimulating

function for insulin on leptin expression and secretion in adipocytes (233-235). *In vivo* the contradiction persists, as some groups report that insulin does not regulate leptin expression or secretion (236, 237), yet others have found that insulin increases plasma leptin levels (238, 239). After induction of peripheral insulin resistance, $IR^{\Delta per}$ mice exhibit an increase in circulating leptin concentrations. In contrast, similar to previously published transgenic models of lipodystrophy (240), $IR^{\Delta wb}$ mice display very low circulating leptin levels. However, when correlated to the amount of epigonadal fat, leptin levels are tremendously increased to a similar extent in $IR^{\Delta per}$ mice and in $IR^{\Delta wb}$ mice. Thus, insulin appears to inhibit leptin secretion in a white adipose tissue-autonomous manner, consistent with the idea that loss of insulin receptor signaling specifically in adipocytes results in a rise in leptin secretion from the adipose tissue. In $IR^{\Delta wb}$ mice, although adipocyte-autonomous leptin secretion is increased, absolute levels of circulating leptin are reduced as a consequence of the dramatic reduction in white adipose tissue mass. In $IR^{\Delta per}$ mice, however, the rise in serum leptin concentrations remains visible (Fig. 60).

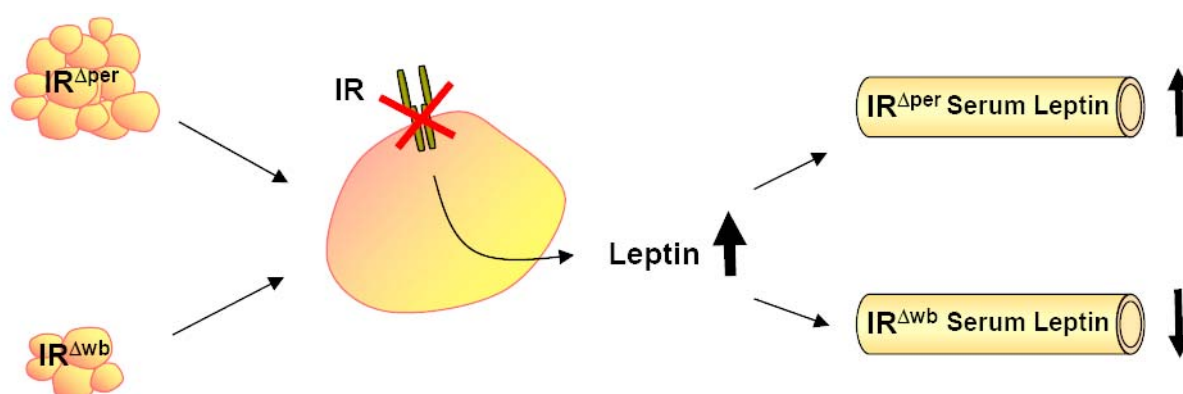


Fig. 60: Proposed model for the effects of insulin resistance on circulating leptin levels.

As a result of the loss peripheral insulin receptor signaling, leptin secretion is disinhibited, resulting in an increase in circulating leptin levels detectable in $IR^{\Delta per}$ mice. In $IR^{\Delta wb}$ mice, however, this effect is masked by a dramatic reduction in white adipose tissue mass.

Concomitantly, adiponectin concentrations of $IR^{\Delta per}$ mice and $IR^{\Delta wb}$ mice were found to be highly upregulated when correlated to white adipose tissue mass. This at first appears paradoxical, since it is well established that total plasma adiponectin is reduced in insulin resistant subjects. However, other studies have previously reported a contradictory hyperadiponectinemia in patients with severe insulin resistance due to

loss-of-function mutations in the insulin receptor (241). Strikingly, mutations in Akt2, a signaling molecule downstream of the insulin receptor in its signal transduction pathway, lead to low leptin and adiponectin concentrations, indicating that elevated adiponectin concentrations in the presence of impaired insulin receptor function may reflect a loss of inhibition of adiponectin expression by an Akt2-independent insulin signaling pathway in adipocytes (241). Further studies revealed that hyperadiponectinemia with loss of insulin receptor function was not dependent on developmental receptor dysfunction (242), a fact supported by the inducible IR^{Δper} and IR^{Δwb} mouse models of insulin resistance here employed.

4.2.3 Hepatic Stat-3 activation and its role in peripheral glucose homeostasis

Leptin mediates its effects by binding to the long isoform of the leptin receptor (ObRb) (243, 244). Both IR^{Δwb} and IR^{Δper} mice show an increase in mRNA expression of the hepatic long isoform of the leptin receptor, as well as a rise in shedding of hepatic ObRb as binding protein (245). Upregulation of ObRb expression in liver could therefore be either a direct consequence of impaired insulin action in hepatocytes or other peripheral tissues as it is observed to similar extents in both mouse models, or a secondary effect caused by increased leptin concentrations as has previously been published (246). However, a similar increase in ObR expression in hepatocyte-specific insulin receptor knockout mice indicates that insulin suppresses ObR expression in liver in a cell-autonomous fashion (247).

Binding of leptin to the leptin receptor leads to receptor homodimerization followed by activation of the Janus Kinases (JAK) which in turn recruit and activate Signal transducer and activator of transcription (Stat) proteins. Activated Stat proteins dimerize and translocate to the nucleus, where they bind to the DNA and activate transcription of target genes (for review see (248)). In addition to elevated leptin levels and increased ObRb mRNA and protein expression, IR^{Δper} mice exhibit significantly increased phosphorylation of hepatic Stat-3. In contrast, expression and tyrosine phosphorylation of Stat-3 in IR^{Δwb} mice that display low plasma leptin concentrations in the presence of elevated ObRb mRNA and protein expression are unaltered.

Also, IL-6 mRNA expression in the liver is significantly increased in IR^{Δper} mice after induction of insulin receptor deficiency, whereas it is unaltered in IR^{Δwb} mice,

indicating a role for central insulin action in the regulation of hepatic IL-6 mRNA expression. Since Stat-3 is not only a target of leptin, but has recently been demonstrated to be a target of the brain insulin signaling pathway by regulation of hepatic IL-6 expression (199, 249), activation of hepatic Stat-3 may either result through intact neuronal insulin signal transduction leading to an upregulation of hepatic IL-6 mRNA expression or as a direct consequence of leptin signaling through the hepatic ObRb.

IR^{Δwb} mice, lacking CNS insulin signaling, suffer from more severe hyperglycemia than IR^{Δper} mice. Restoration of Stat-3 tyrosine phosphorylation in IR^{Δwb} mice results in a significant improvement of hyperglycemia to normal blood glucose levels. Although these experiments cannot ultimately rule out whether improved glucose metabolism in IR^{Δper} mice versus IR^{Δwb} mice is a consequence of Stat-3 phosphorylation caused by maintained IL-6 regulation controlled by insulin signaling in the brain or by elevated leptin concentrations in the presence of increased hepatic ObRb expression, these differential phenotypes of IR^{Δper} and IR^{Δwb} mice provide additional evidence for a physiologically relevant role of activated hepatic Stat-3 signaling in glucose homeostasis in mice.

4.2.4 Effects of peripheral and central insulin deficiency on insulin concentrations and its secretion from the pancreatic β cell

Pancreatic β cell insulin receptor knockout mice (βIRKO) suffer a loss of glucose-stimulated insulin secretion (131). Strikingly, the IR^{Δper} mice exhibited no detectable impairment in this pathway despite showing an insulin receptor deletion of more than 95% in pancreas. A diminished first-phase insulin secretion is an early marker of β cell deterioration, yet this appears not to be the case in IR^{Δper} mice. Fasting plasma insulin levels in IR^{Δwb} mice were significantly higher than those found in IR^{Δper} mice, consistent with a more severe degree of insulin resistance in this mouse model due to higher blood glucose concentrations. Accordingly, although a slight increase in insulin levels upon administration of an exogenous glucose challenge could be detected, the characteristic biphasic pattern of insulin secretion was not detectable. Though significantly enlarged, no structural defects could be detected in pancreatic islets of IR^{Δper} and IR^{Δwb} mice, nor was the distribution of β cells altered in either mouse model. This is a clear indication that the insulin receptor is not required for acute β cell

hyperproliferation, since β cell hyperplasia still occurs and the response to exogenously administered glucose remains unaltered.

4.3 IGF-1 receptor signaling in the central nervous system

4.3.1 Contribution of central IGF-1 receptor signaling to insulin-mediated effects in the periphery

Over the past few years it has become widely acknowledged that insulin has profound effects in the CNS, where it modulates a variety of functions including the regulation of energy homeostasis, sympathetic activity and peripheral glucose homeostasis (134, 221, 250, 251). However, the contribution of central IGF-1 receptor signaling to these processes has so far not been evaluated and may provide novel insights with respect to the pathogenesis of type 2 diabetes and the development of neurodegenerative disorders. To this end, IGF-1R ^{Δ Syn} mice lacking the IGF-1 receptor specifically in Synapsin-1-expressing neurons were generated and efficient reduction in IGF-1 receptor protein expression was demonstrated in the hippocampus and in the parietal cortex of this mouse model.

Analysis of energy and glucose homeostasis in IGF-1R ^{Δ Syn} mice and control littermates indicate that the loss of IGF-1 receptor signal transduction in the hippocampus and cortex has no apparent influence on the regulation of blood glucose or leptin and insulin concentrations. Furthermore, administration of an exogenous glucose or insulin challenge is counter-regulated in a manner comparable to littermate controls.

However, IGF-1R ^{Δ Syn} mice display a reduced body weight compared to controls 3 weeks after birth, at the age of weaning. Whether this reduced body weight is a result of an intrauterine growth retardation or arises from a postnatal growth deficit, potentially due to a deficiency in locating or in memorizing the location of the mother's teat, remains to be determined. The reduced body weight is compensated for as early as one week after weaning and no further differences in body weight between IGF-1R ^{Δ Syn} mice and littermate controls were detected. Concomitantly, epigonadal fat pads and body composition of adult mice lacking central IGF-1 receptor signaling are indistinguishable from those of controls.

In conclusion, IGF-1 receptor signaling in Synapsin-1-expressing neurons apparently has no impact on peripheral glucose or energy homeostasis in the presence of normal insulin signaling. However, one of the key regions involved in the regulation of food intake and energy expenditure is the hypothalamus. Thus, it remains to be determined whether deletion of the IGF-1 receptor in this particular region has any influence on peripheral metabolic actions.

4.3.2 Neuroprotective effects of IGF-1 receptor signaling

Several *in vitro* and *in vivo* studies have revealed IGF-1 to be a neuroprotective factor of hippocampal neurons with respect to the formation of neurodegenerative diseases such as Alzheimer's and Huntington's disease. IGF-1 significantly protected rat primary hippocampal neurons against neurotoxicity induced by A β derivatives (252). Moreover, in a rat model of Huntington's disease, icv infusion of IGF-1 significantly attenuated striatal degeneration after injection of the NMDA receptor agonist quinolinate (253).

Injection of kainic acid (KA), a non-NMDA glutamate receptor agonist, induces excitatory neurotoxicity through acute membrane depolarization and latent cellular toxicity which results in neuronal apoptosis predominantly in the hippocampus. Loss of central IGF-1 receptor signaling, particularly in the hippocampus, would potentially result in a higher susceptibility of IGF-1R Δ Syn mice to KA therefore leading to more severe seizures and increased apoptosis. Upon neuronal degeneration, the Nissl bodies of a neuron disintegrate and dispersion of the Nissl substance occurs, a process called chromatolysis. Staining of Nissl bodies therefore serves as an adequate indicator of neuronal damage. Interestingly, no differences could be detected in seizure initiation time and strength or in the brain morphology after KA injection between IGF-1R Δ Syn mice and littermate controls, indicating that loss of IGF-1 receptor signaling in Synapsin-1-expressing neurons is potentially insufficient to abrogate IGF-1-mediated neuroprotection. This might also explain the indistinguishable weight of brain tissues of IGF-1R Δ Syn mice and littermate controls, whereas IGF-1-deficient mice display a severely reduced brain size, particularly a diminished dentate gyrus granule cell layer (208). On the other hand, mice with an overactivation of Ras, a signaling molecule downstream of the IGF-1 receptor, exhibit severe brain hypertrophy (206). The

activation status of Ras and whether loss of Ras activation is compensated for by a signaling redundancy via the insulin receptor remains to be elucidated.

4.3.3 IGF-1 receptor signaling in learning and memory formation

Many neurodegenerative disorders, such as Alzheimer's disease, are associated with disorders of learning and memory. Since declarative memory cannot be properly assessed in animal models, spatial memory formation in rodents is determined using the Morris water maze task (188). IGF-1R^{ΔSyn} mice performed poorly in this test, suggesting a significant impairment in the formation of long-term memories. The elevated plus maze task (193) was designed to assess stress behavior in combination with anxiety or depression. IGF-1R^{ΔSyn} mice did not display any signs of anxiety in the elevated plus maze, since, in contrast to control littermates, they did not exhibit preference for the closed arms of the maze, indicating that the loss of central IGF-1 receptor signaling has an anxiolytic effect. Conversely, the performance of IGF-1R^{ΔSyn} mice did not differ from that of controls when analyzing the spontaneous novelty paradigm. However, previous studies have shown that hippocampal damage rarely produces significant deficits on object recognition tasks in rodents, suggesting that the hippocampus is not a central component necessary to discriminate familiarity of previously encountered objects (254).

Western blot analyses reveal a significant reduction of IGF-1 receptor protein expression in the hippocampus and to a lesser degree in the parietal cortex of the brain. The parietal lobe has been implicated in the integration of sensory information determining spatial orientation and navigation, while the hippocampus is required for the formation of declarative memory. Loss of IGF-1 receptor signaling in these brain regions has a significant impact on the formation and recollection of spatial memories and results in reduced anxiety-like behavior. Thus, the present study clearly establishes a critical role for IGF-1 signaling in memory formation and/or retention.

4.4 Perspectives and experimental approaches

In conclusion, this thesis defines CNS insulin action as a pivotal determinant of energy homeostasis, peripheral glucose and fat metabolism in the adult mouse. The data support recent findings on the regulation of hepatic Stat-3 activation by central insulin

and indicate a novel role for CNS insulin action in the regulation of adipocyte metabolism.

Furthermore, this thesis demonstrates that loss of IGF-1 receptor signaling in the hippocampus and in the parietal cortex results in a profound deficit in spatial memory acquisition and has an anxiolytic effect, while peripheral glucose and energy homeostasis remain unaffected.

However, as previously mentioned, to entirely rule out any influence of IGF-1 receptor signaling in the CNS on metabolic processes, further experiments are necessary, including deletion of the IGF-1 receptor in the hypothalamus by crossing mice homozygous for the loxP-flanked IGF-1 receptor allele with mice expressing the Cre recombinase under the control of a promoter expressed specifically in this brain region, such as for example the promoters for steroidogenic factor (Sf) 1 or single-minded (Sim) 1.

In addition, to elucidate the underlying molecular mechanism behind the impaired spatial memory formation, current experiments include the measurement of long-term potentiation (LTP) in IGF-1R^{ΔSyn} mice and littermate controls, as well as the generation of a combined insulin receptor and IGF-1 receptor knockout in the CNS. These experiments will aid in determining a contribution of altered insulin and IGF-1 receptor signaling in the central nervous system to the development of neurodegenerative diseases, obesity and diabetes mellitus type 2.

5 Summary

Much of our understanding about insulin has been gained from murine knockouts of the insulin receptor (IR) gene in the whole body or restricted to individual tissues. Here, two novel inducible mouse models with IR inactivation in all tissues including brain ($IR^{\Delta wb}$) or restricted to peripheral tissues ($IR^{\Delta per}$) are described. Crucially, mouse models with inducible deletion later in life allow for the distinction between developmental and acute effects of insulin resistance.

Compared to $IR^{\Delta per}$ mice, body wide deletion of IR has a more pronounced effect on reducing white adipose tissue mass (WAT), despite a similar reduction in IR expression in WAT of both models. The more pronounced lipodystrophy in $IR^{\Delta wb}$ mice points to a novel regulatory function of central insulin receptor signaling in control of lipogenesis which is substantiated by the ability of intracerebroventricularly applied insulin in C57BL/6 mice to slightly increase adipocyte size, fat mass and white adipose tissue lipoprotein lipase expression. Moreover, loss of insulin receptor signaling in adipocytes results in an increase in leptin secretion from the adipose tissue, indicating that insulin inhibits adipocyte-autonomous leptin secretion. In addition to the increase in leptin secretion, both strains display a dramatic upregulation of hepatic leptin receptor expression, while only $IR^{\Delta per}$ mice exhibit increased Stat-3 phosphorylation and IL-6 expression. $IR^{\Delta wb}$ mice, on the other hand, display a higher degree of impaired peripheral glucose metabolism, which is ameliorated by leptin administration along with Stat-3 phosphorylation. Furthermore, despite exhibiting largely reduced IR expression in pancreas, $IR^{\Delta per}$ mice still secrete insulin in response to an acute glucose challenge, whereas glucose-stimulated insulin secretion is abrogated in $IR^{\Delta wb}$ mice, but both mouse models respond to hyperglycemia with a significant increase in β cell mass.

In conclusion, these findings define CNS insulin action as a pivotal determinant of energy homeostasis and peripheral glucose metabolism in the adult mouse and support recent findings on the regulation of hepatic IL-6 mRNA by central insulin. Nevertheless, leptin-activated Stat-3 phosphorylation in liver may alternatively lead to improved glucose metabolism in $IR^{\Delta wb}$ mice.

Furthermore, deletion of the insulin-like growth factor (IGF-) 1 receptor in the central nervous system reveals a significant role for IGF-1 receptor signaling in hippocampal learning and spatial memory acquisition and defines IGF-1R as a potential new therapeutic target in the treatment of conditions linked to anxiety-like behavior.

6 Zusammenfassung

Der heutige Wissensstand über Insulin wurde zum größten Teil aus der Analyse von „Knockout“-Mäusen des Insulinrezeptor (IR) Gens im gesamten Körper oder in spezifischen Geweben gewonnen. Hier werden zwei neue, induzierbare Mausmodelle beschrieben, in denen der IR entweder in allen Geweben inklusive Gehirn ($IR^{\Delta wb}$) oder nur in peripheren Geweben ($IR^{\Delta per}$) inaktiviert werden kann. Die Möglichkeit einer Gendeletion, die erst im adulten Tier induziert wird, ist essentiell für die Differenzierung zwischen akuten und entwicklungsabhängigen Effekten der Insulinresistenz. Trotz gleichartiger IR-Inaktivierung im weißen Fettgewebe beider Mausmodelle, bewirkt die körperweite Deletion des IR eine stärkere Reduktion der weißen Fettmasse im Vergleich zu $IR^{\Delta per}$ Mäusen. Diese erhöhte Lipodystrophie in $IR^{\Delta wb}$ Mäusen deutet auf eine neue regulatorische Funktion des zentralen IR-Signalweges in der Kontrolle der Lipogenese; eine Hypothese, die durch die Erkenntnis unterstützt wird, dass intracerebroventrikular infundiertes Insulin in C57BL/6 Mäusen zu einer Erhöhung von Adipozytengröße, Fettmasse und Lipoprotein Lipase mRNA Expression führt. Darüberhinaus resultiert der Verlust der IR-Signaltransduktion in Adipozyten in einer erhöhten Leptinsekretion. Beide Mausmodelle weisen ebenfalls eine erhöhte hepatische Leptinrezeptor Expression auf, wobei dies nur in $IR^{\Delta per}$ Mäusen auch zu einer verstärkten Stat-3-Phosphorylierung und einer gesteigerten IL-6 mRNA Expression führt. Im Gegensatz dazu weisen $IR^{\Delta wb}$ Mäuse eine stärkere Beeinträchtigung des peripheren Glukosemetabolismus auf, der, ebenso wie die Stat-3-Phosphorylierung, durch chronische Leptininfusion normalisiert wird. Beide Mausmodelle reagieren auf Hyperglykämie mit einer signifikanten Zunahme der β -Zellmasse, wobei die Glukose-stimulierte Insulinsekretion nur noch in $IR^{\Delta per}$ Mäusen funktioniert. Zusammenfassend belegen diese Ergebnisse eindeutig, dass die zentrale Insulinsignaltransduktion wesentlich für die Regulation des peripheren Energiehaushaltes und Glukosemetabolismus der Maus ist. Zudem unterstützen sie bereits vorhandene Erkenntnisse zur Regulation hepatischer IL-6 mRNA durch zentrales Insulin. Allerdings besteht die Möglichkeit, dass die Leptin-aktivierte Stat-3-Phosphorylierung in der Leber von $IR^{\Delta wb}$ Mäusen zur Verminderung der Hyperglykämie führt.

Des Weiteren weist die Deletion des IGF-1 Rezeptorgens im zentralen Nervensystem auf eine relevante Rolle der IGF-1 Signaltransduktion bei der Bildung

räumlicher Erinnerungen hin und liefert einen neuen potenziellen Ansatz für die Behandlung von Angstzuständen.

7 References

1. Centers for Disease Control and Prevention. 2005. National diabetes fact sheet: general information and national estimates on diabetes in the United States, 2005.: Atlanta, GA: U.S. Department of Health and Human Services, Centers for Disease Control and Prevention, 2005.
2. King, K.M., and Rubin, G. 2003. A history of diabetes: from antiquity to discovering insulin. *Br J Nurs* 12:1091-1095.
3. Sanders, L.J. 2002. From Thebes to Toronto and the 21st Century: An Incredible Journey. *Diabetes Spectrum* 15:56-60.
4. MacCracken, J., and Hoel, D. 1997. From ants to analogues. Puzzles and promises in diabetes management. *Postgrad Med* 101:138-140, 143-135, 149-150.
5. Willis, T. 1685. The London practice of physick. Basset & Crooke, London, 1685:238-255, 273-234.
6. Dobson, M. 1776. Experiments and observations on the urine in diabetes. *Medical Observations and Inquiries*, London.
7. Cawley, T. 1788. A singular case of diabetes, consisting entirely in the quantity of urine: With an inquiry into the different theories of the disease. *Lond Med J* 9:286-308.
8. Von Mering, J., and Minkowski, O. 1890. Diabetes mellitus nach Pankreasextirpation. *Arch Exp Pathol Pharmacol* 26:371-387.
9. Benedum, J. 1999. The early history of endocrine cell transplantation. *J Mol Med* 77:30-35.
10. Sharpey-Schafer, E.A. 1916. *The Endocrine organs: an introduction to the study of internal secretion*: London: Longmans, Green. 156 pp.
11. Banting, F.G., Best, C.H., Collip, J.B., Campbell, W.R., and Fletcher, A.A. 1922. Pancreatic extracts in the treatment of diabetes mellitus. Preliminary report. *CMAJ* 22:141-146.
12. Steiner, D.F., Cunningham, D., Spigelman, L., and Aten, B. 1967. Insulin biosynthesis: evidence for a precursor. *Science* 157:697-700.
13. Orci, L., Ravazzola, M., Amherdt, M., Madsen, O., Vassalli, J.D., and Perrelet, A. 1985. Direct identification of prohormone conversion site in insulin-secreting cells. *Cell* 42:671-681.

References

14. Davidson, H.W., Rhodes, C.J., and Hutton, J.C. 1988. Intraorganellar calcium and pH control proinsulin cleavage in the pancreatic beta cell via two distinct site-specific endopeptidases. *Nature* 333:93-96.
15. Docherty, K., and Hutton, J.C. 1983. Carboxypeptidase activity in the insulin secretory granule. *FEBS Lett* 162:137-141.
16. Davidson, H.W., and Hutton, J.C. 1987. The insulin-secretory-granule carboxypeptidase H. Purification and demonstration of involvement in proinsulin processing. *Biochem J* 245:575-582.
17. Steiner, D.F., Clark, J.L., Nolan, C., Rubenstein, A.H., Margoliash, E., Aten, B., and Oyer, P.E. 1969. Proinsulin and the biosynthesis of insulin. *Recent Prog Horm Res* 25:207-282.
18. Duckworth, W.C., Bennett, R.G., and Hamel, F.G. 1998. Insulin degradation: progress and potential. *Endocr Rev* 19:608-624.
19. Birnbaum, M.J. 1992. The insulin-sensitive glucose transporter. *Int Rev Cytol* 137:239-297.
20. Cushman, S.W., and Wardzala, L.J. 1980. Potential mechanism of insulin action on glucose transport in the isolated rat adipose cell. Apparent translocation of intracellular transport systems to the plasma membrane. *J Biol Chem* 255:4758-4762.
21. Cushman, S.W., Wardzala, L.J., Simpson, I.A., Karnieli, E., Hissin, P.J., Wheeler, T.J., Hinkle, P.C., and Salans, L.B. 1984. Insulin-induced translocation of intracellular glucose transporters in the isolated rat adipose cell. *Fed Proc* 43:2251-2255.
22. Pilkis, S.J., and Granner, D.K. 1992. Molecular physiology of the regulation of hepatic gluconeogenesis and glycolysis. *Annu Rev Physiol* 54:885-909.
23. Saltiel, A.R., and Kahn, C.R. 2001. Insulin signalling and the regulation of glucose and lipid metabolism. *Nature* 414:799-806.
24. Shier, P., and Watt, V.M. 1989. Primary structure of a putative receptor for a ligand of the insulin family. *J Biol Chem* 264:14605-14608.
25. Ullrich, A., Gray, A., Tam, A.W., Yang-Feng, T., Tsubokawa, M., Collins, C., Henzel, W., Le Bon, T., Kathuria, S., Chen, E., et al. 1986. Insulin-like growth factor I receptor primary structure: comparison with insulin receptor suggests structural determinants that define functional specificity. *Embo J* 5:2503-2512.
26. Rosen, O.M. 1987. After insulin binds. *Science* 237:1452-1458.

27. Jacobs, S., Hazum, E., Shechter, Y., and Cuatrecasas, P. 1979. Insulin receptor: covalent labeling and identification of subunits. *Proc Natl Acad Sci U S A* 76:4918-4921.
28. Kasuga, M., Hedo, J.A., Yamada, K.M., and Kahn, C.R. 1982. The structure of insulin receptor and its subunits. Evidence for multiple nonreduced forms and a 210,000 possible proreceptor. *J Biol Chem* 257:10392-10399.
29. Van Obberghen, E., Ksauga, M., Le Cam, A., Hedo, J.A., Itin, A., and Harrison, L.C. 1981. Biosynthetic labeling of insulin receptor: studies of subunits in cultured human IM-9 lymphocytes. *Proc Natl Acad Sci U S A* 78:1052-1056.
30. Kasuga, M., Fujita-Yamaguchi, Y., Blithe, D.L., and Kahn, C.R. 1983. Tyrosine-specific protein kinase activity is associated with the purified insulin receptor. *Proc Natl Acad Sci U S A* 80:2137-2141.
31. Chou, C.K., Dull, T.J., Russell, D.S., Gherzi, R., Lebwohl, D., Ullrich, A., and Rosen, O.M. 1987. Human insulin receptors mutated at the ATP-binding site lack protein tyrosine kinase activity and fail to mediate postreceptor effects of insulin. *J Biol Chem* 262:1842-1847.
32. Ebina, Y., Araki, E., Taira, M., Shimada, F., Mori, M., Craik, C.S., Siddle, K., Pierce, S.B., Roth, R.A., and Rutter, W.J. 1987. Replacement of lysine residue 1030 in the putative ATP-binding region of the insulin receptor abolishes insulin- and antibody-stimulated glucose uptake and receptor kinase activity. *Proc Natl Acad Sci U S A* 84:704-708.
33. Ebina, Y., Ellis, L., Jarnagin, K., Edery, M., Graf, L., Clauser, E., Ou, J.H., Masiarz, F., Kan, Y.W., Goldfine, I.D., et al. 1985. The human insulin receptor cDNA: the structural basis for hormone-activated transmembrane signalling. *Cell* 40:747-758.
34. Seino, S., Seino, M., and Bell, G.I. 1990. Human insulin-receptor gene. *Diabetes* 39:129-133.
35. Seino, S., Seino, M., Nishi, S., and Bell, G.I. 1989. Structure of the human insulin receptor gene and characterization of its promoter. *Proc Natl Acad Sci U S A* 86:114-118.
36. Braciale, V.L., Gavin, J.R., 3rd, and Braciale, T.J. 1982. Inducible expression of insulin receptors on T lymphocyte clones. *J Exp Med* 156:664-669.
37. Harbeck, M.C., Louie, D.C., Howland, J., Wolf, B.A., and Rothenberg, P.L. 1996. Expression of insulin receptor mRNA and insulin receptor substrate 1 in pancreatic islet beta-cells. *Diabetes* 45:711-717.

References

38. Marks, J.L., Porte, D., Jr., Stahl, W.L., and Baskin, D.G. 1990. Localization of insulin receptor mRNA in rat brain by in situ hybridization. *Endocrinology* 127:3234-3236.
39. Czech, M.P., Lewis, R.E., and Corvera, S. 1989. Multifunctional glycoprotein receptors for insulin and the insulin-like growth factors. *Ciba Found Symp* 145:27-41; discussion 42-24.
40. Perdue, J.F. 1984. Chemistry, structure, and function of insulin-like growth factors and their receptors: a review. *Can J Biochem Cell Biol* 62:1237-1245.
41. Kahn, C.R., Baird, K.L., Jarrett, D.B., and Flier, J.S. 1978. Direct demonstration that receptor crosslinking or aggregation is important in insulin action. *Proc Natl Acad Sci U S A* 75:4209-4213.
42. Eck, M.J., Dhe-Paganon, S., Trub, T., Nolte, R.T., and Shoelson, S.E. 1996. Structure of the IRS-1 PTB domain bound to the juxtamembrane region of the insulin receptor. *Cell* 85:695-705.
43. Miralpeix, M., Sun, X.J., Backer, J.M., Myers, M.G., Jr., Araki, E., and White, M.F. 1992. Insulin stimulates tyrosine phosphorylation of multiple high molecular weight substrates in Fao hepatoma cells. *Biochemistry* 31:9031-9039.
44. White, M.F., Livingston, J.N., Backer, J.M., Lauris, V., Dull, T.J., Ullrich, A., and Kahn, C.R. 1988. Mutation of the insulin receptor at tyrosine 960 inhibits signal transmission but does not affect its tyrosine kinase activity. *Cell* 54:641-649.
45. Burks, D.J., Pons, S., Towery, H., Smith-Hall, J., Myers, M.G., Jr., Yenush, L., and White, M.F. 1997. Heterologous pleckstrin homology domains do not couple IRS-1 to the insulin receptor. *J Biol Chem* 272:27716-27721.
46. Burks, D.J., Wang, J., Towery, H., Ishibashi, O., Lowe, D., Riedel, H., and White, M.F. 1998. IRS pleckstrin homology domains bind to acidic motifs in proteins. *J Biol Chem* 273:31061-31067.
47. Jacobs, A.R., LeRoith, D., and Taylor, S.I. 2001. Insulin receptor substrate-1 pleckstrin homology and phosphotyrosine-binding domains are both involved in plasma membrane targeting. *J Biol Chem* 276:40795-40802.
48. Sun, X.J., Rothenberg, P., Kahn, C.R., Backer, J.M., Araki, E., Wilden, P.A., Cahill, D.A., Goldstein, B.J., and White, M.F. 1991. Structure of the insulin receptor substrate IRS-1 defines a unique signal transduction protein. *Nature* 352:73-77.

49. Sun, X.J., Wang, L.M., Zhang, Y., Yenush, L., Myers, M.G., Jr., Glasheen, E., Lane, W.S., Pierce, J.H., and White, M.F. 1995. Role of IRS-2 in insulin and cytokine signalling. *Nature* 377:173-177.
50. Lavan, B.E., Fantin, V.R., Chang, E.T., Lane, W.S., Keller, S.R., and Lienhard, G.E. 1997. A novel 160-kDa phosphotyrosine protein in insulin-treated embryonic kidney cells is a new member of the insulin receptor substrate family. *J Biol Chem* 272:21403-21407.
51. Holgado-Madruga, M., Emllet, D.R., Moscatello, D.K., Godwin, A.K., and Wong, A.J. 1996. A Grb2-associated docking protein in EGF- and insulin-receptor signalling. *Nature* 379:560-564.
52. Lavan, B.E., Lane, W.S., and Lienhard, G.E. 1997. The 60-kDa phosphotyrosine protein in insulin-treated adipocytes is a new member of the insulin receptor substrate family. *J Biol Chem* 272:11439-11443.
53. Lehr, S., Kotzka, J., Herkner, A., Sikmann, A., Meyer, H.E., Krone, W., and Muller-Wieland, D. 2000. Identification of major tyrosine phosphorylation sites in the human insulin receptor substrate Gab-1 by insulin receptor kinase in vitro. *Biochemistry* 39:10898-10907.
54. Sciacchitano, S., and Taylor, S.I. 1997. Cloning, tissue expression, and chromosomal localization of the mouse IRS-3 gene. *Endocrinology* 138:4931-4940.
55. De Fea, K., and Roth, R.A. 1997. Protein kinase C modulation of insulin receptor substrate-1 tyrosine phosphorylation requires serine 612. *Biochemistry* 36:12939-12947.
56. Myers, M.G., Jr., Backer, J.M., Sun, X.J., Shoelson, S., Hu, P., Schlessinger, J., Yoakim, M., Schaffhausen, B., and White, M.F. 1992. IRS-1 activates phosphatidylinositol 3'-kinase by associating with src homology 2 domains of p85. *Proc Natl Acad Sci U S A* 89:10350-10354.
57. Myers, M.G., Jr., Sun, X.J., Cheatham, B., Jachna, B.R., Glasheen, E.M., Backer, J.M., and White, M.F. 1993. IRS-1 is a common element in insulin and insulin-like growth factor-I signaling to the phosphatidylinositol 3'-kinase. *Endocrinology* 132:1421-1430.
58. Skolnik, E.Y., Batzer, A., Li, N., Lee, C.H., Lowenstein, E., Mohammadi, M., Margolis, B., and Schlessinger, J. 1993. The function of GRB2 in linking the insulin receptor to Ras signaling pathways. *Science* 260:1953-1955.
59. Rocchi, S., Tartare-Deckert, S., Sawka-Verhelle, D., Gamha, A., and van Obberghen, E. 1996. Interaction of SH2-containing protein tyrosine phosphatase 2 with the insulin receptor and the insulin-like growth factor-I receptor: studies

References

- of the domains involved using the yeast two-hybrid system. *Endocrinology* 137:4944-4952.
60. Katso, R., Okkenhaug, K., Ahmadi, K., White, S., Timms, J., and Waterfield, M.D. 2001. Cellular function of phosphoinositide 3-kinases: implications for development, homeostasis, and cancer. *Annu Rev Cell Dev Biol* 17:615-675.
 61. Skolnik, E.Y., Margolis, B., Mohammadi, M., Lowenstein, E., Fischer, R., Drepps, A., Ullrich, A., and Schlessinger, J. 1991. Cloning of PI3 kinase-associated p85 utilizing a novel method for expression/cloning of target proteins for receptor tyrosine kinases. *Cell* 65:83-90.
 62. Whitman, M., Downes, C.P., Keeler, M., Keller, T., and Cantley, L. 1988. Type I phosphatidylinositol kinase makes a novel inositol phospholipid, phosphatidylinositol-3-phosphate. *Nature* 332:644-646.
 63. Vanhaesebroeck, B., and Alessi, D.R. 2000. The PI3K-PDK1 connection: more than just a road to PKB. *Biochem J* 346 Pt 3:561-576.
 64. Cheatham, B., and Kahn, C.R. 1995. Insulin action and the insulin signaling network. *Endocr Rev* 16:117-142.
 65. Evans, M.J., and Kaufman, M.H. 1981. Establishment in culture of pluripotential cells from mouse embryos. *Nature* 292:154-156.
 66. Smithies, O., Gregg, R.G., Boggs, S.S., Koralewski, M.A., and Kucherlapati, R.S. 1985. Insertion of DNA sequences into the human chromosomal beta-globin locus by homologous recombination. *Nature* 317:230-234.
 67. Thomas, K.R., Folger, K.R., and Capecchi, M.R. 1986. High frequency targeting of genes to specific sites in the mammalian genome. *Cell* 44:419-428.
 68. Capecchi, M.R. 1989. Altering the genome by homologous recombination. *Science* 244:1288-1292.
 69. Kuhn, R., and Schwenk, F. 1997. Advances in gene targeting methods. *Curr Opin Immunol* 9:183-188.
 70. Rajewsky, K., Gu, H., Kuhn, R., Betz, U.A., Muller, W., Roes, J., and Schwenk, F. 1996. Conditional gene targeting. *J Clin Invest* 98:600-603.
 71. Sternberg, N., and Hamilton, D. 1981. Bacteriophage P1 site-specific recombination. I. Recombination between loxP sites. *J Mol Biol* 150:467-486.
 72. Sternberg, N., Hamilton, D., and Hoess, R. 1981. Bacteriophage P1 site-specific recombination. II. Recombination between loxP and the bacterial chromosome. *J Mol Biol* 150:487-507.

73. Sauer, B., and Henderson, N. 1988. Site-specific DNA recombination in mammalian cells by the Cre recombinase of bacteriophage P1. *Proc Natl Acad Sci U S A* 85:5166-5170.
74. Gu, H., Zou, Y.R., and Rajewsky, K. 1993. Independent control of immunoglobulin switch recombination at individual switch regions evidenced through Cre-loxP-mediated gene targeting. *Cell* 73:1155-1164.
75. Kano, M., Igarashi, H., Saito, I., and Masuda, M. 1998. Cre-loxP-mediated DNA flip-flop in mammalian cells leading to alternate expression of retrovirally transduced genes. *Biochem Biophys Res Commun* 248:806-811.
76. Lam, K.P., and Rajewsky, K. 1998. Rapid elimination of mature autoreactive B cells demonstrated by Cre-induced change in B cell antigen receptor specificity in vivo. *Proc Natl Acad Sci U S A* 95:13171-13175.
77. Abremski, K., Hoess, R., and Sternberg, N. 1983. Studies on the properties of P1 site-specific recombination: evidence for topologically unlinked products following recombination. *Cell* 32:1301-1311.
78. Kilby, N.J., Snaith, M.R., and Murray, J.A. 1993. Site-specific recombinases: tools for genome engineering. *Trends Genet* 9:413-421.
79. Dymecki, S.M. 1996. A modular set of FLP, FRT and lacZ fusion vectors for manipulating genes by site-specific recombination. *Gene* 171:197-201.
80. McLeod, M., Craft, S., and Broach, J.R. 1986. Identification of the crossover site during FLP-mediated recombination in the *Saccharomyces cerevisiae* plasmid 2 microns circle. *Mol Cell Biol* 6:3357-3367.
81. Thomas, K.R., and Capecchi, M.R. 1987. Site-directed mutagenesis by gene targeting in mouse embryo-derived stem cells. *Cell* 51:503-512.
82. Thomas, K.R., Deng, C., and Capecchi, M.R. 1992. High-fidelity gene targeting in embryonic stem cells by using sequence replacement vectors. *Mol Cell Biol* 12:2919-2923.
83. Bradley, A., Evans, M., Kaufman, M.H., and Robertson, E. 1984. Formation of germ-line chimaeras from embryo-derived teratocarcinoma cell lines. *Nature* 309:255-256.
84. Robertson, E., Bradley, A., Kuehn, M., and Evans, M. 1986. Germ-line transmission of genes introduced into cultured pluripotential cells by retroviral vector. *Nature* 323:445-448.
85. Gossler, A., Doetschman, T., Korn, R., Serfling, E., and Kemler, R. 1986. Transgenesis by means of blastocyst-derived embryonic stem cell lines. *Proc Natl Acad Sci U S A* 83:9065-9069.

References

86. Schwartzberg, P.L., Goff, S.P., and Robertson, E.J. 1989. Germ-line transmission of a c-abl mutation produced by targeted gene disruption in ES cells. *Science* 246:799-803.
87. Zijlstra, M., Li, E., Sajjadi, F., Subramani, S., and Jaenisch, R. 1989. Germ-line transmission of a disrupted beta 2-microglobulin gene produced by homologous recombination in embryonic stem cells. *Nature* 342:435-438.
88. Rickert, R.C., Rajewsky, K., and Roes, J. 1995. Impairment of T-cell-dependent B-cell responses and B-1 cell development in CD19-deficient mice. *Nature* 376:352-355.
89. Testa, G., Zhang, Y., Vintersten, K., Benes, V., Pijnappel, W.W., Chambers, I., Smith, A.J., Smith, A.G., and Stewart, A.F. 2003. Engineering the mouse genome with bacterial artificial chromosomes to create multipurpose alleles. *Nat Biotechnol* 21:443-447.
90. Plum, L., Wunderlich, F.T., Baudler, S., Krone, W., and Bruning, J.C. 2005. Transgenic and knockout mice in diabetes research: novel insights into pathophysiology, limitations, and perspectives. *Physiology (Bethesda)* 20:152-161.
91. Passinen, S., Haverinen, M., Pekki, A., Rauta, J., Paranko, J., Syvala, H., Tuohimaa, P., and Ylikomi, T. 1999. Only a small portion of the cytoplasmic progesterone receptor is associated with Hsp90 in vivo. *J Cell Biochem* 74:458-467.
92. Allan, G.F., Leng, X., Tsai, S.Y., Weigel, N.L., Edwards, D.P., Tsai, M.J., and O'Malley, B.W. 1992. Hormone and antihormone induce distinct conformational changes which are central to steroid receptor activation. *J Biol Chem* 267:19513-19520.
93. Guiochon-Mantel, A., Loosfelt, H., Lescop, P., Sar, S., Atger, M., Perrot-Appinat, M., and Milgrom, E. 1989. Mechanisms of nuclear localization of the progesterone receptor: evidence for interaction between monomers. *Cell* 57:1147-1154.
94. Tyagi, R.K., Amazit, L., Lescop, P., Milgrom, E., and Guiochon-Mantel, A. 1998. Mechanisms of progesterone receptor export from nuclei: role of nuclear localization signal, nuclear export signal, and ran guanosine triphosphate. *Mol Endocrinol* 12:1684-1695.
95. Brocard, J., Feil, R., Chambon, P., and Metzger, D. 1998. A chimeric Cre recombinase inducible by synthetic, but not by natural ligands of the glucocorticoid receptor. *Nucleic Acids Res* 26:4086-4090.

96. Kellendonk, C., Tronche, F., Casanova, E., Anlag, K., Opherk, C., and Schutz, G. 1999. Inducible site-specific recombination in the brain. *J Mol Biol* 285:175-182.
97. Schwenk, F., Kuhn, R., Angrand, P.O., Rajewsky, K., and Stewart, A.F. 1998. Temporally and spatially regulated somatic mutagenesis in mice. *Nucleic Acids Res* 26:1427-1432.
98. Picard, D. 1994. Regulation of protein function through expression of chimaeric proteins. *Curr Opin Biotechnol* 5:511-515.
99. Feil, R., Wagner, J., Metzger, D., and Chambon, P. 1997. Regulation of Cre recombinase activity by mutated estrogen receptor ligand-binding domains. *Biochem Biophys Res Commun* 237:752-757.
100. Seibler, J., Zevnik, B., Kuter-Luks, B., Andreas, S., Kern, H., Hennek, T., Rode, A., Heimann, C., Faust, N., Kauselmann, G., et al. 2003. Rapid generation of inducible mouse mutants. *Nucleic Acids Res* 31:e12.
101. Casanova, E., Fehsenfeld, S., Lemberger, T., Shimshek, D.R., Sprengel, R., and Mantamadiotis, T. 2002. ER-based double iCre fusion protein allows partial recombination in forebrain. *Genesis* 34:208-214.
102. Forde, A., Constien, R., Grone, H.J., Hammerling, G., and Arnold, B. 2002. Temporal Cre-mediated recombination exclusively in endothelial cells using Tie2 regulatory elements. *Genesis* 33:191-197.
103. Kuhbandner, S., Brummer, S., Metzger, D., Chambon, P., Hofmann, F., and Feil, R. 2000. Temporally controlled somatic mutagenesis in smooth muscle. *Genesis* 28:15-22.
104. Fire, A., Xu, S., Montgomery, M.K., Kostas, S.A., Driver, S.E., and Mello, C.C. 1998. Potent and specific genetic interference by double-stranded RNA in *Caenorhabditis elegans*. *Nature* 391:806-811.
105. Elbashir, S.M., Lendeckel, W., and Tuschl, T. 2001. RNA interference is mediated by 21- and 22-nucleotide RNAs. *Genes Dev* 15:188-200.
106. Bernstein, E., Caudy, A.A., Hammond, S.M., and Hannon, G.J. 2001. Role for a bidentate ribonuclease in the initiation step of RNA interference. *Nature* 409:363-366.
107. Grishok, A., Pasquinelli, A.E., Conte, D., Li, N., Parrish, S., Ha, I., Baillie, D.L., Fire, A., Ruvkun, G., and Mello, C.C. 2001. Genes and mechanisms related to RNA interference regulate expression of the small temporal RNAs that control *C. elegans* developmental timing. *Cell* 106:23-34.

References

108. Ketting, R.F., Fischer, S.E., Bernstein, E., Sijen, T., Hannon, G.J., and Plasterk, R.H. 2001. Dicer functions in RNA interference and in synthesis of small RNA involved in developmental timing in *C. elegans*. *Genes Dev* 15:2654-2659.
109. Song, J.J., Liu, J., Tolia, N.H., Schneiderman, J., Smith, S.K., Martienssen, R.A., Hannon, G.J., and Joshua-Tor, L. 2003. The crystal structure of the Argonaute2 PAZ domain reveals an RNA binding motif in RNAi effector complexes. *Nat Struct Biol* 10:1026-1032.
110. Yan, K.S., Yan, S., Farooq, A., Han, A., Zeng, L., and Zhou, M.M. 2003. Structure and conserved RNA binding of the PAZ domain. *Nature* 426:468-474.
111. Zamore, P.D., Tuschl, T., Sharp, P.A., and Bartel, D.P. 2000. RNAi: double-stranded RNA directs the ATP-dependent cleavage of mRNA at 21 to 23 nucleotide intervals. *Cell* 101:25-33.
112. McManus, M.T., and Sharp, P.A. 2002. Gene silencing in mammals by small interfering RNAs. *Nat Rev Genet* 3:737-747.
113. Paddison, P.J., Caudy, A.A., and Hannon, G.J. 2002. Stable suppression of gene expression by RNAi in mammalian cells. *Proc Natl Acad Sci U S A* 99:1443-1448.
114. Svoboda, P., Stein, P., and Schultz, R.M. 2001. RNAi in mouse oocytes and preimplantation embryos: effectiveness of hairpin dsRNA. *Biochem Biophys Res Commun* 287:1099-1104.
115. Brummelkamp, T.R., Bernards, R., and Agami, R. 2002. A system for stable expression of short interfering RNAs in mammalian cells. *Science* 296:550-553.
116. Paddison, P.J., Caudy, A.A., Bernstein, E., Hannon, G.J., and Conklin, D.S. 2002. Short hairpin RNAs (shRNAs) induce sequence-specific silencing in mammalian cells. *Genes Dev* 16:948-958.
117. Coumoul, X., Shukla, V., Li, C., Wang, R.H., and Deng, C.X. 2005. Conditional knockdown of *Fgfr2* in mice using Cre-LoxP induced RNA interference. *Nucleic Acids Res* 33:e102.
118. Oberdoerffer, P., Kanellopoulou, C., Heissmeyer, V., Paeper, C., Borowski, C., Aifantis, I., Rao, A., and Rajewsky, K. 2005. Efficiency of RNA interference in the mouse hematopoietic system varies between cell types and developmental stages. *Mol Cell Biol* 25:3896-3905.
119. Ventura, A., Meissner, A., Dillon, C.P., McManus, M., Sharp, P.A., Van Parijs, L., Jaenisch, R., and Jacks, T. 2004. Cre-lox-regulated conditional RNA interference from transgenes. *Proc Natl Acad Sci U S A* 101:10380-10385.

120. Seibler, J., Kleinridders, A., Kuter-Luks, B., Niehaves, S., Bruning, J.C., and Schwenk, F. 2007. Reversible gene knockdown in mice using a tight, inducible shRNA expression system. *Nucleic Acids Res* 35:e54.
121. Duvillie, B., Cordonnier, N., Deltour, L., Dandoy-Dron, F., Itier, J.M., Monthieux, E., Jami, J., Joshi, R.L., and Bucchini, D. 1997. Phenotypic alterations in insulin-deficient mutant mice. *Proc Natl Acad Sci U S A* 94:5137-5140.
122. Accili, D., Drago, J., Lee, E.J., Johnson, M.D., Cool, M.H., Salvatore, P., Asico, L.D., Jose, P.A., Taylor, S.I., and Westphal, H. 1996. Early neonatal death in mice homozygous for a null allele of the insulin receptor gene. *Nat Genet* 12:106-109.
123. Abe, H., Yamada, N., Kamata, K., Kuwaki, T., Shimada, M., Osuga, J., Shionoiri, F., Yahagi, N., Kadowaki, T., Tamemoto, H., et al. 1998. Hypertension, hypertriglyceridemia, and impaired endothelium-dependent vascular relaxation in mice lacking insulin receptor substrate-1. *J Clin Invest* 101:1784-1788.
124. Araki, E., Lipes, M.A., Patti, M.E., Bruning, J.C., Haag, B., 3rd, Johnson, R.S., and Kahn, C.R. 1994. Alternative pathway of insulin signalling in mice with targeted disruption of the IRS-1 gene. *Nature* 372:186-190.
125. Tamemoto, H., Kadowaki, T., Tobe, K., Yagi, T., Sakura, H., Hayakawa, T., Terauchi, Y., Ueki, K., Kaburagi, Y., Satoh, S., et al. 1994. Insulin resistance and growth retardation in mice lacking insulin receptor substrate-1. *Nature* 372:182-186.
126. Withers, D.J., Gutierrez, J.S., Towery, H., Burks, D.J., Ren, J.M., Previs, S., Zhang, Y., Bernal, D., Pons, S., Shulman, G.I., et al. 1998. Disruption of IRS-2 causes type 2 diabetes in mice. *Nature* 391:900-904.
127. Liu, S.C., Wang, Q., Lienhard, G.E., and Keller, S.R. 1999. Insulin receptor substrate 3 is not essential for growth or glucose homeostasis. *J Biol Chem* 274:18093-18099.
128. Fantin, V.R., Wang, Q., Lienhard, G.E., and Keller, S.R. 2000. Mice lacking insulin receptor substrate 4 exhibit mild defects in growth, reproduction, and glucose homeostasis. *Am J Physiol Endocrinol Metab* 278:E127-133.
129. Itoh, M., Yoshida, Y., Nishida, K., Narimatsu, M., Hibi, M., and Hirano, T. 2000. Role of Gab1 in heart, placenta, and skin development and growth factor- and cytokine-induced extracellular signal-regulated kinase mitogen-activated protein kinase activation. *Mol Cell Biol* 20:3695-3704.

References

130. Bard-Chapeau, E.A., Hevener, A.L., Long, S., Zhang, E.E., Olefsky, J.M., and Feng, G.S. 2005. Deletion of Gab1 in the liver leads to enhanced glucose tolerance and improved hepatic insulin action. *Nat Med* 11:567-571.
131. Kulkarni, R.N., Bruning, J.C., Winnay, J.N., Postic, C., Magnuson, M.A., and Kahn, C.R. 1999. Tissue-specific knockout of the insulin receptor in pancreatic beta cells creates an insulin secretory defect similar to that in type 2 diabetes. *Cell* 96:329-339.
132. Bluher, M., Michael, M.D., Peroni, O.D., Ueki, K., Carter, N., Kahn, B.B., and Kahn, C.R. 2002. Adipose tissue selective insulin receptor knockout protects against obesity and obesity-related glucose intolerance. *Dev Cell* 3:25-38.
133. Bruning, J.C., Michael, M.D., Winnay, J.N., Hayashi, T., Horsch, D., Accili, D., Goodyear, L.J., and Kahn, C.R. 1998. A muscle-specific insulin receptor knockout exhibits features of the metabolic syndrome of NIDDM without altering glucose tolerance. *Mol Cell* 2:559-569.
134. Bruning, J.C., Gautam, D., Burks, D.J., Gillette, J., Schubert, M., Orban, P.C., Klein, R., Krone, W., Muller-Wieland, D., and Kahn, C.R. 2000. Role of brain insulin receptor in control of body weight and reproduction. *Science* 289:2122-2125.
135. Michael, M.D., Kulkarni, R.N., Postic, C., Previs, S.F., Shulman, G.I., Magnuson, M.A., and Kahn, C.R. 2000. Loss of insulin signaling in hepatocytes leads to severe insulin resistance and progressive hepatic dysfunction. *Mol Cell* 6:87-97.
136. Terauchi, Y., Iwamoto, K., Tamemoto, H., Komeda, K., Ishii, C., Kanazawa, Y., Asanuma, N., Aizawa, T., Akanuma, Y., Yasuda, K., et al. 1997. Development of non-insulin-dependent diabetes mellitus in the double knockout mice with disruption of insulin receptor substrate-1 and beta cell glucokinase genes. Genetic reconstitution of diabetes as a polygenic disease. *J Clin Invest* 99:861-866.
137. Nakae, J., Biggs, W.H., 3rd, Kitamura, T., Cavenee, W.K., Wright, C.V., Arden, K.C., and Accili, D. 2002. Regulation of insulin action and pancreatic beta-cell function by mutated alleles of the gene encoding forkhead transcription factor Foxo1. *Nat Genet* 32:245-253.
138. Guillam, M.T., Hummler, E., Schaerer, E., Yeh, J.I., Birnbaum, M.J., Beermann, F., Schmidt, A., Deriaz, N., and Thorens, B. 1997. Early diabetes and abnormal postnatal pancreatic islet development in mice lacking Glut-2. *Nat Genet* 17:327-330.
139. Katz, E.B., Stenbit, A.E., Hatton, K., DePinho, R., and Charron, M.J. 1995. Cardiac and adipose tissue abnormalities but not diabetes in mice deficient in GLUT4. *Nature* 377:151-155.

140. Bruning, J.C., Winnay, J., Bonner-Weir, S., Taylor, S.I., Accili, D., and Kahn, C.R. 1997. Development of a novel polygenic model of NIDDM in mice heterozygous for IR and IRS-1 null alleles. *Cell* 88:561-572.
141. Liu, J.P., Baker, J., Perkins, A.S., Robertson, E.J., and Efstratiadis, A. 1993. Mice carrying null mutations of the genes encoding insulin-like growth factor I (Igf-1) and type 1 IGF receptor (Igf1r). *Cell* 75:59-72.
142. Powell-Braxton, L., Hollingshead, P., Giltinan, D., Pitts-Meek, S., and Stewart, T. 1993. Inactivation of the IGF-I gene in mice results in perinatal lethality. *Ann N Y Acad Sci* 692:300-301.
143. Baker, J., Liu, J.P., Robertson, E.J., and Efstratiadis, A. 1993. Role of insulin-like growth factors in embryonic and postnatal growth. *Cell* 75:73-82.
144. Joshi, R.L., Lamothe, B., Cordonnier, N., Mesbah, K., Monthieux, E., Jami, J., and Bucchini, D. 1996. Targeted disruption of the insulin receptor gene in the mouse results in neonatal lethality. *Embo J* 15:1542-1547.
145. Fisher, S.J., and Kahn, C.R. 2003. Insulin signaling is required for insulin's direct and indirect action on hepatic glucose production. *J Clin Invest* 111:463-468.
146. Baumgartl, J., Baudler, S., Scherner, M., Babaev, V., Makowski, L., Suttles, J., McDuffie, M., Fazio, S., Kahn, C.R., Hotamisligil, G.S., et al. 2006. Myeloid lineage cell-restricted insulin resistance protects apolipoproteinE-deficient mice against atherosclerosis. *Cell Metab* 3:247-256.
147. Vicent, D., Ilany, J., Kondo, T., Naruse, K., Fisher, S.J., Kisanuki, Y.Y., Bursell, S., Yanagisawa, M., King, G.L., and Kahn, C.R. 2003. The role of endothelial insulin signaling in the regulation of vascular tone and insulin resistance. *J Clin Invest* 111:1373-1380.
148. LeRoith, D., Werner, H., Beitner-Johnson, D., and Roberts, C.T., Jr. 1995. Molecular and cellular aspects of the insulin-like growth factor I receptor. *Endocr Rev* 16:143-163.
149. De Meyts, P. 1994. The structural basis of insulin and insulin-like growth factor-I receptor binding and negative co-operativity, and its relevance to mitogenic versus metabolic signalling. *Diabetologia* 37 Suppl 2:S135-148.
150. Soos, M.A., and Siddle, K. 1989. Immunological relationships between receptors for insulin and insulin-like growth factor I. Evidence for structural heterogeneity of insulin-like growth factor I receptors involving hybrids with insulin receptors. *Biochem J* 263:553-563.
151. Moxham, C.P., Duronio, V., and Jacobs, S. 1989. Insulin-like growth factor I receptor beta-subunit heterogeneity. Evidence for hybrid tetramers composed of

References

- insulin-like growth factor I and insulin receptor heterodimers. *J Biol Chem* 264:13238-13244.
152. Rother, K.I., Imai, Y., Caruso, M., Beguinot, F., Formisano, P., and Accili, D. 1998. Evidence that IRS-2 phosphorylation is required for insulin action in hepatocytes. *J Biol Chem* 273:17491-17497.
153. Baudry, A., Lamothe, B., Bucchini, D., Jami, J., Montarras, D., Pinset, C., and Joshi, R.L. 2001. IGF-1 receptor as an alternative receptor for metabolic signaling in insulin receptor-deficient muscle cells. *FEBS Lett* 488:174-178.
154. Lamothe, B., Baudry, A., Christoffersen, C.T., De Meyts, P., Jami, J., Bucchini, D., and Joshi, R.L. 1998. Insulin receptor-deficient cells as a new tool for dissecting complex interplay in insulin and insulin-like growth factors. *FEBS Lett* 426:381-385.
155. Di Cola, G., Cool, M.H., and Accili, D. 1997. Hypoglycemic effect of insulin-like growth factor-1 in mice lacking insulin receptors. *J Clin Invest* 99:2538-2544.
156. Fernandez, A.M., Kim, J.K., Yakar, S., Dupont, J., Hernandez-Sanchez, C., Castle, A.L., Filmore, J., Shulman, G.I., and Le Roith, D. 2001. Functional inactivation of the IGF-I and insulin receptors in skeletal muscle causes type 2 diabetes. *Genes Dev* 15:1926-1934.
157. Anlar, B., Sullivan, K.A., and Feldman, E.L. 1999. Insulin-like growth factor-I and central nervous system development. *Horm Metab Res* 31:120-125.
158. Unger, J.W., and Betz, M. 1998. Insulin receptors and signal transduction proteins in the hypothalamo-hypophyseal system: a review on morphological findings and functional implications. *Histol Histopathol* 13:1215-1224.
159. Schubert, M., Brazil, D.P., Burks, D.J., Kushner, J.A., Ye, J., Flint, C.L., Farhang-Fallah, J., Dikkes, P., Warot, X.M., Rio, C., et al. 2003. Insulin receptor substrate-2 deficiency impairs brain growth and promotes tau phosphorylation. *J Neurosci* 23:7084-7092.
160. Schubert, M., Gautam, D., Surjo, D., Ueki, K., Baudler, S., Schubert, D., Kondo, T., Alber, J., Galldiks, N., Kustermann, E., et al. 2004. Role for neuronal insulin resistance in neurodegenerative diseases. *Proc Natl Acad Sci U S A* 101:3100-3105.
161. Lichtenwalner, R.J., Forbes, M.E., Sonntag, W.E., and Riddle, D.R. 2006. Adult-onset deficiency in growth hormone and insulin-like growth factor-I decreases survival of dentate granule neurons: insights into the regulation of adult hippocampal neurogenesis. *J Neurosci Res* 83:199-210.

162. Dudek, H., Datta, S.R., Franke, T.F., Birnbaum, M.J., Yao, R., Cooper, G.M., Segal, R.A., Kaplan, D.R., and Greenberg, M.E. 1997. Regulation of neuronal survival by the serine-threonine protein kinase Akt. *Science* 275:661-665.
163. Gasparini, L., and Xu, H. 2003. Potential roles of insulin and IGF-1 in Alzheimer's disease. *Trends Neurosci* 26:404-406.
164. Carro, E., Trejo, J.L., Gomez-Isla, T., LeRoith, D., and Torres-Aleman, I. 2002. Serum insulin-like growth factor I regulates brain amyloid-beta levels. *Nat Med* 8:1390-1397.
165. Gasparini, L., Gouras, G.K., Wang, R., Gross, R.S., Beal, M.F., Greengard, P., and Xu, H. 2001. Stimulation of beta-amyloid precursor protein trafficking by insulin reduces intraneuronal beta-amyloid and requires mitogen-activated protein kinase signaling. *J Neurosci* 21:2561-2570.
166. Niikura, T., Hashimoto, Y., Okamoto, T., Abe, Y., Yasukawa, T., Kawasumi, M., Hiraki, T., Kita, Y., Terashita, K., Kouyama, K., et al. 2001. Insulin-like growth factor I (IGF-I) protects cells from apoptosis by Alzheimer's V642I mutant amyloid precursor protein through IGF-I receptor in an IGF-binding protein-sensitive manner. *J Neurosci* 21:1902-1910.
167. Woods, S.C., Rushing, P.A., and Seeley, R.J. 2001. Neuropeptides and the control of energy homeostasis. *Nestle Nutr Workshop Ser Clin Perform Programme* 5:93-112; discussion 112-115.
168. Rosenzweig, E.S., and Barnes, C.A. 2003. Impact of aging on hippocampal function: plasticity, network dynamics, and cognition. *Prog Neurobiol* 69:143-179.
169. Wu, W.W., Oh, M.M., and Disterhoft, J.F. 2002. Age-related biophysical alterations of hippocampal pyramidal neurons: implications for learning and memory. *Ageing Res Rev* 1:181-207.
170. Gould, E., and Gross, C.G. 2002. Neurogenesis in adult mammals: some progress and problems. *J Neurosci* 22:619-623.
171. van Praag, H., Schinder, A.F., Christie, B.R., Toni, N., Palmer, T.D., and Gage, F.H. 2002. Functional neurogenesis in the adult hippocampus. *Nature* 415:1030-1034.
172. Kempermann, G., Kuhn, H.G., and Gage, F.H. 1998. Experience-induced neurogenesis in the senescent dentate gyrus. *J Neurosci* 18:3206-3212.
173. Shors, T.J., Townsend, D.A., Zhao, M., Kozorovitskiy, Y., and Gould, E. 2002. Neurogenesis may relate to some but not all types of hippocampal-dependent learning. *Hippocampus* 12:578-584.

References

174. Mattson, M.P., Maudsley, S., and Martin, B. 2004. A neural signaling triumvirate that influences ageing and age-related disease: insulin/IGF-1, BDNF and serotonin. *Ageing Res Rev* 3:445-464.
175. Lichtenwalner, R.J., Forbes, M.E., Bennett, S.A., Lynch, C.D., Sonntag, W.E., and Riddle, D.R. 2001. Intracerebroventricular infusion of insulin-like growth factor-I ameliorates the age-related decline in hippocampal neurogenesis. *Neuroscience* 107:603-613.
176. Sun, L.Y., Evans, M.S., Hsieh, J., Panici, J., and Bartke, A. 2005. Increased neurogenesis in dentate gyrus of long-lived Ames dwarf mice. *Endocrinology* 146:1138-1144.
177. Sambrook, J., and Russell, D.W. 2001. *Molecular Cloning: A Laboratory Manual*: CSHL Press. 2344 pp.
178. Mullis, K.B., and Faloona, F.A. 1987. Specific synthesis of DNA in vitro via a polymerase-catalyzed chain reaction. *Methods Enzymol* 155:335-350.
179. Saiki, R.K., Gelfand, D.H., Stoffel, S., Scharf, S.J., Higuchi, R., Horn, G.T., Mullis, K.B., and Erlich, H.A. 1988. Primer-directed enzymatic amplification of DNA with a thermostable DNA polymerase. *Science* 239:487-491.
180. Chomczynski, P., and Qasba, P.K. 1984. Alkaline transfer of DNA to plastic membrane. *Biochem Biophys Res Commun* 122:340-344.
181. Koch, L. 2004. Konditionale Inaktivierung des murinen Igflr-Gens. In *Mathematisch-Naturwissenschaftliche Fakultät*. Cologne: University of Cologne. 128.
182. Kontgen, F., and Stewart, C.L. 1993. Simple screening procedure to detect gene targeting events in embryonic stem cells. *Methods Enzymol* 225:878-890.
183. Mansour, S.L., Thomas, K.R., and Capecchi, M.R. 1988. Disruption of the proto-oncogene int-2 in mouse embryo-derived stem cells: a general strategy for targeting mutations to non-selectable genes. *Nature* 336:348-352.
184. Laemmli, U.K. 1970. Cleavage of structural proteins during the assembly of the head of bacteriophage T4. *Nature* 227:680-685.
185. Hogan, B., Costantini, F., and Lacey, E. 1986. *Manipulating the mouse embryo: A Laboratory Manual*. Cold Spring Harbor, New York: Cold Spring Harbor Laboratory Press.
186. Silver, L.M. 1995. *Mouse Genetics: Concepts and Applications*: Oxford University Press. 376 Seiten pp.

187. Zhu, Y., Romero, M.I., Ghosh, P., Ye, Z., Charnay, P., Rushing, E.J., Marth, J.D., and Parada, L.F. 2001. Ablation of NF1 function in neurons induces abnormal development of cerebral cortex and reactive gliosis in the brain. *Genes Dev* 15:859-876.
188. Morris, R. 1984. Developments of a water-maze procedure for studying spatial learning in the rat. *J Neurosci Methods* 11:47-60.
189. Carro, E., Trejo, J.L., Busiguina, S., and Torres-Aleman, I. 2001. Circulating insulin-like growth factor I mediates the protective effects of physical exercise against brain insults of different etiology and anatomy. *J Neurosci* 21:5678-5684.
190. Carro, E., Trejo, J.L., Gerber, A., Loetscher, H., Torrado, J., Metzger, F., and Torres-Aleman, I. 2006. Therapeutic actions of insulin-like growth factor I on APP/PS2 mice with severe brain amyloidosis. *Neurobiol Aging* 27:1250-1257.
191. Fernandez, A.M., de la Vega, A.G., and Torres-Aleman, I. 1998. Insulin-like growth factor I restores motor coordination in a rat model of cerebellar ataxia. *Proc Natl Acad Sci U S A* 95:1253-1258.
192. Pellow, S., Chopin, P., File, S.E., and Briley, M. 1985. Validation of open:closed arm entries in an elevated plus-maze as a measure of anxiety in the rat. *J Neurosci Methods* 14:149-167.
193. Montgomery, K.C. 1955. The relation between fear induced by novel stimulation and exploratory behavior. *J Comp Physiol Psychol* 48:254-260.
194. Sohal, D.S., Nghiem, M., Crackower, M.A., Witt, S.A., Kimball, T.R., Tymitz, K.M., Penninger, J.M., and Molkentin, J.D. 2001. Temporally regulated and tissue-specific gene manipulations in the adult and embryonic heart using a tamoxifen-inducible Cre protein. *Circ Res* 89:20-25.
195. Seibler, J., Kuter-Luks, B., Kern, H., Streu, S., Plum, L., Mauer, J., Kuhn, R., Bruning, J.C., and Schwenk, F. 2005. Single copy shRNA configuration for ubiquitous gene knockdown in mice. *Nucleic Acids Res* 33:e67.
196. Fain, J.N., Kovacev, V.P., and Scow, R.O. 1966. Antilipolytic effect of insulin in isolated fat cells of the rat. *Endocrinology* 78:773-778.
197. Kovacev, V.P., and Scow, R.O. 1966. Effect of hormones on fatty acid release by rat adipose tissue in vivo. *Am J Physiol* 210:1199-1208.
198. Lavis, V.R., and Williams, R.H. 1973. Lipolytic effects of high concentrations of insulin on isolated fat cells. Enhancement of the response to lipolytic hormones. *Diabetes* 22:629-636.

References

199. Inoue, H., Ogawa, W., Asakawa, A., Okamoto, Y., Nishizawa, A., Matsumoto, M., Teshigawara, K., Matsuki, Y., Watanabe, E., Hiramatsu, R., et al. 2006. Role of hepatic STAT3 in brain-insulin action on hepatic glucose production. *Cell Metab* 3:267-275.
200. Konner, A.C., Janoschek, R., Plum, L., Jordan, S.D., Rother, E., Ma, X., Xu, C., Enriori, P., Hampel, B., Barsh, G.S., et al. 2007. Insulin Action in AgRP-Expressing Neurons Is Required for Suppression of Hepatic Glucose Production. *Cell Metab* 5:438-449.
201. Holzenberger, M., Leneuve, P., Hamard, G., Ducos, B., Perin, L., Binoux, M., and Le Bouc, Y. 2000. A targeted partial invalidation of the insulin-like growth factor I receptor gene in mice causes a postnatal growth deficit. *Endocrinology* 141:2557-2566.
202. Hoesche, C., Sauerwald, A., Veh, R.W., Krippel, B., and Kilimann, M.W. 1993. The 5'-flanking region of the rat synapsin I gene directs neuron-specific and developmentally regulated reporter gene expression in transgenic mice. *J Biol Chem* 268:26494-26502.
203. Altman, J., and Das, G.D. 1965. Autoradiographic and histological evidence of postnatal hippocampal neurogenesis in rats. *J Comp Neurol* 124:319-335.
204. Cameron, H.A., Woolley, C.S., McEwen, B.S., and Gould, E. 1993. Differentiation of newly born neurons and glia in the dentate gyrus of the adult rat. *Neuroscience* 56:337-344.
205. Corotto, F.S., Henegar, J.A., and Maruniak, J.A. 1993. Neurogenesis persists in the subependymal layer of the adult mouse brain. *Neurosci Lett* 149:111-114.
206. Heumann, R., Goemans, C., Bartsch, D., Lingenhohl, K., Waldmeier, P.C., Hengerer, B., Allegrini, P.R., Schellander, K., Wagner, E.F., Arendt, T., et al. 2000. Transgenic activation of Ras in neurons promotes hypertrophy and protects from lesion-induced degeneration. *J Cell Biol* 151:1537-1548.
207. Gartner, U., Alpar, A., Reimann, F., Seeger, G., Heumann, R., and Arendt, T. 2004. Constitutive Ras activity induces hippocampal hypertrophy and remodeling of pyramidal neurons in synRas mice. *J Neurosci Res* 77:630-641.
208. Beck, K.D., Powell-Braxton, L., Widmer, H.R., Valverde, J., and Hefti, F. 1995. Igf1 gene disruption results in reduced brain size, CNS hypomyelination, and loss of hippocampal granule and striatal parvalbumin-containing neurons. *Neuron* 14:717-730.
209. Trejo, J.L., Carro, E., and Torres-Aleman, I. 2001. Circulating insulin-like growth factor I mediates exercise-induced increases in the number of new neurons in the adult hippocampus. *J Neurosci* 21:1628-1634.

210. Aberg, M.A., Aberg, N.D., Hedbacker, H., Oscarsson, J., and Eriksson, P.S. 2000. Peripheral infusion of IGF-I selectively induces neurogenesis in the adult rat hippocampus. *J Neurosci* 20:2896-2903.
211. Sperk, G. 1994. Kainic acid seizures in the rat. *Prog Neurobiol* 42:1-32.
212. Amaducci, L., and Tesco, G. 1994. Aging as a major risk for degenerative diseases of the central nervous system. *Curr Opin Neurol* 7:283-286.
213. Ennaceur, A., and Delacour, J. 1988. A new one-trial test for neurobiological studies of memory in rats. 1: Behavioral data. *Behav Brain Res* 31:47-59.
214. Lillioja, S., Mott, D.M., Spraul, M., Ferraro, R., Foley, J.E., Ravussin, E., Knowler, W.C., Bennett, P.H., and Bogardus, C. 1993. Insulin resistance and insulin secretory dysfunction as precursors of non-insulin-dependent diabetes mellitus. Prospective studies of Pima Indians. *N Engl J Med* 329:1988-1992.
215. Martin, B.C., Warram, J.H., Krolewski, A.S., Bergman, R.N., Soeldner, J.S., and Kahn, C.R. 1992. Role of glucose and insulin resistance in development of type 2 diabetes mellitus: results of a 25-year follow-up study. *Lancet* 340:925-929.
216. Nigro, J., Osman, N., Dart, A.M., and Little, P.J. 2006. Insulin resistance and atherosclerosis. *Endocr Rev* 27:242-259.
217. Plum, L., Belgardt, B.F., and Bruning, J.C. 2006. Central insulin action in energy and glucose homeostasis. *J Clin Invest* 116:1761-1766.
218. Semenkovich, C.F. 2006. Insulin resistance and atherosclerosis. *J Clin Invest* 116:1813-1822.
219. Buettner, C., Patel, R., Muse, E.D., Bhanot, S., Monia, B.P., McKay, R., Obici, S., and Rossetti, L. 2005. Severe impairment in liver insulin signaling fails to alter hepatic insulin action in conscious mice. *J Clin Invest* 115:1306-1313.
220. Gelling, R.W., Morton, G.J., Morrison, C.D., Niswender, K.D., Myers, M.G., Jr., Rhodes, C.J., and Schwartz, M.W. 2006. Insulin action in the brain contributes to glucose lowering during insulin treatment of diabetes. *Cell Metab* 3:67-73.
221. Obici, S., Feng, Z., Karkanias, G., Baskin, D.G., and Rossetti, L. 2002. Decreasing hypothalamic insulin receptors causes hyperphagia and insulin resistance in rats. *Nat Neurosci* 5:566-572.
222. Obici, S., Zhang, B.B., Karkanias, G., and Rossetti, L. 2002. Hypothalamic insulin signaling is required for inhibition of glucose production. *Nat Med* 8:1376-1382.

References

223. Okamoto, H., Obici, S., Accili, D., and Rossetti, L. 2005. Restoration of liver insulin signaling in Insr knockout mice fails to normalize hepatic insulin action. *J Clin Invest* 115:1314-1322.
224. Edgerton, D.S., Lautz, M., Scott, M., Everett, C.A., Stettler, K.M., Neal, D.W., Chu, C.A., and Cherrington, A.D. 2006. Insulin's direct effects on the liver dominate the control of hepatic glucose production. *J Clin Invest* 116:521-527.
225. Cherrington, A.D. 2005. The role of hepatic insulin receptors in the regulation of glucose production. *J Clin Invest* 115:1136-1139.
226. Theander-Carrillo, C., Wiedmer, P., Cettour-Rose, P., Nogueiras, R., Perez-Tilve, D., Pfluger, P., Castaneda, T.R., Muzzin, P., Schurmann, A., Szanto, I., et al. 2006. Ghrelin action in the brain controls adipocyte metabolism. *J Clin Invest* 116:1983-1993.
227. Manin, M., Balage, M., Larue-Achagiotis, C., and Grizard, J. 1988. Chronic intracerebroventricular infusion of insulin failed to alter brain insulin-binding sites, food intake, and body weight. *J Neurochem* 51:1689-1695.
228. Coll, A.P., Farooqi, I.S., and O'Rahilly, S. 2007. The hormonal control of food intake. *Cell* 129:251-262.
229. Zhang, Y., Proenca, R., Maffei, M., Barone, M., Leopold, L., and Friedman, J.M. 1994. Positional cloning of the mouse obese gene and its human homologue. *Nature* 372:425-432.
230. Sliker, L.J., Sloop, K.W., Surface, P.L., Kriauciunas, A., LaQuier, F., Manetta, J., Bue-Valleskey, J., and Stephens, T.W. 1996. Regulation of expression of ob mRNA and protein by glucocorticoids and cAMP. *J Biol Chem* 271:5301-5304.
231. Murakami, T., Iida, M., and Shima, K. 1995. Dexamethasone regulates obese expression in isolated rat adipocytes. *Biochem Biophys Res Commun* 214:1260-1267.
232. MacDougald, O.A., Hwang, C.S., Fan, H., and Lane, M.D. 1995. Regulated expression of the obese gene product (leptin) in white adipose tissue and 3T3-L1 adipocytes. *Proc Natl Acad Sci U S A* 92:9034-9037.
233. Gettys, T.W., Harkness, P.J., and Watson, P.M. 1996. The beta 3-adrenergic receptor inhibits insulin-stimulated leptin secretion from isolated rat adipocytes. *Endocrinology* 137:4054-4057.
234. Bradley, R.L., and Cheatham, B. 1999. Regulation of ob gene expression and leptin secretion by insulin and dexamethasone in rat adipocytes. *Diabetes* 48:272-278.

-
235. Barr, V.A., Malide, D., Zarnowski, M.J., Taylor, S.I., and Cushman, S.W. 1997. Insulin stimulates both leptin secretion and production by rat white adipose tissue. *Endocrinology* 138:4463-4472.
236. Vidal, H., Auboeuf, D., De Vos, P., Staels, B., Riou, J.P., Auwerx, J., and Laville, M. 1996. The expression of ob gene is not acutely regulated by insulin and fasting in human abdominal subcutaneous adipose tissue. *J Clin Invest* 98:251-255.
237. Dagogo-Jack, S., Fanelli, C., Paramore, D., Brothers, J., and Landt, M. 1996. Plasma leptin and insulin relationships in obese and nonobese humans. *Diabetes* 45:695-698.
238. Malmstrom, R., Taskinen, M.R., Karonen, S.L., and Yki-Jarvinen, H. 1996. Insulin increases plasma leptin concentrations in normal subjects and patients with NIDDM. *Diabetologia* 39:993-996.
239. Kolaczynski, J.W., Nyce, M.R., Considine, R.V., Boden, G., Nolan, J.J., Henry, R., Mudaliar, S.R., Olefsky, J., and Caro, J.F. 1996. Acute and chronic effects of insulin on leptin production in humans: Studies in vivo and in vitro. *Diabetes* 45:699-701.
240. Shimomura, I., Hammer, R.E., Richardson, J.A., Ikemoto, S., Bashmakov, Y., Goldstein, J.L., and Brown, M.S. 1998. Insulin resistance and diabetes mellitus in transgenic mice expressing nuclear SREBP-1c in adipose tissue: model for congenital generalized lipodystrophy. *Genes Dev* 12:3182-3194.
241. Semple, R.K., Soos, M.A., Luan, J., Mitchell, C.S., Wilson, J.C., Gurnell, M., Cochran, E.K., Gorden, P., Chatterjee, V.K., Wareham, N.J., et al. 2006. Elevated plasma adiponectin in humans with genetically defective insulin receptors. *J Clin Endocrinol Metab* 91:3219-3223.
242. Semple, R.K., Halberg, N.H., Burling, K., Soos, M.A., Schraw, T., Luan, J., Cochran, E.K., Dunger, D.B., Wareham, N.J., Scherer, P.E., et al. 2007. Paradoxical elevation of high-molecular weight adiponectin in acquired extreme insulin resistance due to insulin receptor antibodies. *Diabetes* 56:1712-1717.
243. Tartaglia, L.A., Dembski, M., Weng, X., Deng, N., Culpepper, J., Devos, R., Richards, G.J., Campfield, L.A., Clark, F.T., Deeds, J., et al. 1995. Identification and expression cloning of a leptin receptor, OB-R. *Cell* 83:1263-1271.
244. Baumann, H., Morella, K.K., White, D.W., Dembski, M., Bailon, P.S., Kim, H., Lai, C.F., and Tartaglia, L.A. 1996. The full-length leptin receptor has signaling capabilities of interleukin 6-type cytokine receptors. *Proc Natl Acad Sci U S A* 93:8374-8378.

References

245. Ge, H., Huang, L., Pourbahrami, T., and Li, C. 2002. Generation of soluble leptin receptor by ectodomain shedding of membrane-spanning receptors in vitro and in vivo. *J Biol Chem* 277:45898-45903.
246. Cohen, P., Yang, G., Yu, X., Soukas, A.A., Wolfish, C.S., Friedman, J.M., and Li, C. 2005. Induction of leptin receptor expression in the liver by leptin and food deprivation. *J Biol Chem* 280:10034-10039.
247. Cohen, S.E., Kokkotou, E., Biddinger, S.B., Kondo, T., Gebhardt, R., Kratzsch, J., Mantzoros, C.S., and Kahn, C.R. 2007. High circulating leptin receptors with normal leptin sensitivity in liver-specific insulin receptor knock-out (LIRKO) mice. *J Biol Chem* 282:23672-23678.
248. Margetic, S., Gazzola, C., Pegg, G.G., and Hill, R.A. 2002. Leptin: a review of its peripheral actions and interactions. *Int J Obes Relat Metab Disord* 26:1407-1433.
249. Inoue, H., Ogawa, W., Ozaki, M., Haga, S., Matsumoto, M., Furukawa, K., Hashimoto, N., Kido, Y., Mori, T., Sakaue, H., et al. 2004. Role of STAT-3 in regulation of hepatic gluconeogenic genes and carbohydrate metabolism in vivo. *Nat Med* 10:168-174.
250. Rahmouni, K., Morgan, D.A., Morgan, G.M., Liu, X., Sigmund, C.D., Mark, A.L., and Haynes, W.G. 2004. Hypothalamic PI3K and MAPK differentially mediate regional sympathetic activation to insulin. *J Clin Invest* 114:652-658.
251. Strubbe, J.H., and Mein, C.G. 1977. Increased feeding in response to bilateral injection of insulin antibodies in the VMH. *Physiol Behav* 19:309-313.
252. Dore, S., Kar, S., and Quirion, R. 1997. Insulin-like growth factor I protects and rescues hippocampal neurons against beta-amyloid- and human amylin-induced toxicity. *Proc Natl Acad Sci U S A* 94:4772-4777.
253. Escartin, C., Boyer, F., Bemelmans, A.P., Hantraye, P., and Brouillet, E. 2004. Insulin growth factor-1 protects against excitotoxicity in the rat striatum. *Neuroreport* 15:2251-2254.
254. Mumby, D.G. 2001. Perspectives on object-recognition memory following hippocampal damage: lessons from studies in rats. *Behav Brain Res* 127:159-181.

8 Acknowledgements

My sincere gratitude goes to Prof. Dr. Jens C. Brüning for providing me with this project and the opportunity to work in his lab.

I would like to thank Prof. Dr. Thomas Langer, Prof. Dr. Siegfried Roth and Dr. Ursula Lichtenberg for agreeing to form my thesis committee.

My graduate studies would not have been the same without the social and academic challenges and diversions provided by my fellow colleagues in the Department of Mouse Genetics and Metabolism. I would like to gratefully acknowledge Dr. Thomas Wunderlich for his help with gene targeting strategies and Southern blot analysis, Sigrid Irlenbusch for aiding with ES and EF cell culture, Brigitte Hampel for immunohistochemical stainings, Christine Könner for her help with animal operations and Dr. André Kleinriders for letting me bug him about all the little things right from the start. I thank all my colleagues for stimulating discussions, help with experiments and general advice. I am especially grateful to Julia Baumgartl for her support and friendship.

Finally, I am forever indebted to my family, my parents Raymonde and Ulrich Koch, my sister Claire Buhl, and Andrew Croxford for all their love and support, endless patience and encouragement when it was most required.

9 Erklärung

Ich versichere, daß ich die von mir vorgelegte Dissertation selbständig angefertigt, die benutzten Quellen und Hilfsmittel vollständig angegeben und die Stellen der Arbeit - einschließlich Tabellen, Karten und Abbildungen -, die anderen Werken im Wortlaut oder dem Sinn nach entnommen sind, in jedem Einzelfall als Entlehnung kenntlich gemacht habe; daß diese Dissertation noch keiner anderen Fakultät oder Universität zur Prüfung vorgelegen hat; daß sie - abgesehen von unten angegebenen Teilpublikationen - noch nicht veröffentlicht worden ist sowie, daß ich eine solche Veröffentlichung vor Abschluß des Promotionsverfahrens nicht vornehmen werde. Die Bestimmungen dieser Promotionsordnung sind mir bekannt. Die von mir vorgelegte Dissertation ist von Prof. Dr. Jens C. Brüning betreut worden.

Köln, Dezember 2007

Linda Koch

Teilpublikationen

Koch, L., Wunderlich, F.T., Seibler, J., Könner, A.C., Hampel, B., Irlenbusch, S., Brabant, G., Kahn, C.R., Schwenk, F., and Brüning, J.C. *Central insulin action regulates peripheral glucose and fat metabolism in mice*. J Clin Invest. 2008 Jun 2;118(6):2132-2147.

Klötting, N., Koch, L., Wunderlich, F.T., Kern, M., Ruschke, K., Krone, W., Brüning, J.C., and Blüher, M. 2008. Autocrine IGF-1 action in adipocytes controls systemic IGF-1 concentrations and growth. (in press)

Ibrahim, H., Stachelscheid, H., Koch, L., Schmitz, A., Wunderlich, F.T., Michels, C., Wickenhauser, C., Haase, I., Brüning, J.C., and Niessen, C.M. 2007. Insulin/IGF-1 signaling control proliferative potential of interfollicular epidermal progenitor cells via Rac. (submitted)

10 Curriculum Vitae

Persönliche Daten

Name	Linda Koch
Geburt	15.06.1979 in Köln
Adresse	Berrenrather St. 365, 50937 Köln
Email	linkoc@gmx.de
Nationalität	deutsch/französisch

Bildungsweg

Seit 04/2004	Promotion in der Abteilung Mausgenetik und Metabolismus des Instituts für Genetik der Universität zu Köln
1998 - 2004	Studium der Biologie an der Mathematisch-Naturwissenschaftlichen Fakultät der Universität zu Köln Diplomarbeit in der Abteilung Mausgenetik und Metabolismus des Instituts für Genetik der Universität zu Köln zum Thema: „Konditionale Inaktivierung des murinen Igf-1 Rezeptor Gens“ Diplomprüfungen im Hauptfach Genetik und in den Nebenfächern Biochemie und Zoologie
1998	Studiensemester Biologie (Lehramt, SekI) und Englisch (Lehramt, SekI) am Erziehungswissenschaftlichen Institut der Universität zu Köln
1988 - 1997	Deutsche Schule Lissabon, Portugal (Abschluss: Reifeprüfung)
1985-1988	Katholische Grundschule Mechernich

Publikationen

2006	Plum, L., Ma, X., Hampel, B., Balthasar, N., Coppari, R., Munzberg, H., Shanabrough, M., Burdakov, D., Rother, E., Janoschek, R., Alber, J., Belgardt, B.F., Koch, L., Seibler, J., Schwenk, F., Fekete, C., Suzuki, A., Mak, T. W., Krone, W., Horvath, T.L., Ashcroft, F.M., and Bruning, J.C. 2006. <i>Enhanced PIP3 signaling in POMC neurons causes KATP channel activation and leads to diet-sensitive obesity.</i> J Clin Invest 116:1886-1901
2006	Janoschek, R., Plum, L., Koch, L., Munzberg, H., Diano, S., Shanabrough, M., Muller, W., Horvath, T.L., and Bruning, J.C. 2006. <i>gp130 signaling in proopiomelanocortin neurons mediates the acute anorectic response to centrally applied ciliary neurotrophic factor.</i> Proc Natl Acad Sci U S A 103:10707-10712